Geosynthetic Reinforced Soil Performance Testing—Axial Load Deformation Relationships

PUBLICATION NO. FHWA-HRT-13-066

AUGUST 2013

U.S. Department of Transportation
Federal Highway Administration

Research, Development, and Technology
Turner-Fairbank Highway Research Center
6300 Georgetown Pike
McLean, VA 22101-2296

FOREWORD

The use of geosynthetic reinforced soil (GRS) for load bearing applications such as bridge abutments and integrated bridge systems (IBS) has expanded among transportation agencies looking to save time and money while delivering a better and safe product to the traveling public. GRS has been identified by the Federal Highway Administration (FHWA) as a proven, market-ready technology, and is being actively promoted through its Every Day Counts (EDC) initiative. FHWA interim design guidance for GRS abutments and IBSs is presented in Publication No. FHWA-HRT-11-026. The guidance includes the procedure and use of the GRS performance tests, also termed a mini-pier experiment. This report presents a database of nineteen performance tests performed by the FHWA, largely at the Turner-Fairbank Highway Research Center. It also presents findings, conclusions, and suggestions regarding various design parameters related to the performance of GRS, such as backfill material, reinforcement strength, reinforcement spacing, facing confinement, secondary reinforcement, and compaction.

A reliability analysis for load and resistance factor design (LRFD) was performed based on the results of this performance testing to determine a calibrated resistance factor for the soil-geosynthetic capacity equation. The results of this analysis can also be used by bridge designers to estimate capacity and deformation of GRS. In addition, an insight into the behavior of GRS as a new composite material due to the close reinforcement spacing is described.

Jorge E. Pagán-Ortiz
Director, Office of Infrastructure
Research and Development

TECHNICAL REPORT DOCUMENTATION PAGE

1. Report No. FHWA-HRT-13-066	2. Government Accession No.	3. Recipient's Catalog No.
4. Title and Subtitle Geosynthetic Reinforced Soil Performance Testing—Axial Load Deformation Relationships		5. Report Date August 2013
		6. Performing Organization Code: HRDI-40
7. Author(s) Nicks, J.E., Adams, M.T., Ooi, P.S.K., Stabile, T.		8. Performing Organization Report No.
9. Performing Organization Name and Address Turner-Fairbank Highway Research Center 6300 Georgetown Pike McLean, VA 22101		10. Work Unit No.
		11. Contract or Grant No. N/A
12. Sponsoring Agency Name and Address Office of Infrastructure R&D FHWA Research, Development and Technology 6300 Georgetown Pike McLean, VA 22101		13. Type of Report and Period Covered Technical
		14. Sponsoring Agency Code

15. Supplementary Notes
The FHWA Contracting Officer's Technical Representative (COTR) was Mike Adams, HRDI-40.

16. Abstract

The geosynthetic reinforced soil (GRS) performance test (PT), also called a mini-pier experiment, consists of constructing alternating layers of compacted granular fill and geosynthetic reinforcement with a facing element that is frictionally connected, then axially loading the GRS mass while measuring deformation to monitor performance. This large element load test provides material strength properties of a particular GRS composite built with unique combinations of reinforcement, compacted fill, and facing elements. This report describes the procedure and provides axial load- deformation results for a series of PTs conducted in both Defiance County, OH, as part of the Federal Highway Administration's (FHWA) Every Day Counts (EDC) GRS Validation Sessions and in McLean, VA, at the FHWA's Turner-Fairbank Highway Research Center as part of a parametric study.

The primary objectives of this research report are to: (1) build a database of GRS material properties that can be used by designers for GRS abutments and integrated bridge systems; (2) evaluate the relationship between reinforcement strength and spacing; (3) quantify the contribution of the frictionally connected facing elements at the service limit and strength limit states; (4) assess the new internal stability design method proposed by Adams et al. 2011 for GRS; and (5) perform a reliability analysis of the proposed soil-geosynthetic capacity equation for LRFD calibration. [1,11]

17. Key Words Geosynthetic reinforced soil, performance test, mini-pier experiment, abutment, integrated bridge system, geotextile, capacity, deformation		18. Distribution Statement	
19. Security Classif. (of this report) Unclassified	20. Security Classif. (of this page) Unclassified	21. No. of Pages 169	22. Price

Form DOT F 1700.7 (8-72) Reproduction of completed page authorized

SI* (MODERN METRIC) CONVERSION FACTORS

APPROXIMATE CONVERSIONS TO SI UNITS

Symbol	When You Know	Multiply By	To Find	Symbol
		LENGTH		
in	inches	25.4	millimeters	mm
ft	feet	0.305	meters	m
yd	yards	0.914	meters	m
mi	miles	1.61	kilometers	km
		AREA		
in^2	square inches	645.2	square millimeters	mm^2
ft^2	square feet	0.093	square meters	m^2
yd^2	square yard	0.836	square meters	m^2
ac	acres	0.405	hectares	ha
mi^2	square miles	2.59	square kilometers	km^2
		VOLUME		
fl oz	fluid ounces	29.57	milliliters	mL
gal	gallons	3.785	liters	L
ft^3	cubic feet	0.028	cubic meters	m^3
yd^3	cubic yards	0.765	cubic meters	m^3
		NOTE: volumes greater than 1000 L shall be shown in m^3		
		MASS		
oz	ounces	28.35	grams	g
lb	pounds	0.454	kilograms	kg
T	short tons (2000 lb)	0.907	megagrams (or "metric ton")	Mg (or "t")
		TEMPERATURE (exact degrees)		
^oF	Fahrenheit	5 (F-32)/9 or (F-32)/1.8	Celsius	^oC
		ILLUMINATION		
fc	foot-candles	10.76	lux	lx
fl	foot-Lamberts	3.426	$candela/m^2$	cd/m^2
		FORCE and PRESSURE or STRESS		
lbf	poundforce	4.45	newtons	N
lbf/in^2	poundforce per square inch	6.89	kilopascals	kPa

APPROXIMATE CONVERSIONS FROM SI UNITS

Symbol	When You Know	Multiply By	To Find	Symbol
		LENGTH		
mm	millimeters	0.039	inches	in
m	meters	3.28	feet	ft
m	meters	1.09	yards	yd
km	kilometers	0.621	miles	mi
		AREA		
mm^2	square millimeters	0.0016	square inches	in^2
m^2	square meters	10.764	square feet	ft^2
m^2	square meters	1.195	square yards	yd^2
ha	hectares	2.47	acres	ac
km^2	square kilometers	0.386	square miles	mi^2
		VOLUME		
mL	milliliters	0.034	fluid ounces	fl oz
L	liters	0.264	gallons	gal
m^3	cubic meters	35.314	cubic feet	ft^3
m^3	cubic meters	1.307	cubic yards	yd^3
		MASS		
g	grams	0.035	ounces	oz
kg	kilograms	2.202	pounds	lb
Mg (or "t")	megagrams (or "metric ton")	1.103	short tons (2000 lb)	T
		TEMPERATURE (exact degrees)		
^oC	Celsius	1.8C+32	Fahrenheit	^oF
		ILLUMINATION		
lx	lux	0.0929	foot-candles	fc
cd/m^2	$candela/m^2$	0.2919	foot-Lamberts	fl
		FORCE and PRESSURE or STRESS		
N	newtons	0.225	poundforce	lbf
kPa	kilopascals	0.145	poundforce per square inch	lbf/in^2

*SI is the symbol for the International System of Units. Appropriate rounding should be made to comply with Section 4 of ASTM E380.
(Revised March 2003)

TABLE OF CONTENTS

LIST OF FIGURES

LIST OF TABLES

LIST OF ABBREVIATIONS AND SYMBOLS

Abbreviations

AASHTO	American Association of State Highway and Transportation Officials
CMU	Concrete masonry unit
DC	Defiance County, OH
EDC	Every Day Counts initiative
FHWA	Federal Highway Administration
GP-GM	Poorly graded-silty gravel
GRS	Geosynthetic reinforced soil
IBS	Integrated bridge systems
LFD	Load factor design
LRFD	Load and resistance factor design
LSDS	Large scale direct shear
LVDT	Linear voltage displacement transducers
MARV	Minimum average roll value
POT	Potentiometer
PT	Performance test
SRW	Segmental retaining wall
TFHRC	Turner-Fairbank Highway Research Center
USCS	Unified Soil Classification System

Symbols

β	Reliability index
β_s	Slope angle
β_T	Target reliability index

γ	Unit weight of the backfill
γ_b	Bulk unit weight of the facing block
γ_d	Maximum dry density
γ_D	Load factor for dead load
γ_L	Load factor for live load
γ_{GRS}	Unit weight of the GRS composite
γ_i	Load factor for load component i
δ	Interface friction angle between the geosynthetic and the facing element for a frictionally connected GRS composite
$\varepsilon_{@q=4000psf}$	Measured vertical strain at an applied load of 4000 psf
$\varepsilon_{@qult}$	Measured vertical strain at failure
ε_{max}	Maximum recorded vertical strain
ε_v	Vertical strain
$\varepsilon_{v,compact}$	Vertical strain for a compacted GRS composite
$\varepsilon_{v,uncompact}$	Vertical strain for an uncompacted GRS composite
λ	Bias, ratio of measured to predicted
λ_D	Bias factor for dead load
λ_L	Bias factor for live load
λ_R	Bias factor for resistance
ν_{GRS}	Poisson's ratio of the GRS
ρ	Vertical displacement
σ	Applied normal stress
σ_c	External confining stress due to the facing

σ_h	Total lateral stress within the GRS composite at a given depth and location
τ	Shear strength of soil
ϕ	Peak friction angle
ϕ_{GRS}	Friction angle of the GRS composite
Φ	Resistance factor
Φ_{cap}	Resistance factor for capacity
ω	Optimum moisture content
a	Footing offset from the edge of the wall face (i.e., setback distance)
b	Footing width on top of the GRS composite
B	Base width of the GRS composite
B_{total}	Total width of the PT with the CMU facing
c	Cohesion of the backfill
c_{GRS}	Cohesion of the GRS composite
Cc	Coefficient of Curvature
Cu	Coefficient of Uniformity
d	Depth of the facing block unit perpendicular to the wall face
d_{max}	Maximum aggregate size
D_{10}	Aggregate size in which 10 percent of the sample is finer
D_{30}	Aggregate size in which 30 percent of the sample is finer
D_{60}	Aggregate size in which 60 percent of the sample is finer
D_{85}	Aggregate size in which 85 percent of the sample is finer
E_o	Initial stress-strain ratio
$E_{o,CMU}$	Initial stress-strain ratio for tests with CMU facing
$E_{o,\ no\ CMU}$	Initial stress-strain ratio for tests without any facing

E_{GRS}	Young's modulus of the GRS composite
E_R	Ratio of stress to strain for the reload cycle
$\bar{g}$	Mean safety margin
H	Height of the GRS composite
K_{ar}	Coefficient of active earth pressure for the backfill
K_{pr}	Coefficient of passive earth pressure for the backfill
L	Length of footing/bearing area
$N_{\gamma q}$	Bearing capacity factor
N_{cq}	Bearing capacity factor
N_s	Stability factor
S_{GRS}	Plane strain stiffness of a strip footing on top of GRS
S_{PT}	Stiffness of the unconfined GRS column
S_v	Reinforcement spacing
T_f	Wide width tensile strength of the geosynthetic, expressed as the minimum average roll value (MARV)
$T_{req,c}$	Required reinforcement strength in the direction perpendicular to the wall face
q	Applied stress
$q_{@\varepsilon=0.5\%}$	Applied stress at 0.5 percent vertical strain
$q_{@\varepsilon=0.5\%,\ predicted}$	Predicted applied stress at 0.5 percent vertical strain
$q_{@\varepsilon=5\%}$	Applied stress at 5 percent vertical strain
q_{max}	Maximum applied pressure during testing
$q_{ult,an,c}$	Ultimate capacity using semi-empirical theory
$q_{ult,emp}$	Measured failure pressure
$q_{ult,emp\ CMU}$	Measured failure pressure for tests with CMU facing
$q_{ult,emp\ no\ CMU}$	Measured failure pressure for tests without any facing

$q_{ult,PS}$	Ultimate capacity of strip footing under plane strain conditions
$q_{ult,PT}$	Ultimate capacity of the GRS column
Q	Load
Q_D	Dead load
Q_L	Live load
Q_i	Load component i
R	Resistance
V_{dmax}	Coefficient of variation of the maximum aggregate size
V_D	Coefficient of variation of the dead load
V_{Kp}	Coefficient of variation of the coefficient for passive earth pressure
V_L	Coefficient of variation of the live load
V_M	Coefficient of variation of the model
V_Q	Coefficient of variation of the loads
V_R	Coefficient of variation of the resistance
V_{Tf}	Coefficient of variation of the reinforcement strength
W	Factor accounting for the effect of reinforcement spacing and aggregate size
z	Standard normal variable

1. INTRODUCTION

The Federal Highway Administration (FHWA) has developed a standard test method to describe the load-deformation behavior of a frictionally connected geosynthetic reinforced soil (GRS) composite material which can be used to predict performance of a GRS abutment.[1] The GRS performance test (PT), also called a mini-pier experiment, consists of constructing alternating layers of compacted granular fill and geosynthetic reinforcement with a facing element that is frictionally connected, then axially loading the GRS mass while measuring deformation to monitor performance. This large element load test provides material strength properties of a particular GRS composite built with different combinations of reinforcement, compacted fill, and facing elements. This report describes the procedure and provides axial load versus deformation results for a series of PTs conducted in both Defiance County, OH, as part of the FHWA's Every Day Counts (EDC) GRS Validation Sessions and in McLean, VA, at the FHWA's Turner-Fairbank Highway Research Center (TFHRC) as part of a parametric study.

1.1 BACKGROUND

The FHWA first demonstrated the concept of a mini-pier experiment in 2000 with the "Vegas Mini-Pier" experiment, shown in figure 1.[1,2] The pier was 8 ft tall with square inside dimensions of 3.5 ft, which represents a height (H) to base width (B) ratio of 2 (figure 2 through figure 4). This H/B ratio is consistent with typical triaxial testing for soils.[3]

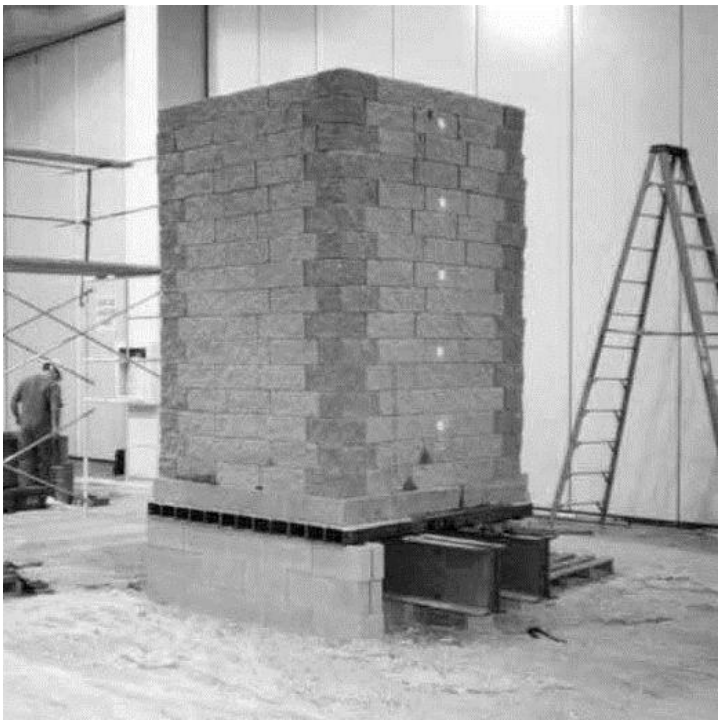

Figure 1. Photo. Vegas mini-pier experiment.

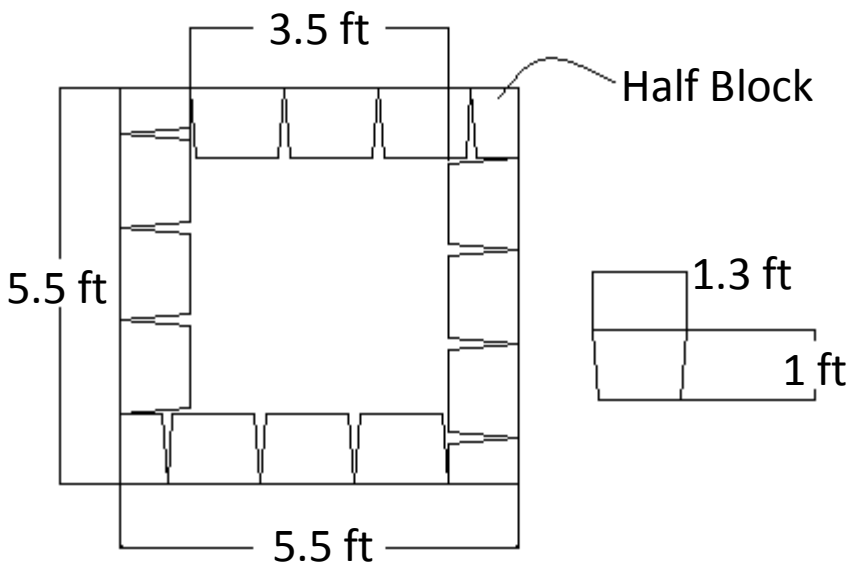

Figure 2. Illustration. Plan view of Vegas mini-pier experiment.

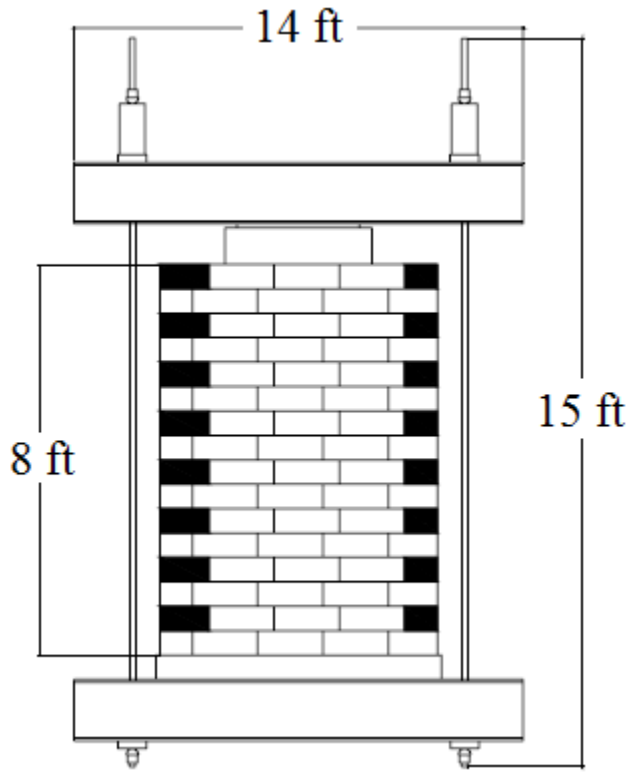

Figure 3. Illustration. Face view of Vegas mini-pier experiment.

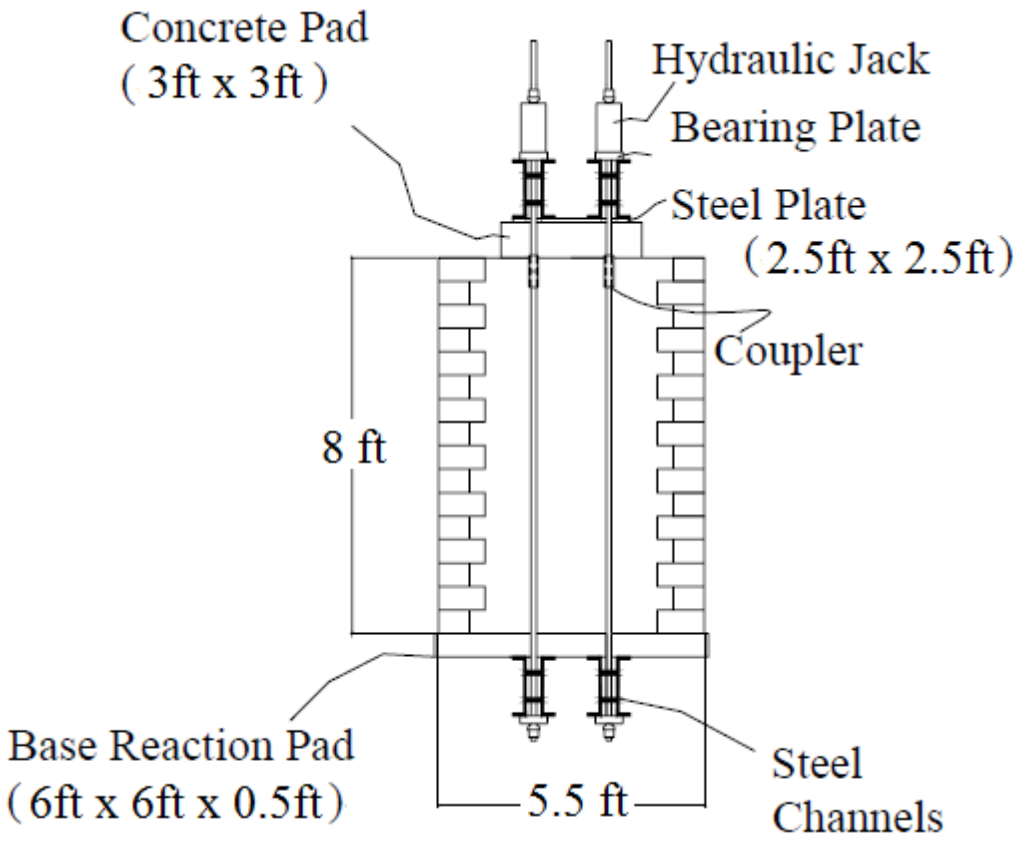

Figure 4. Illustration. Side view of Vegas mini-pier experiment.

The materials used for the GRS pier were a poorly graded-silty gravel (GP-GM, according to the Unified Soil Classification System, or USCS) soil with a 2,400 lb/ft (ultimate wide width tensile strength) geotextile spaced every 6 inches frictionally connected to segmental retaining wall (SRW) blocks for the facing. The top two courses of block, 1 ft from the top of the mini-pier, had two intermediate bearing bed reinforcement layers as shown in figure 5. The resulting pier was loaded up to 146 psi; however, time constraints and stroke limitations for the jacks prevented loading to failure of the composite. Since then, several additional performance tests have been completed, with the largest load carrying capacity reported at 176 psi.[4,5]

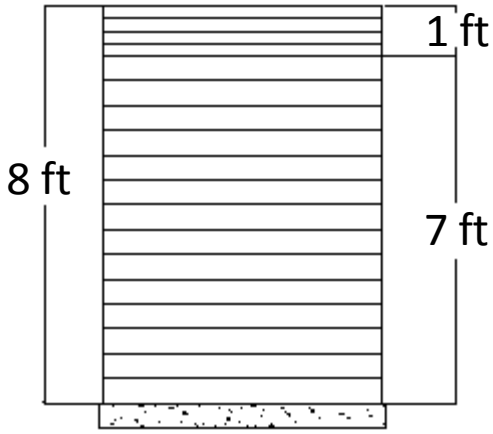

Figure 5. Illustration. Reinforcement schedule for Vegas mini-pier experiment.

The concept of testing GRS material has been previously applied on smaller scale models ranging from small triaxial sized samples to 2-ft cubed specimens in smaller capacity test frames.[6,7] Several large scale tests have also been conducted.[7,8,9] For the aggregates recommended by FHWA for bridge support, large scale tests are required to adequately predict performance of a full-scale GRS abutment.[1] The proposed FHWA PT has been shown to accurately predict both the strength limit and the service limit for GRS abutments.[5]

1.2 CURRENT PERFORMANCE TESTS

To investigate GRS material further, the FHWA conducted a series of 19 PTs as part of this research. The layout for these PTs was a slight modification of the Vegas Mini-Pier experiment. Since these tests were conducted with concrete masonry units (CMU) for the facing, as opposed to SRW blocks used in the Vegas PT, different test dimensions were needed to retain the H/B ratio of 2 throughout testing. For CMUs, the typical performance test is 6.4 ft tall with square inside dimensions of 3.2 ft (figure 6 and figure 7). The parameters that varied among tests were reinforcement spacing (from 4 to 16 inches), geotextile strength (from 1,400 to 4,800 lb/ft, soil type (open-graded and well-graded), and frictionally connected facing element (concrete masonry unit facing and no facing).

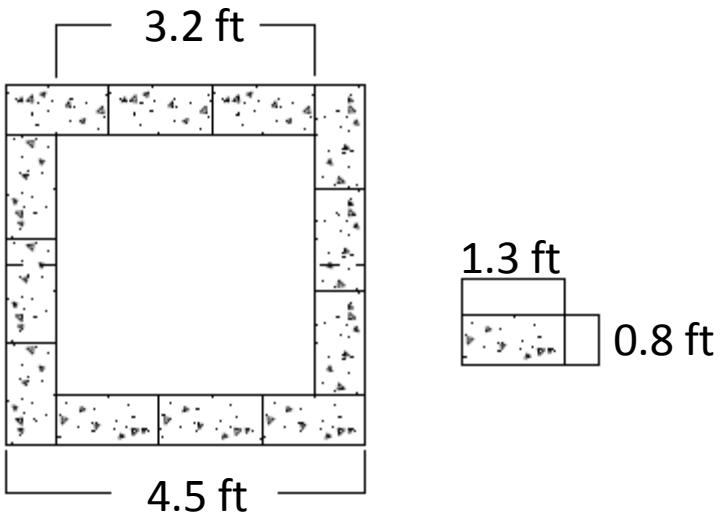

Figure 6. Illustration. Plan view of Defiance County experiment.

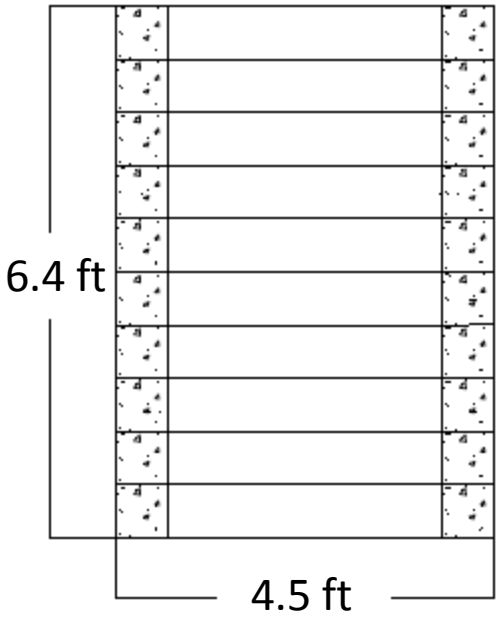

Figure 7. Illustration. Elevation view of Defiance County (DC) test.

1.3 INTERNAL STABILITY DESIGN

The results of the PT are primarily used in the design of GRS abutments.[1] The resulting stress-strain curve can be used to describe the strength limit state for capacity and the service limit state for deformation (vertical and lateral) due to an applied load. It is the only method currently available to describe both the capacity and deformation behavior of GRS for load bearing applications; American Association of State Highway and Transportation Officials (AASHTO) (2012) does not provide any guidance for these GRS limit states.[10]

In addition to the empirically based design using PT results, a semi-empirical method is also presented by FHWA for internal stability design of GRS abutments and integrated bridge systems, based on basic soil mechanics principles for the relationship between vertical and lateral stress but is fit to the available data at the time.[1] The ultimate capacity is determined according to the equation presented in figure 8.[11] Note that in design, the effect of confining stress (due to the facing element) and cohesion is ignored, which for a CMU facing and the select granular fill specified for GRS abutments is an appropriate assumption.[5]

$$q_{ult,an,c} = \left[\sigma_c + W\left(\frac{T_f}{S_v}\right)\right] K_{pr} + 2c\sqrt{K_{pr}}$$

Figure 8. Equation. Ultimate vertical capacity for a GRS composite.

Where $q_{ult,an,c}$ is the ultimate capacity using semi-empirical theory, σ_c is the external confining stress due to the facing, W is a factor accounting for the effect of reinforcement spacing and aggregate size (figure 9), T_f is the minimum average roll value (MARV) for wide width tensile strength of the geosynthetic, K_{pr} is the coefficient of passive earth pressure for the backfill, and c is the cohesion of the backfill.

$$W = 0.7^{\left(\frac{S_v}{6d_{max}}\right)}$$

Figure 9. Equation. W factor.

Where S_v is the reinforcement spacing and d_{max} is the maximum aggregate size. The constant of 0.7 in the W-factor is the ratio of average force in the reinforcement to the maximum force in the reinforcement and the $6d_{max}$ term is an approximation of the minimum distance between reinforcement layers where the grain size of the soil will not significantly impact the composite behavior of the GRS.[12]

A variant of figure 8 is also used to determine the required reinforcement strength at a given applied stress (figure 10). The method provides engineers with the minimum strength of reinforcement needed to prevent failure of the GRS composite at that given applied stress. Note that figure 10 will not represent the actual load on the reinforcement at working stress once increased reinforcement strengths are used in the field since this will change the conditions. The actual load on the reinforcement is difficult to estimate; instead, the service limit for the reinforcement is based on limiting reinforcement strain to 2 percent.[1]

$$T_{req,c} = \left[\frac{\sigma_h - \sigma_C - 2c\sqrt{K_{ar}}}{W}\right] S_v$$

Figure 10. Equation. Required reinforcement strength.

Where $T_{req,c}$ is the required reinforcement strength in the direction perpendicular to the wall face, σ_h is the total lateral stress within the GRS composite at a given depth and location, σ_c is the external confining stress due to the facing, c is the cohesion of the reinforced backfill, K_{ar} is the coefficient of active earth pressure for the backfill, W is a factor accounting for the effect of

reinforcement spacing and aggregate size (figure 9), and S_v is the reinforcement spacing. As with the ultimate capacity equation, the effect of confining stress (due to the facing element) and cohesion is ignored when determining the required reinforcement strength in the design of GRS abutments, leading to added conservatism in the design method.[5]

The soil-geosynthetic composite capacity equation (figure 8) and the required reinforcement strength equation (figure 10) have been previously validated against the results of 16 different types of tests, including previous performance tests (figure 12 and figure 13, respectively). The research study presented in this report will add to this database to further quantify the predictive capability of these equations.

Note that the predictions for capacity and required reinforcement strength used the estimated confining stress calculated according to figure 11, and the measured cohesion from soil testing, both of which would be ignored in design. In addition, the minimum average roll value (MARV) for the reinforcement, which is a property value calculated as the average strength for a roll less two standard deviations, was used to calibrate the predictive equations since the actual strength of the reinforcement for each test was not measured or precisely known, and the MARV is an industry value common for all geosynthetics specified in practice.

$$\sigma_c = \gamma_b d \tan\delta$$

Figure 11. Equation. Confining stress.[11]

Where γ_b is the bulk unit weight of the facing block, d is the depth of the facing block unit perpendicular to the wall face, and δ is the interface friction angle between the geosynthetic and the facing element for a frictionally connected GRS composite.

Note that the friction angle and cohesion terms used to calculate the earth pressure coefficients and lateral stress within the ultimate capacity (figure 8) and required reinforcement strength (figure 10) equations were measured using a large scale direct shear (LSDS) test on the backfill alone according to ASTM D3080.[13] The peak strength of the reinforced backfill material was selected as it is a commonly reported value and easiest to ascertain from typical testing. More details are provided in section 2.1.3.

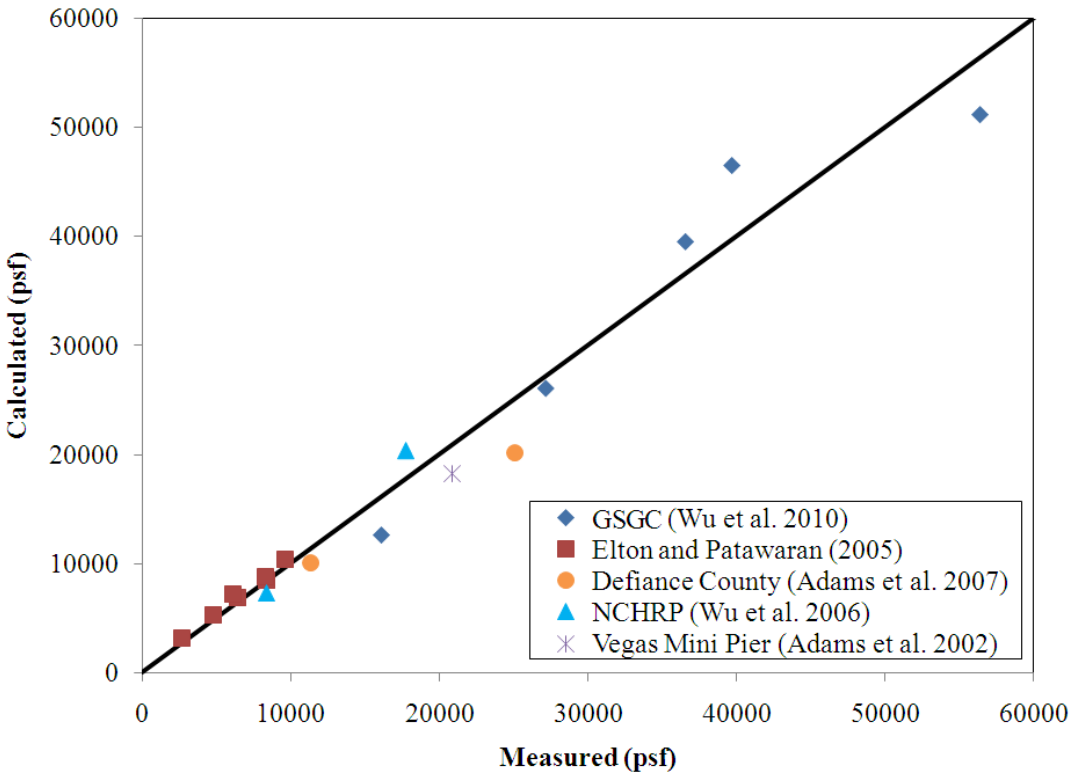

Figure 12. Graph. Predictive capability of the soil-geosynthetic composite capacity equation.[(5)]

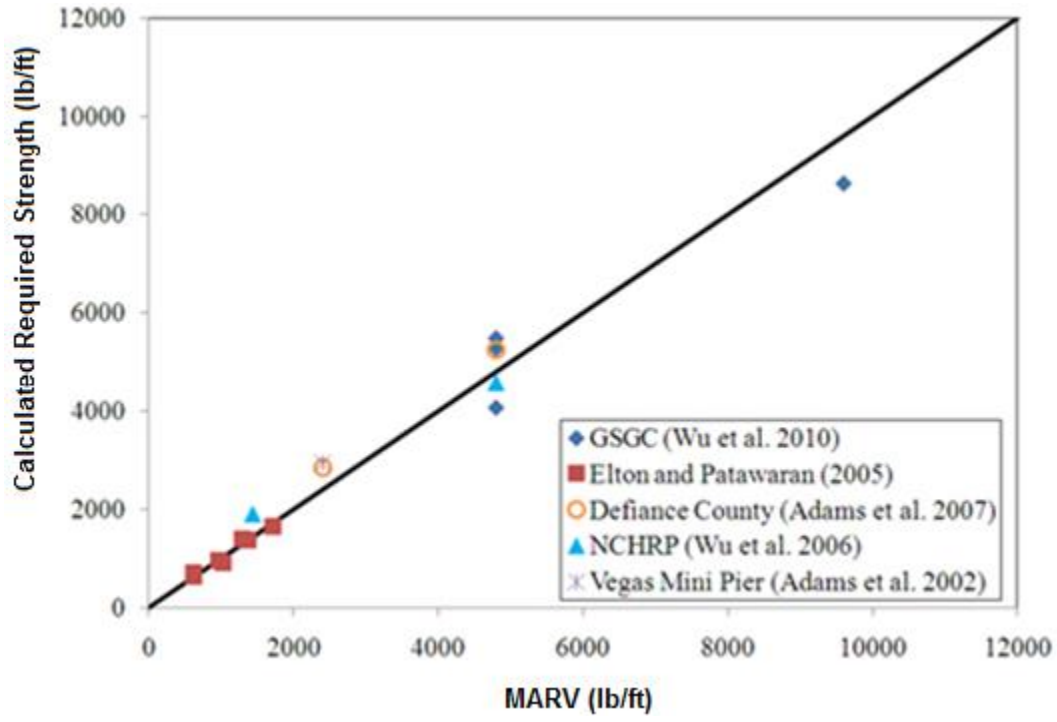

Figure 13. Graph. Predictive capability of the required reinforcement strength equation.[(5)]

1.4 OBJECTIVES

The results of the PT parametric study will be used for several purposes. The primary objectives of this research report are to: (1) build a database of GRS material properties that can be used by designers or for Load and Resistance Factor Design (LRFD) calibration; (2) evaluate the relationship between reinforcement strength and spacing; (3) quantify the contribution of the frictionally connected facing elements at the service limit and strength limit states; (4) assess the new internal stability design method proposed by Adams et al. 2011a for GRS; and (5) perform a reliability analysis of the proposed soil-geosynthetic capacity equation for LRFD.[1,11] When combining additional measurement techniques (e.g., contact pressure cells, earth pressure cells, etc.), other uses for the PT are possible, such as to study thrust against the face as a function of spacing; however, this is outside the scope of this report.

2. TESTING CONDITIONS

A series of 19 performance tests have been conducted (table 1); 5 at the Defiance County, OH, highway maintenance facility and 14 at the TFHRC.

Table 1. Summary of PT conditions.

Test No.	Backfill				Reinforcement			Facing
	Type	ϕ (°)	c (psf)	d_{max} (inch)	T_f^ (lb/ft)	S_v (inch)	T_f/S_v (lb/ft^2)	
DC-1	8	54	0	½	4,800	7⅝**	7,600	CMU
DC-2	8P*	46	0	¾	4,800	7⅝**	7,600	CMU
DC-3	57	52	0	1	4,800	7⅝**	7,600	CMU
DC-4	9	49	0	⅜	4,800	7⅝**	7,600	CMU
DC-5	8***	54	0	½	4,800	7⅝**	7,600	CMU
TF-1++	8	55	0	½	2,400	7⅝	3,800	CMU
TF-2	21A	53	115	1	2,400	7⅝	3,800	CMU
TF-3	21A	53	115	1	2,400	7⅝	3,800	no CMU
TF-4+	21A	53	115	1	4,800	7⅝	7,600	no CMU
TF-5++	21A	53	115	1	4,800	7⅝	7,600	no CMU
TF-6++	21A	53	115	1	4,800	7⅝	7,600	CMU
TF-7	21A	53	115	1	4,800	7⅝	7,600	no CMU
TF-8	21A	53	115	1	4,800	7⅝**	7,600	no CMU
TF-9	21A	53	115	1	4,800	15¼	3,800	CMU
TF-10	21A	53	115	1	4,800	15¼	3,800	no CMU
TF-11	21A	53	115	1	1,400	$3^{13}/_{16}$	4,400	no CMU
TF-12	21A	53	115	1	1,400	$3^{13}/_{16}$	4,400	CMU
TF-13	21A	53	115	1	3,600	11¼	3,800	no CMU
TF-14	21A	53	115	1	3,600	11¼	3,800	CMU

ϕ = the peak friction angle, c = the cohesion at peak strength, d_{max} = the maximum aggregate size, T_f = the ultimate reinforcement strength, expressed as the minimum average roll value (MARV) from ASTM D4595 testing,[1] and S_v = the reinforcement spacing.

^ MARV value.

*Rounded pea-gravel angularity.

**Two courses of bearing bed reinforcement placed at the top of the PT.

***Uncompacted sample, +technical difficulties required termination during testing.

++Technical difficulties resulted in unloading/reloading of the composite.

2.1 BACKFILL CONDITIONS

In total, six unique backfill types were used in the PTs: (1) an AASHTO No. 8 crushed, manufactured limestone aggregate obtained from Defiance County OH, (2) an AASHTO No. 8 rounded quartz pea gravel (PG) obtained from Defiance County, OH, (3) an AASHTO No. 57 crushed, manufactured limestone aggregate obtained from Defiance County, OH, (4) an AASHTO No. 9 crushed, manufactured limestone aggregate obtained from Defiance County,

OH, (5) an AASHTO No. 8 crushed, manufactured diabase aggregate obtained from Loudon County, VA, and (6) an AASHTO A-1-a aggregate obtained from Loudon County, VA (also referred to locally as a Virginia DOT, or VDOT, 21A material).

2.1.1 Sieve Analysis

All backfills used for testing, except for the AASHTO No. 9 aggregates, meet the FHWA specifications for use in bridge abutments.[1] The gradations of each aggregate are shown in table 2 and figure 14.

Table 2. PT reinforced backfill gradations.

Sieve No.	Percent Passing					
	No. 8 (OH)	**No. 8 PG (OH)**	**No. 57 (OH)**	**No. 9 (OH)**	**No. 8 (VA)**	**A-1-a (VDOT 21A)**
1.5			100.00		100.00	100.00
1			100.00		100.00	100.00
0.75	100.00	100.00	87.91			
0.50	100.00	99.57	35.69		99.69	82.41
0.375	96.99	95.58	14.13	100.00	69.86	71.36
4	26.50	14.60	3.67	94.22	7.78	48.52
8	4.63	6.98	2.41	27.75	1.66	35.24
10					1.39	32.81
16	1.85	4.34	1.47	8.90	1.11	25.40
40					0.93	16.66
50	0.91	2.64		3.66	0.88	
100	0.76			3.22		
200	0.65		0.71	2.82		6.47

Blank cell = no value was measured for that particular sieve number.

Most of the backfills tested are open or poorly graded materials (e.g., AASHTO Nos. 57, 8, and 9); however, the A-1-a material is a well-graded material. Table 3 shows the classification (based on the USCS) along with the maximum aggregate size (d_{max}), other relevant grain sizes for various percent passing values, and the coefficient of curvature (Cc) and coefficient of uniformity (Cu) for each material tested.

Table 3. PT backfill gradation properties.

Aggregate Type	USCS Classification	d_{max} (inch)	D_{85} (inch)	D_{60} (inch)	D_{30} (inch)	D_{10} (inch)	Cc	Cu
8 (OH)	GP	0.50	0.34	0.28	0.20	0.12	1.19	2.36
8 PG (OH)	GP	0.75	0.35	0.29	0.22	0.13	1.30	2.23
57 (OH)	GP	1.00	0.74	0.62	0.47	0.30	1.18	2.05
9 (OH)	SP	0.38	0.17	0.14	0.47	0.05	1.35	2.78
8 (VA)	GP	1.00	0.44	0.35	0.25	0.19	0.96	1.78
A-1-a (VDOT 21A)	GW-GM	1.00	0.57	0.28	0.07	0.01	2.67	46.67

d_{max} = the maximum aggregate size.
D_{85} = the aggregate size in which 85 percent of the sample is finer.
D_{60} = the aggregate size in which 60 percent of the sample is finer.
D_{30} = the aggregate size in which 30 percent of the sample is finer.
D_{10} = the aggregate size in which 10 percent of the sample is finer.
Cc = the coefficient of curvature.
Cu = the coefficient of uniformity.

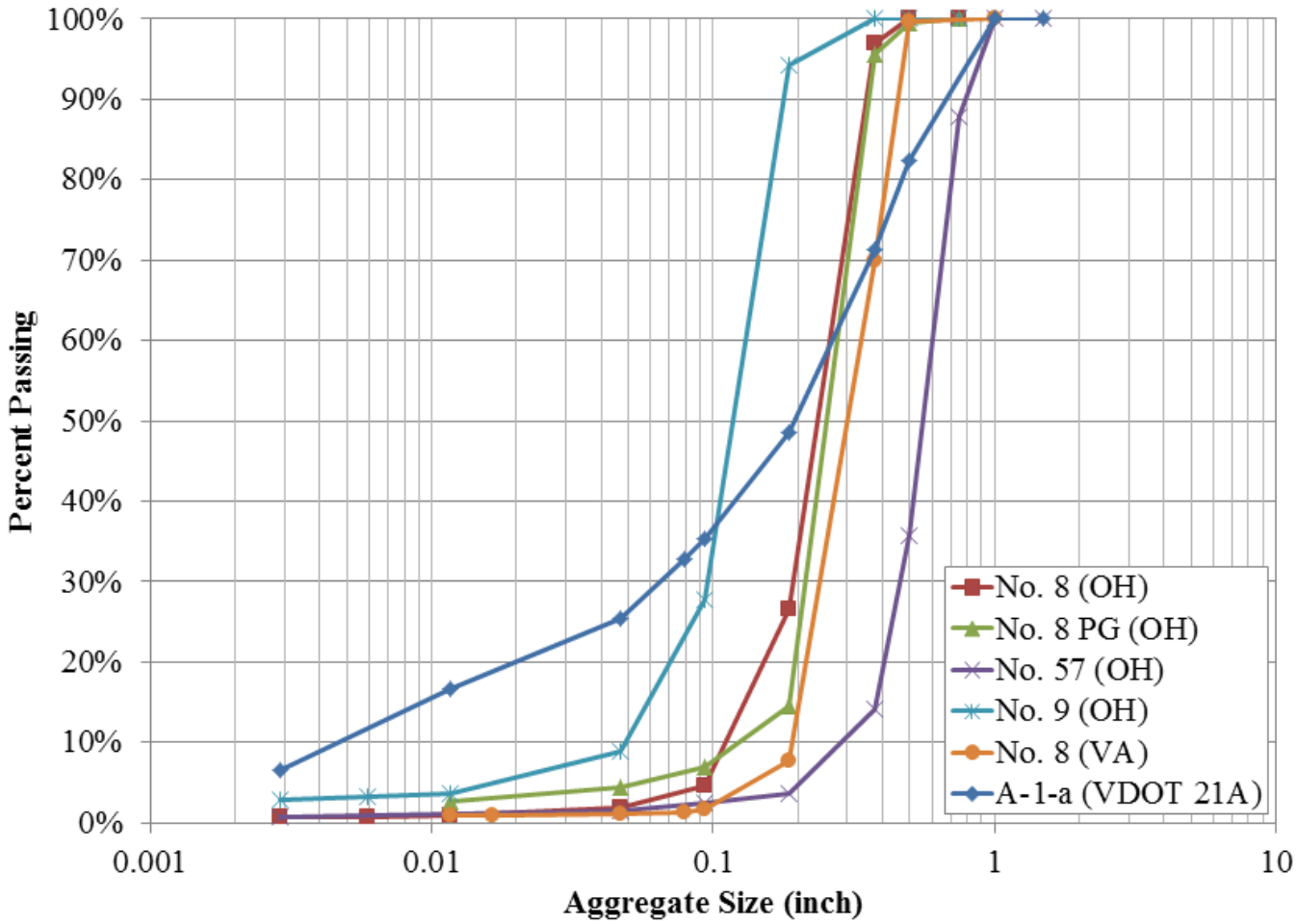

Figure 14. Graph. Reinforced backfill gradations.

2.1.2 Density

To determine the in-place compaction requirements of the backfill material, a standard Proctor test was conducted according to Method D of AASHTO T99 for the AASHTO A-1-a (VDOT 21A) material.[15] In addition, vibratory tests were conducted according to ASTM D4252 for the open-graded materials to determine the maximum dry density.[16] The results are shown in table 4.

Table 4. Maximum dry density for PT aggregates.

Aggregate Type	Max Dry Density, γ_d (pcf)	Optimum Moisture Content, ω (percent)
8 (OH)	101.27	N/A
8 PG (OH)	115.75	N/A
57 (OH)	108.69	N/A
9 (OH)	110.66	N/A
8 (VA)	112.82	N/A
A-1-a (VDOT 21A)	148.90	7.7

N/A = Not applicable, there is no optimum moisture content for open-graded aggregates since they are free draining.

2.1.3 Friction Angle

The strength properties of each aggregate were determined using a large scale direct shear (LSDS) device according to ASTM D3080.[13] The LSDS device at TFHRC is 12 x 12 x 8 inches in dimension and is capable of testing aggregates up to 1.2 inches. For this series of experiments, the unscalped aggregates were tested at four applied normal stresses, 5, 10, 20, and 30 psi, at a shear rate of 0.015 inches/min and a gap size equal to the D_{85} of the material (i.e., the aggregate size where 85 percent of the sample is smaller; see table 3).

The open-graded materials were tested in a dry, uncompacted state prior to the consolidation phase in the LSDS device. The well-graded material (VDOT 21A) was tested at 100 percent of the maximum dry density (i.e., the level of compaction achieved during each PT with the backfill), and at the optimum moisture content (see table 4). Since the shear strength failure envelope for these aggregates is non-linear, the reported cohesion for the well-graded material (VDOT21A) was determined through a series of LSDS tests that were performed with the compacted state fully saturated; note that the resulting peak friction angle in this case was similar to the non-saturated condition.

The results of the LSDS testing are shown in table 5 and in figure 15. Note that the reported friction angle is based on the measured peak strength during testing and assumes a linear Mohr-Coulomb envelope for the range of confining stresses tested. Note that peak strength for these backfill materials is mobilized at typically 0.5- to 1-inch lateral displacement in the LSDS device, which corresponds to about 4- to 8-percent lateral strain for the 12-inch shear box. In the context of the PT though, the GRS composite is tested to failure, sometimes well beyond 8-percent lateral strain. From a theoretical perspective, it may be more appropriate to model the

failure of a GRS composite by using the friction angle at the fully softened state of the backfill material during the LSDS test; however, to conform to the current standard-of-practice, the peak strength of the reinforced backfill material was selected to calibrate the design as it is the commonly reported value and easiest to ascertain from typical testing. Figure 15 provides the raw data for LSDS testing.

Table 5. LSDS testing results.

Aggregate Type	Friction Angle (°)	Cohesion (psf)
8 (OH)	54	0
8 PG (OH)	46	0
57 (OH)	52	0
9 (OH)	53	0
8 (VA)	55	0
A-1-a (VDOT 21A)	54	115

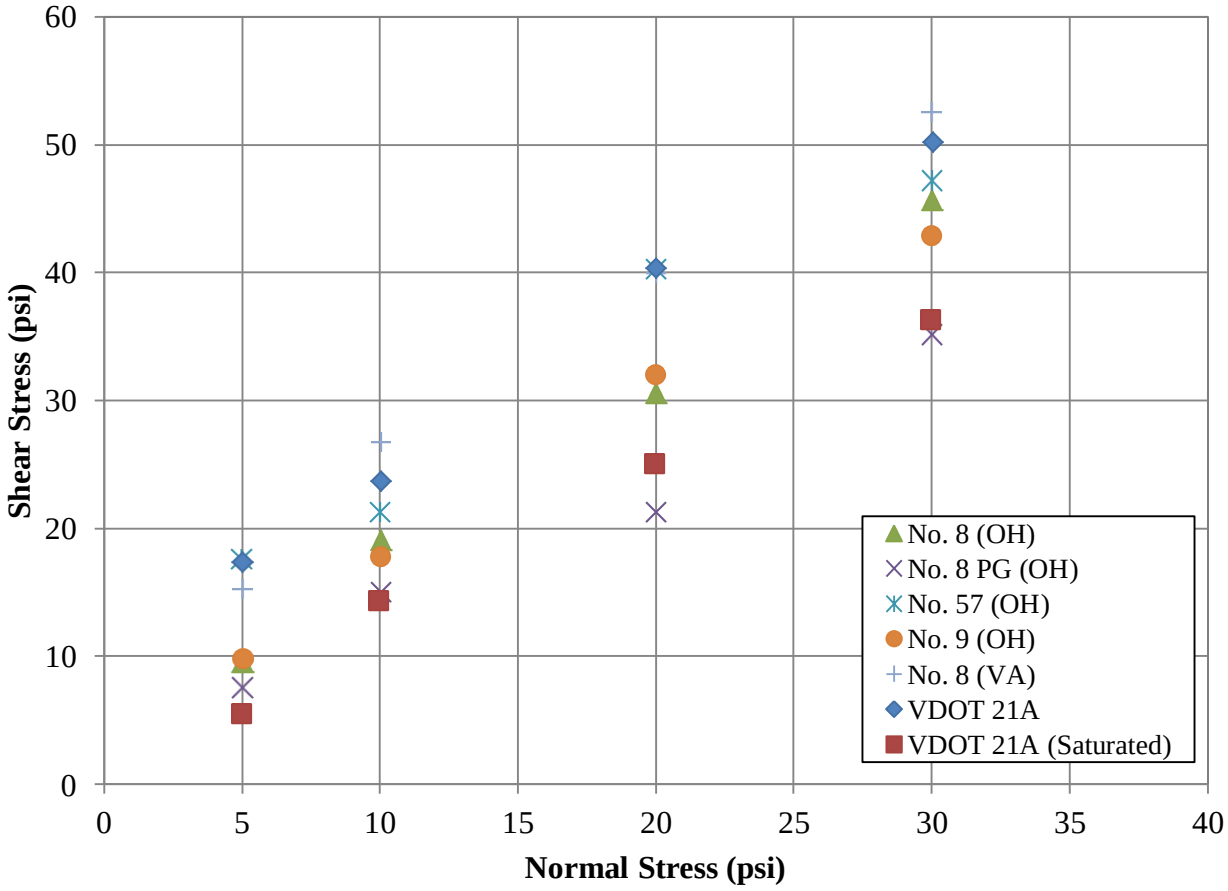

Figure 15. Graph. LSDS testing results.

2.2 REINFORCEMENT CONDITIONS

In all of the tests, a biaxial, woven polypropylene geotextile was used as the reinforcement element; however, different strengths and stiffness of material were used among the PTs. The manufacturer supplied MARV data is shown in table 6. A more recent property of the geosynthetic used in design is the wide width tensile strength at 2-percent strain which provides an indication of GRS performance at the service limit state.[1] Currently, many of the manufacturers do not make this value publicly available, although they can supply it on request. Note that in the field, the actual strength of the reinforcement will be higher than the reported MARV.

Table 6. Geosynthetic reinforcement properties.

	PTs:	TF-11, TF-12	TF-1, TF-2, TF-3	TF-13, TF-14	DC-1, DC-2, DC-3, DC-4, DC-5, TF-4, TF-5, TF-6, TF-7, TF-8, TF-9, TF-10
	Reference:	(17)	(18)	(19)	(18)
Property	**Test Method**	**Minimum Average Roll Value (MARV)[1]**			
Tensile Strength (Grab)	ASTM D4632[20]	200 x 200 lb	315 x 300 lb	450 x 350 lb	600 x 500 lb
Wide Width Tensile	ASTM D4595[14]	1,400 x 1,400 lb/ft	2,400 x 2,400 lb/ft	3,600 x 3,600 lb/ft	4,800 x 4,800 lb/ft
Wide Width Elongation	ASTM D4595[14]	9 x 7 percent	10 x 8 percent	15 x 10 percent	10 x 8 percent
Wide Width Tensile Strength at 5 Percent Strain	ASTM D4595[14]	Not specified	884 x 1,564 lb/ft	1,392 x 1,740 lb/ft	660 x 1,500 lb/ft

[1]Values for the machine (warp) by cross machine (fill) directions, respectively.

2.3 FACING CONDITIONS

A concrete masonry unit (CMU) facing was used on 11 of the 17 tests; the remaining 6 tests were conducted without any facing element. The CMU is a dry-cast, split-faced product with dimensions of 7⅝ x 7⅝ x 15⅝ inches and an approximate weight of 42 lb. The CMUs are frictionally connected to the geotextile reinforcement. The reinforcement overlaps at least 85 percent of the block depth, termed the coverage ratio, as specified by Adams et al. 2011a.[1]

3. TEST SETUP

3.1 LAYOUT

The dimensions for each PT are given in table 7. For each test, the base to height ratio was kept constant at about 2 to mimic triaxial conditions. The height is equivalent to 10 courses of CMU block, while the outside dimensions of the PT with facing are 3.5 blocks wide. For each test, the total width of the PT with the CMU facing (B_{total}) is 54½ inches; the width of the GRS composite itself (B) is 39¼ inches. The footing width on top of the GRS composite (b) is 36 inches.

Table 7. PT dimensions.

Test No	No. Reinf. Layers	S_v (inch)	H (inch)	H/B
DC-1	9	7⅝**	76¼	1.9
DC-2	9	7⅝**	76¼	1.9
DC-3	9	7⅝**	76¼	1.9
DC-4	9	7⅝**	76¼	1.9
DC-5	9	7⅝**	76¼	1.9
TF-1	9	7⅝	76¼	1.9
TF-2	9	7⅝	76¼	1.9
TF-3	9	7⅝	76¼	1.9
TF-4	9	7⅝	76¼	1.9
TF-5	9	7⅝	76¼	1.9
TF-6	9	7⅝	76¼	1.9
TF-7	9	7⅝	76¼	1.9
TF-8	9	7⅝**	76¼	1.9
TF-9	4	15¼	76¼	1.9
TF-10	4	15¼	76¼	1.9
TF-11	19	$3^{13}/_{16}$	76¼	1.9
TF-12	19	$3^{13}/_{16}$	76¼	1.9
TF-13	6	11¼	78¾	2.0
TF-14	6	11¼	78¾	2.0

S_v = the reinforcement spacing, H = the height of the PT,
B = the width of the GRS composite (without the facing element).
**Two courses of bearing bed reinforcement placed at the top of the PT.

Figure 16. Photo. DC-1 GRS PT (before testing).

3.2 LOAD AND REACTION FRAME

The reaction frames were slightly different among the tests. The Defiance County PTs (DC-1 through DC-5) were built on a reinforced concrete base pad similar to the Vegas mini-pier setup (figure 3 and figure 4). The base pad was elevated on CMU blocks to make room for the bottom set of bolted channel beams, while the top set of bolted channels was supported on the top concrete pad which was centered on the GRS composite. The top load pad is supported on the GRS composite, inside the perimeter of the CMU facing; there is an inset of 1⅝ inches around the load pad and the back of the CMU facing (figure 17). The upper and lower channel beams were coupled together with high strength post-tensioning bar. Four hollow core hydraulic jacks were bolted to the top channel beams (figure 18). All jacks were connected to a manifold and controlled with an electric hydraulic pump controlled by a push button solenoid valve. The stroke and capacity of the hollow core jacks were 6 inches and 120 kips, respectively.

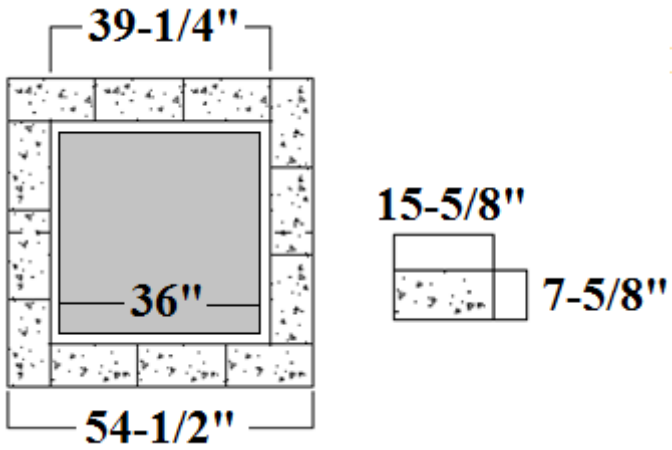

Figure 17. Illustration. Concrete footing on GRS composite, inset from facing.

Figure 18. Photo. Hollow core hydraulic jacks for PT assembly.

A similar reaction frame setup was used for the initial TFHRC PTs (figure 19), except the concrete strong floor was used for the reaction instead of sandwiching the GRS composite between twin sets of bolted channels (figure 4). The top sets of bolted channels were placed on an elastomeric pad and positioned on the top concrete pad to evenly distribute the load delivered from the hydraulic jacks; a 1-inch steel plate was also bolted to the top concrete pad to increase the rigidity of the concrete.

Figure 19. Photo. TF-1 PT setup with reaction frame.

The reaction frame was changed after eccentric loading was observed with the previous setup on the TF-4 test. Subsequent TF tests used a rigid two post frame that provided additional benefits in terms of easier setup and the ability to gang two high-capacity, 600-kips jacks to ensure sufficient stroke to fail any GRS composite without having to reset the loading beam position (figure 20, figure 21, and figure 22). A spherical bearing was used in the two-post frame assembly to maintain a vertical load on the top bearing pad (figure 23). Figure 23 also illustrates that the top concrete load pad was pushed approximately 18 inches into the GRS composite before failure was induced.

Figure 20. Photo. TF-6 PT setup with reaction frame.

Figure 21. Photo. TF-10 PT setup with reaction frame.

Figure 22. Photo. TF-9 at failure with reaction frame.

Figure 23. Photo. Spherical bearing to apply load to the footing on the GRS composite.

3.3 CONSTRUCTION

The method of construction for the mini piers was basically the same for all of the PTs; the GRS composite was built from the bottom up, one course of block at a time. The primary difference in construction between the Defiance County tests and the TFHRC tests was the level of quality control. The five Defiance County tests (DC-1 through DC-5) were each constructed with the same supervisor, but different crews, as part of the FHWA's EDC-GRS Validation Sessions in 2010. The quality control for these tests was therefore limited, which may have impacted the testing results, particularly the stiffness. The 14 PTs conducted at TFHRC were constructed in the Structures Laboratory and were research quality experiments, with consistent construction procedures and compaction control.

At the start of construction for each PT, the first course of block was placed level and centered within the position of the reaction assembly. Aggregate was then infilled using either a front-end loader (for the DC test series) or a concrete dump hopper (for the TF test series). For the TF tests, the squareness of the facing and the verticality of the composite were checked before placement of fill in each course of block by measuring the inside diagonal lengths and checking with a plumb bob on every other lift.

Compaction for the DC tests was performed using a standard 18-inch-wide, gas powered vibratory plate compactor at each lift of aggregate, a nominal 8-inch thickness (height of the CMU block). For the TF tests, it was necessary to compact each 8-inch lift of fill in half layer increments, or at a lift thickness of about 4 inches because a lightweight electric vibratory plate compactor was used for construction; with this equipment, it was impossible to achieve the target

density at the nominal 8-inch lifts. The electric compactor had a 10-square-inch plate, with a weight of 48 lb and an adjustable impact force of 700 lb.

For the well-graded AASHTO A-1-a (VDOT 21A) aggregate, compaction control consisted of testing each nominal 4-inch lift (half the height of a CMU) with a nuclear density gauge to ensure the target density and moisture content (± 2 percent) were met throughout the height of the GRS composite. In the field, density tests are typically performed after the compaction of fill material to the height of CMU block; however, during construction of the TF PTs using well-graded backfill, density testing was performed on nominal 4-inch lifts to test the compaction effort of the lightweight (48 lb) tamper used. For each lift, approximately 100 percent of the standard Proctor value was achieved; the results of the nuclear density gauge for each test are shown in appendix B.

For the open-graded aggregates, compaction was performed until no further compression of the aggregate was observed, which consisted of running the plate compactor across each lift with a minimum of four passes. While it is not common practice to test open-graded aggregates with a nuclear density gauge, backscatter tests were performed on each nominal 4-inch lift for PT TF-1 to collect the surficial density value (appendix B). The percent compaction is based on the maximum index density determined from ASTM D4253 (table 4).[16]

Rodding with a shovel end was also used for each PT to compact the aggregate at the corners and edges of the facing. Once final compaction was achieved to the leveled height of the facing block and before placement of the next course of CMU blocks, any remaining aggregate was brushed off of the facing block so that a smooth surface existed to prevent point loading and ensure even placement of the next layer of block. Depending on the reinforcement schedule, a layer of geotextile reinforcement was then placed over the aggregate with a facing element coverage ratio of at least 85 percent the width of facing element. While the geotextiles used in each test were biaxial, the stiffness in the machine (warp) and cross-machine (fill) directions for the reinforcement was different (table 6). For this reason, the reinforcement was placed in an alternating pattern with each subsequent layer to prevent preferential failure of the PT in the weaker reinforcement direction.

To facilitate construction, two sets of ratchet straps were placed around the facing blocks to secure and maintain block alignment during compaction. During each layer of GRS construction, the lower strap was removed and then used to band the new, upper course of block; the process was repeated until the pier was completed. This process was employed because of the geometry and the reduced footprint of the PT where lateral block movement during compaction is increased compared to a typical in-service bridge abutment (plane strain condition). The ratchet strap on the top course of block was removed after specimen construction was fully completed, prior to loading.

Once the fabric was placed, the next layer of CMU blocks were positioned and the aggregate infilled. This process was repeated for 10 courses of CMU blocks. The concrete footing was then placed on top of the GRS composite and the load frame assembled for testing. Construction of the open-graded aggregate tests took about 4 hours, and 20 hours for the DC tests and TF tests, respectively. The principal difference in time was attributable to the need for compaction in

4-inch lifts, the requirement for nuclear density testing, and the level of quality control. Construction of the well-graded aggregate tests at TF took approximately 30 hours.

3.4 INSTRUMENTATION

Each PT was instrumented to measure the response to the static, vertical applied pressure on the top of the GRS composite. Vertical and lateral deformation was constantly monitored with displacement transducers. Four transducers measured the vertical displacement at the middle of each loading block edge while five transducers measured the horizontal displacement along one face of the specimen (figure 24). For the five PTs conducted in Defiance County, OH, (DC-1 through DC-5) and the first PT conducted at TFHRC (TF-1), linear voltage displacement transducers (LVDT) were used.

String potentiometers (POT) replaced the LVDTs for the remaining tests at TFHRC with CMU blocks (TF-2, TF-6, TF-9, TF-12, TF-14) to measure both vertical and lateral deformation. For the PTs without any facing element (TF-3, TF-4, TF-5, TF-7, TF-8, TF-10, TF-11, TF-13), LVDTs were still used to measure lateral deformation in addition to the string POTs used to measure vertical deformation. The instrumentation layouts for deformation measurements in each test, similar to that shown in figure 24, are presented in appendix C. With the TFHRC PT series, additional instrumentation was included to monitor vertical pressure near the base of the composite, strain on different geotextile layers, and lateral earth pressure behind the face just above the center height of the composite (figure 25). This report focuses on the vertical deformation data, which can be immediately used in the design of GRS composites for load bearing applications.[1]

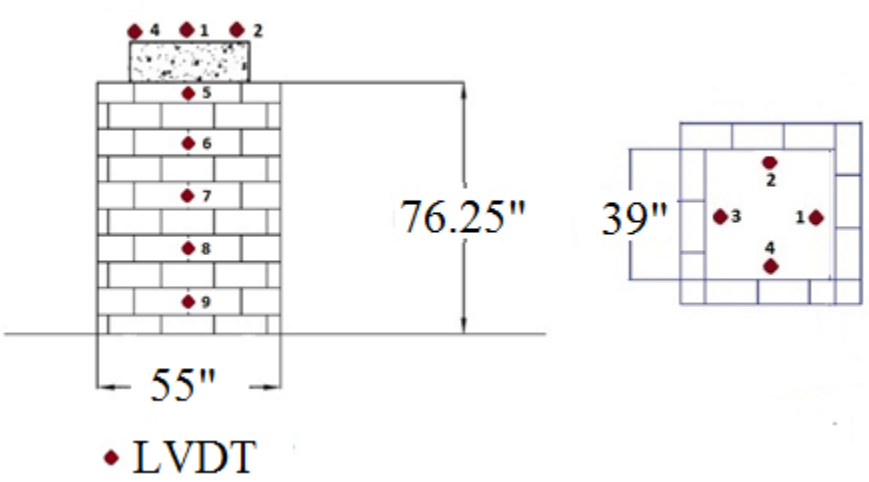

Figure 24. Illustration. Instrumentation layout for DC tests and TF-1.

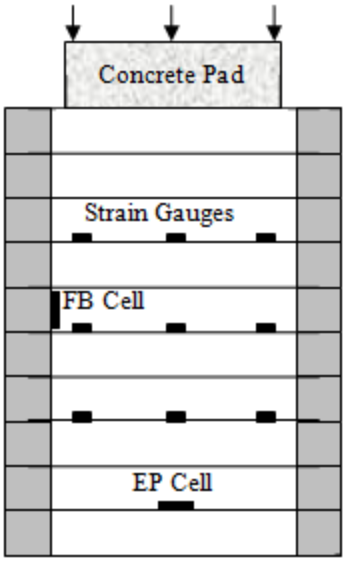

Figure 25. Illustration. General additional instrumentation layout TF PT series.

3.5 LOAD SCHEDULE AND COLLECTION OF DATA

For each TFHRC test, the loading schedule was prepared in the same manner. The basic protocol included estimating the ultimate vertical capacity determined from the semi-empirical equation (figure 8). The estimated capacity was then divided into a minimum of ten load increments to capture the deformation characteristics of each test. In addition, between two and four load increments below the 4,000 psf service limit were included in each test to better define the behavior of the composite at low applied loads.

Each load increment was applied manually using an electric hydraulic pump with a push button controlled solenoid valve. Load was maintained with a strain indicator box calibrated to a load cell placed within the reaction assembly. Hydraulic jack pressure was also checked at each load increment to ensure operation of the system throughout the course of the load test. In each experiment, load was increased, from increment to increment, only when there was no significant change (< 0.003 inch) in settlement between any two time intervals; however, the load increment was held for a minimum of 5 minutes and a maximum of 30 minutes. The data acquisition system was programmed to record settlement at 1-, 3-, 5-, 7-, 15-, 20-, 25-, and 30-minute intervals from the start of each load increment.

The settlement of the top footing, lateral displacement of the face, and geotextile strain were recorded every minute within each load increment. Any vertical earth pressure measurements and lateral stress information were collected at the end of each load increment. Photographs were also taken at the conclusion of each load increment to visually document the test. Typically, each test took about 6 hours to complete.

4. RESULTS DATABASE

The results for each test are presented in table 8. The corresponding vertical stress-strain curves are shown in figure 26 and figure 27 for the Defiance County tests (labeled DC) and the TFHRC tests (labeled TF), respectively. The tabular data for each stress-strain curve shown in figure 26 and figure 27 is given in appendix D. Note that the applied stress and strain are calculated as averages of the measured values (over the period of loading for stress and over the four LVDT/POTs located on the footing for strain at the end of each load increment).

Table 8. PT measured results summary.

	Maximum Tested		Strength Limit	Design Limit		Service Limit
Test No.	**q_{max} (psf)**	**ε_{max} (%)**	**$q_{ult,emp}$ (psf)**	**$q_{@\varepsilon=5\%}$ (psf)**	**$V_{allow,emp} = q_{@\varepsilon=5\%}/3.5$ (psf)**	**$q_{@\varepsilon=0.5\%}$ (psf)**
DC-1	23,310	7.95	23,310	19,983	5,709	3,065
DC-2	22,709	7.07	22,709	19,399	5,543	2,171
DC-3	18,447	5.82	N/A	16,182	4,623	1,324
DC-4	26,730	7.64	N/A	17,350	4,957	2,212
DC-5	21,539	10.42	21,539	11,761	3,360	316
TF-1	20,487	10.9	20,487	13,409	3,831	2,075
TF-2	25,260	11.46	25,260	18,711	5,346	4,759
TF-3	17,491	13.8	17,491	12,120	3,463	3,417
TF-4	14,240	4.4	N/A	N/A[1]	N/A[1]	3,705
TF-5	25,920	17.9	25,920	15,581	4,452	1,815
TF-6	43,828	15.7	43,828	22,007	6,288	3,704
TF-7	26,546	12.5	26,546	13,684	3,910	2,224
TF-8	29,134	17.8	29,134	13,797	3,942	1,753
TF-9	22,310	15.6	22,310	13,527	3,865	2,955
TF-10	10,330	14.27	10,330	7,374	2,107	1,586
TF-11	23,249	12.79	23,249	13,316	3,805	2,839
TF-12	29,030	13.37	29,030	18,573	5,307	4,028
TF-13	12,960	12.32	12,960	8,641	2,469	2,398
TF-14	23,562	12.69	23,562	16,748	4,785	2,037

q_{max} = the maximum applied pressure during testing, ε_{max} = the maximum recorded vertical strain, $q_{ult,emp}$ is the measured failure pressure, $q_{@\varepsilon=5\%}$ = the applied stress at 5 percent vertical strain, $V_{allow,emp}$ is the total allowable pressure on the GRS,(1) $q_{@\varepsilon=0.5\%}$ = the applied stress at 0.5 percent vertical strain.

N/A = Not applicable, did not fail composite. N/A[1] = Not applicable, composite did not reach 5-percent vertical strain before it was terminated.

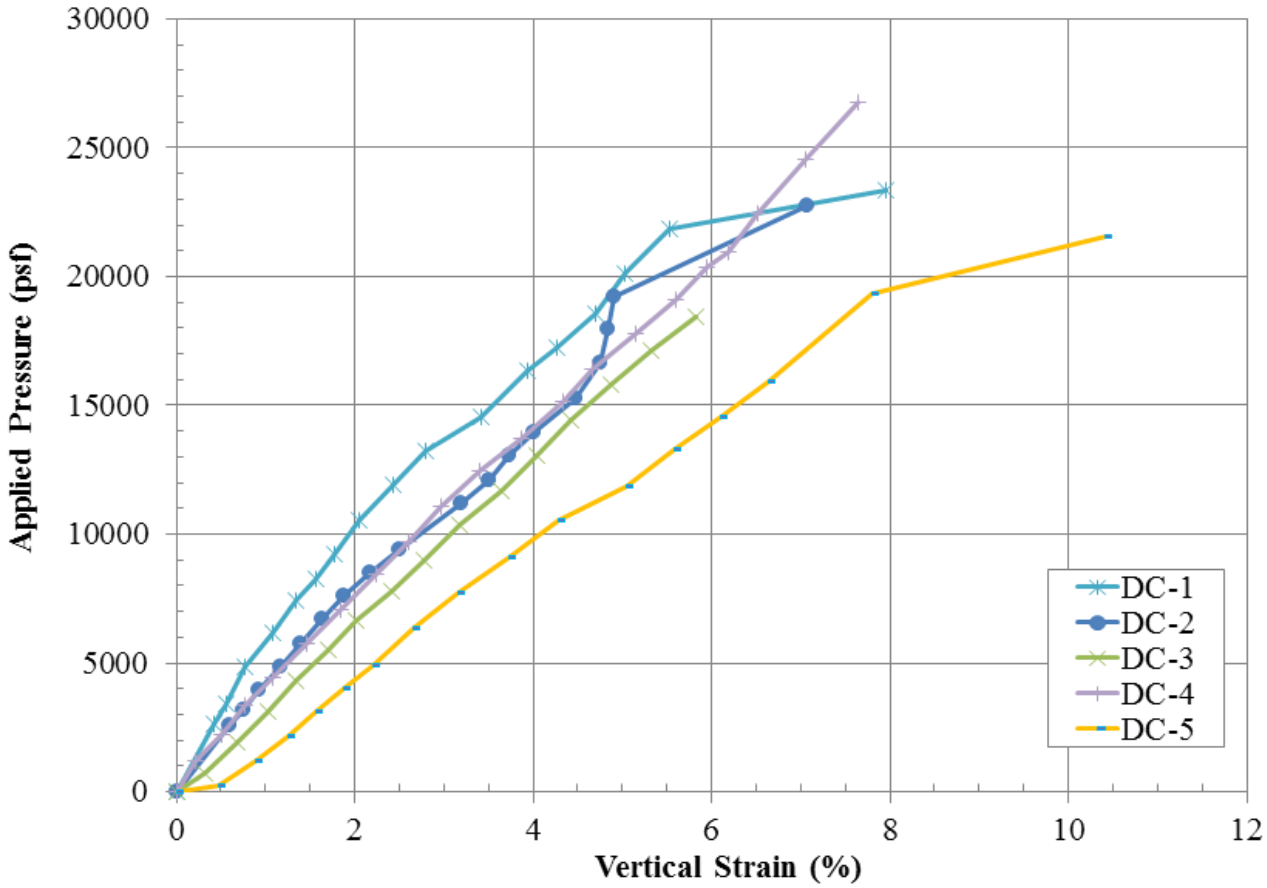

Figure 26. Graph. Load-deformation behavior for the Defiance County PTs.

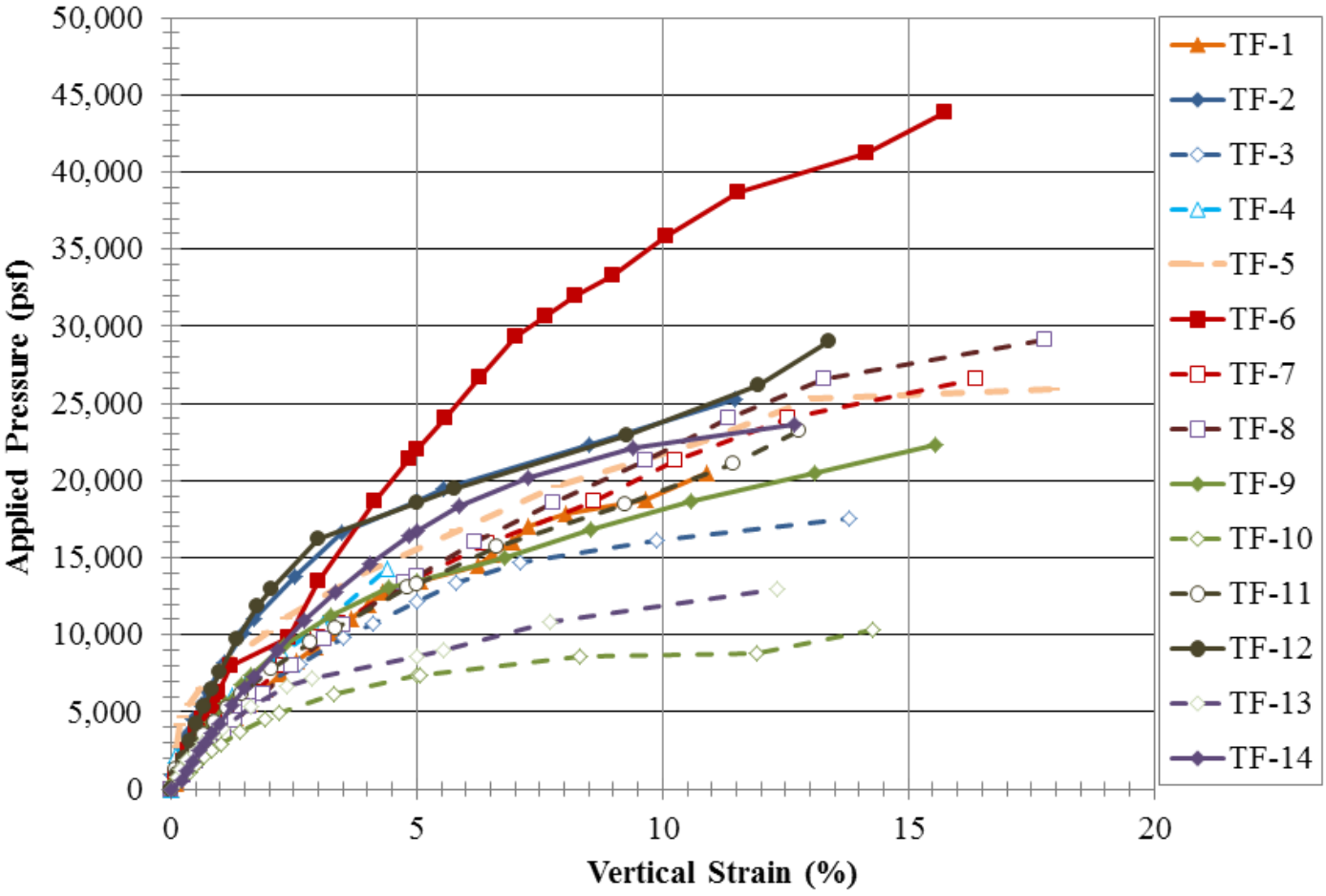

Figure 27. Graph. Load-deformation behavior for the Turner Fairbank PTs.

Note that two Defiance County (DC-3 and DC-4) and one TFHRC test (TF-4) were prematurely terminated before failure of the GRS composite. For the DC tests, the 6-inch stroke of the hydraulic jacks limited the amount of deformation that could be applied to the samples without resetting the experiment, which did not occur. For the TF test, the applied load on TF-4 was not uniform, leading to tilting of the footing (figure 28). Analysis of the data shows this to be the case.

Figure 28. Photo. Tilting of the footing during TF-4 testing.

The TF-4 data plotted on the family of load test curves shown in figure 27 is the average measured settlement from the four string POTs located on each side of the top of the footing. Figure 29 shows the settlement data for each POT, along with the average, for the TF-4 test. As indicated visually (figure 28), the measurements (figure 29) confirm that the footing titled towards sides 3 and 4 of the footing. Figure 28 also illustrates the composite behavior of GRS (i.e., the soil and geosynthetic tend to move together as one material).

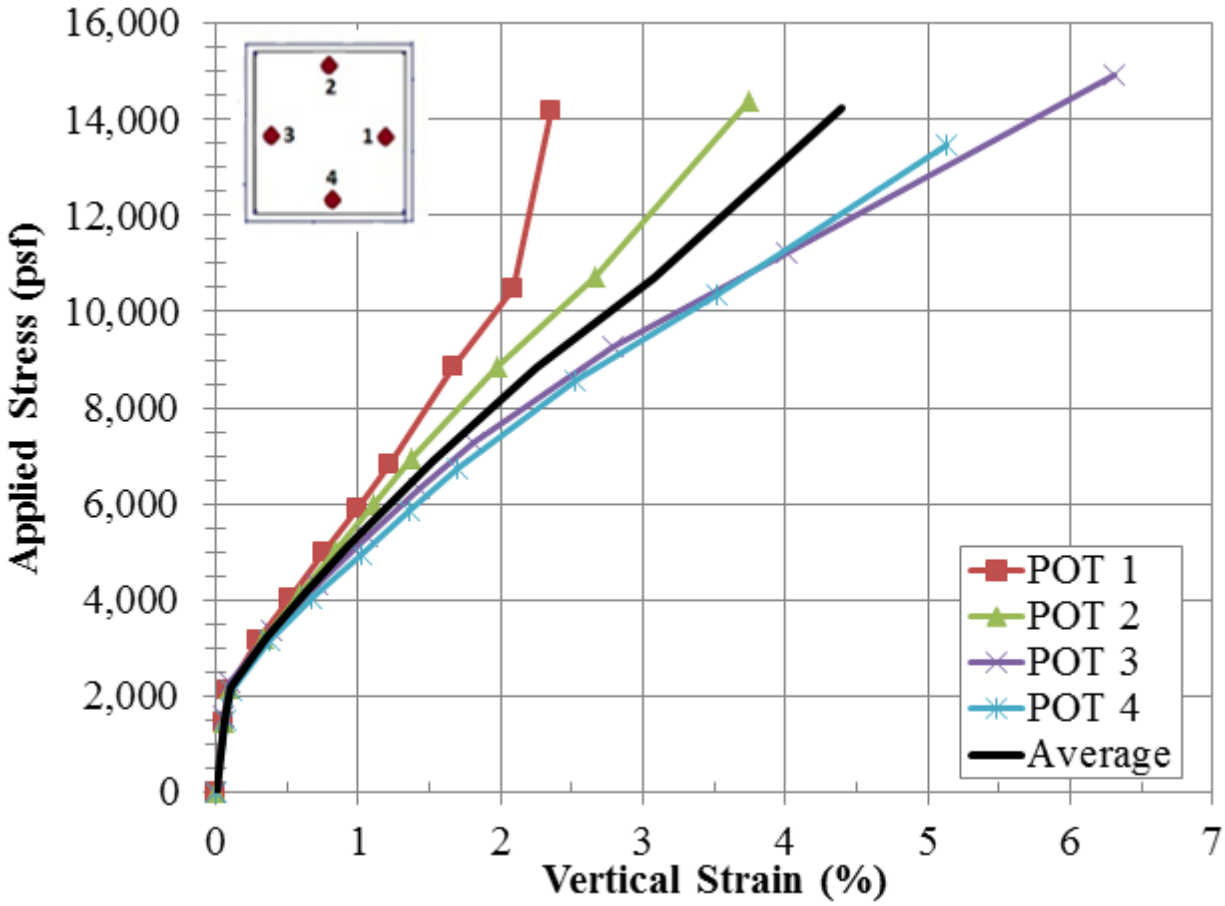

Figure 29. Graph. TF-4 results.

4.1 UNLOAD/RELOAD BEHAVIOR

TF-1, TF-5 and TF-6 experienced technical difficulties during testing that resulted in an unloading/reloading of the composite (figure 30, figure 31 and figure 32, respectively). The load test curves shown in figure 27 were corrected to omit the unload/reload cycles.

Due to a power outage at TFHRC during testing for TF-1 (figure 30), the GRS composite was unloaded for a period of over 40 hours (1.7 days); the maximum applied stress prior to unloading of the composite was 12,761 psf. After reestablishing power, the sample was then reloaded with the approximate same loading schedule as the initial load until failure of the composite was reached at 20,487 psf. The initial ratio of stress to strain (E_o) is equal to approximately 320 ksf, while the reload response was considerably stiffer by a factor of over 6, with a reload ratio of stress to strain (E_R) around 2,070 ksf.

For TF-5 (figure 31), the GRS composite was initially loaded and reloaded twice at low applied loads (less than 4,700 psf). The string potentiometers were reset in each case. An additional unloaded cycle then occurred for a period of 12 minutes 50 seconds in order to reset the single hollow-core jack because of the stroke limitation (hence, the change to the use of two jacks in series starting with TF-6). After resetting the jack, the sample was then reloaded at the approximate same loading schedule as the initial load. The last reload cycle that occurred during

TF-5 was at an applied stress of about 25,000 psf (14th load increment). The failure load was measured at 25,920 psf meaning the unload/reload cycle occurred near failure when the GRS composite had already experienced considerable spalling and necking because of the lack of the facing element. The initial ratio of stress to strain for virgin loading (E_o) of TF-5 during the first applied loading sequence is about 560 ksf. The first and second reload cycles were considerably stiffer, both with a reload ratio of stress to strain equal to approximately 2,900 ksf, supporting the shakedown concept. The last reload cycle; however, is not as stiff as the first two. It is hypothesized by the authors that the strain hardening effect observed in TF-1 was not as pronounced during TF-5 at higher applied loads because the GRS composite had necked considerably prior to the last reload cycle. TF-7 was therefore conducted to determine if there was an effect of the necking of the sample on the capacity of the composite.

The two unload/reload cycles that occurred during TF-6 were at applied stresses of approximately 4,500 psf and 8,000 psf (5th and 10th load increment, respectively). Figure 32 indicates that preloading of the GRS composite resulted in strain hardening to produce a stiffer response during the reload cycle. The reload response is similar during both cycles, with a ratio of stress to strain (E_R) equal to approximately 3,000 ksf, compared to the ratio for the initial, virgin loading (E_o) equal to approximately 750 ksf, an increase by a factor of four.

Typical values of the soil modulus for shallow foundation applications is between about 200 to 400 ksf for natural foundation soils.[21] Based on the results of this series of PTs, GRS composites are stiffer, with modulus values between about 320 and 750 ksf. Preloading results in an even stiffer composite. The strain hardening effect due to preloading was observed during the FHWA GRS Pier load test in 1995 and in-service, with the preloaded GRS abutments for the Blackhawk bridge built in Central City, CO, in 1998.[22,23] To study the possible shakedown phenomenon and resulting response under repeated unload/reload cycles, additional performance testing under cyclic load is needed.

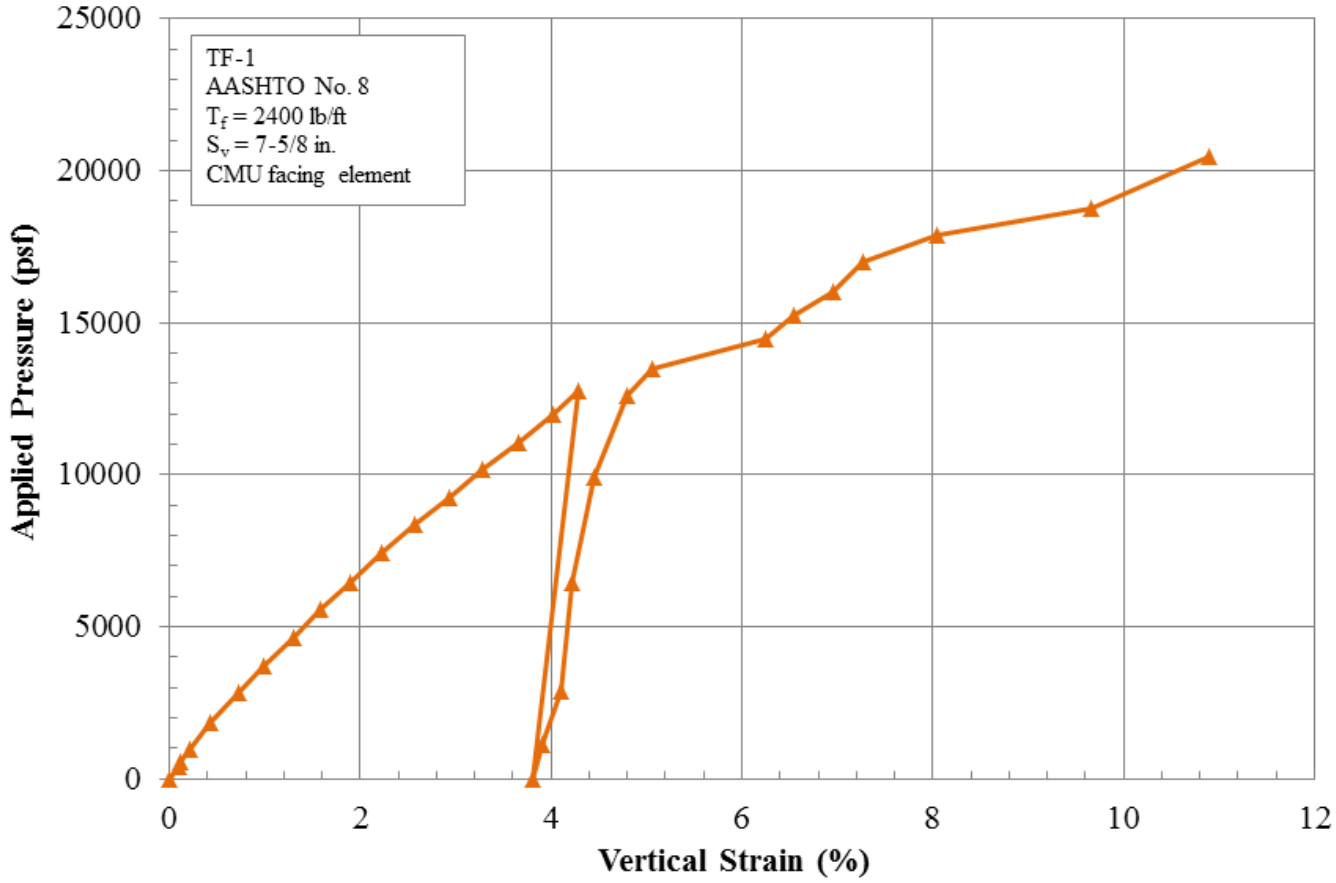

Figure 30. Graph. TF-1 results.

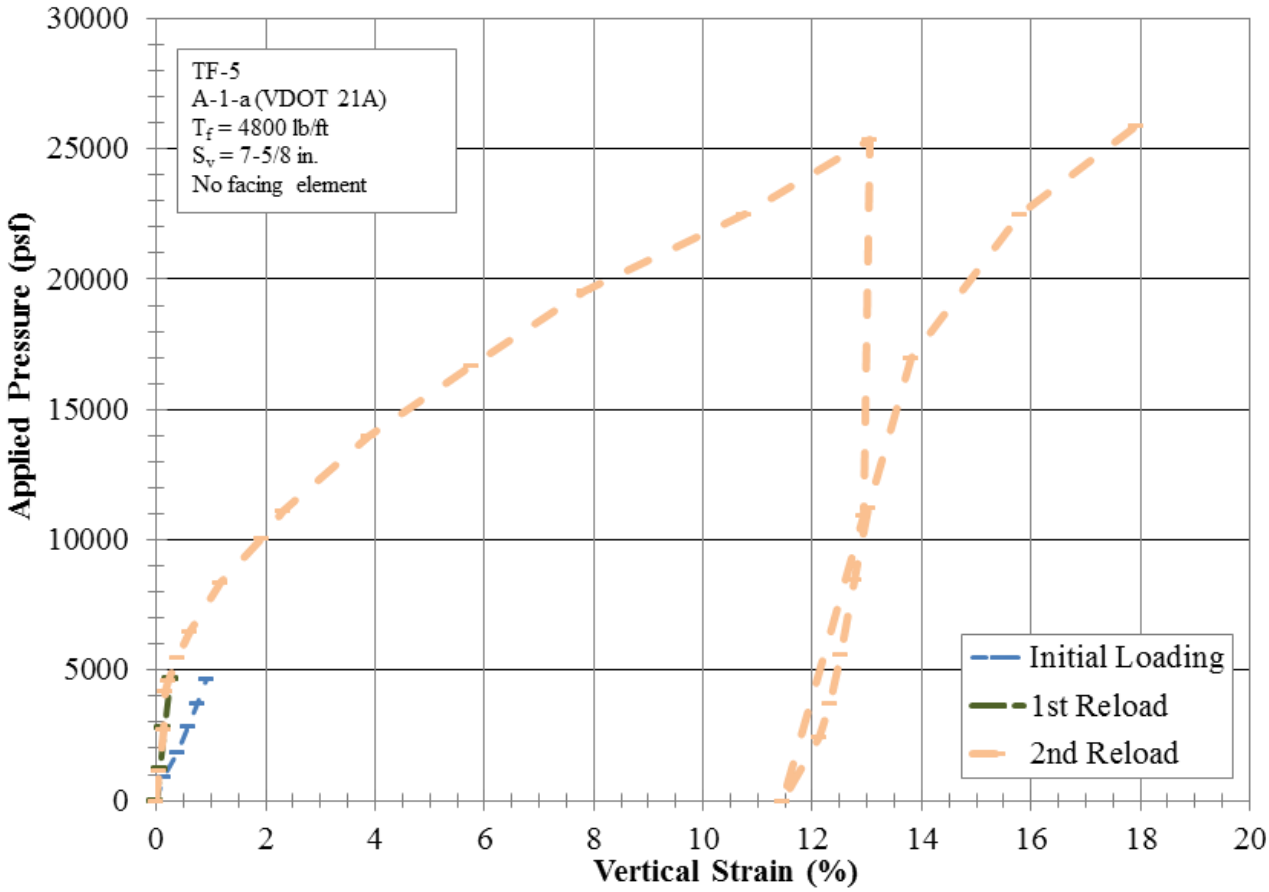

Figure 31. Graph. TF-5 results.

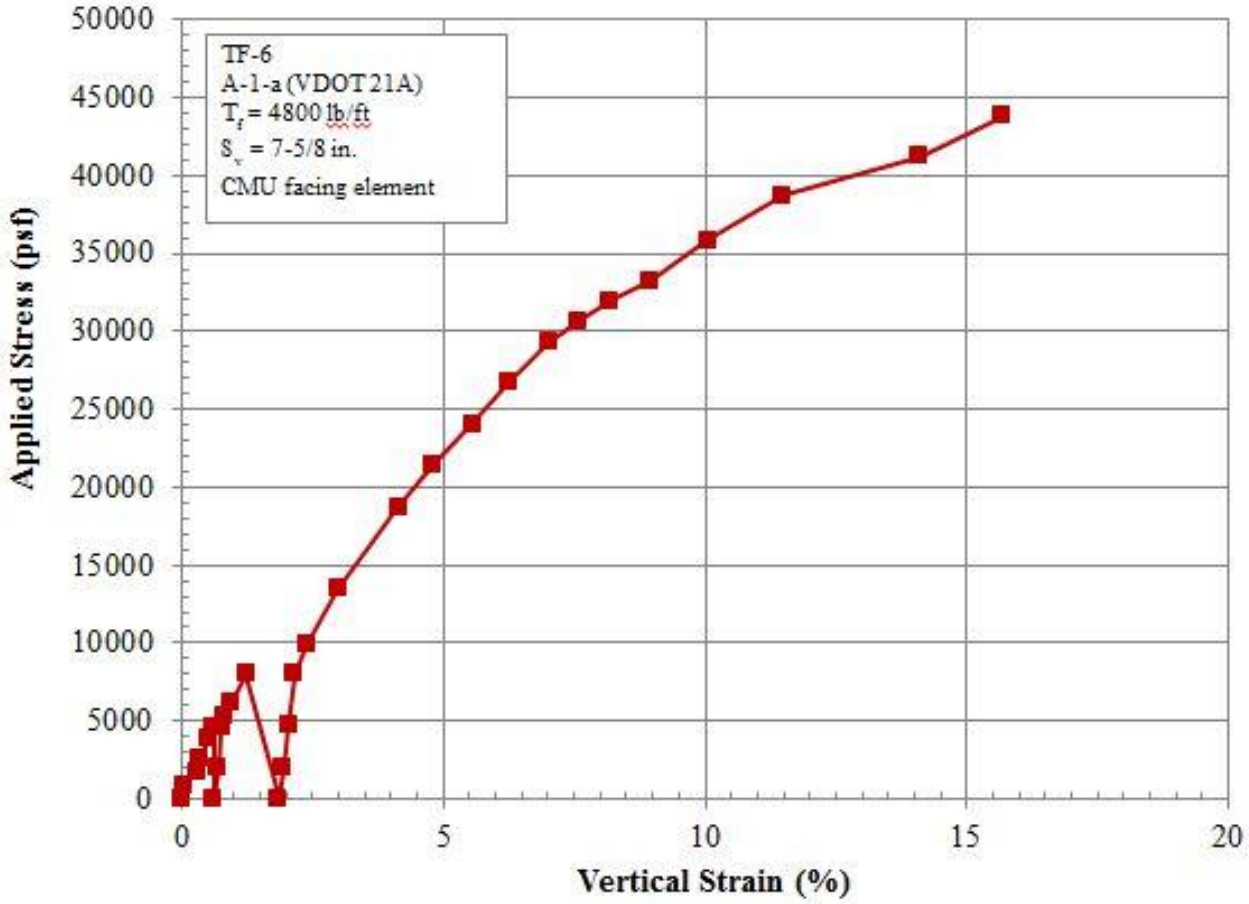

Figure 32. Graph. TF-6 results.

4.2 REPEATABILITY

The repeatability of the test method was indirectly measured through four PTs (TF-4, TF-5, TF-7, and TF-8, see TABLE 1) on nearly identical GRS composites (figure 33). Note that TF-4 was prematurely terminated due to uneven loading and settlement and TF-8 had two courses of bearing bed reinforcement at the top. For TF-5, the stress-strain curve for both the initial loading sequence is plotted to compare to the other tests at lower applied loads, with the stress-strain curve starting on the second reload cycle also plotted to compare to the other tests at higher applied loads. All of the tests were performed without CMU facing. The results indicate good agreement and suggest that the performance test produces repeatable results.

4.3 COMPOSITE BEHAVIOR

The new internal stability design method proposed by Adams et al. 2011a for GRS accounts for functions of the geosynthetic reinforcement beyond simple tensile inclusions and takes into account the backfill and reinforcement spacing comprising the GRS composite material.[1] In this model, connection, reinforcement pullout, and other mechanisms associated with a tie-back design model are not modes of failures for closely spaced GRS.[10] Adding to the understanding of the composite behavior, conducting PTs without a CMU facing allowed for the failure surface for each GRS composite to be visually observed.

For the PTs with reinforcement spacing less than 12 inches, a shear surface formed through the composite (figure 34, figure 35, and figure 36), leading to rupture of the reinforcement. The same mode of failure was not seen for the 15¼-inch spaced system (figure 37) where failure was determined by the soil between the sheets of geotextile, and the full strength of the reinforcement was never developed.

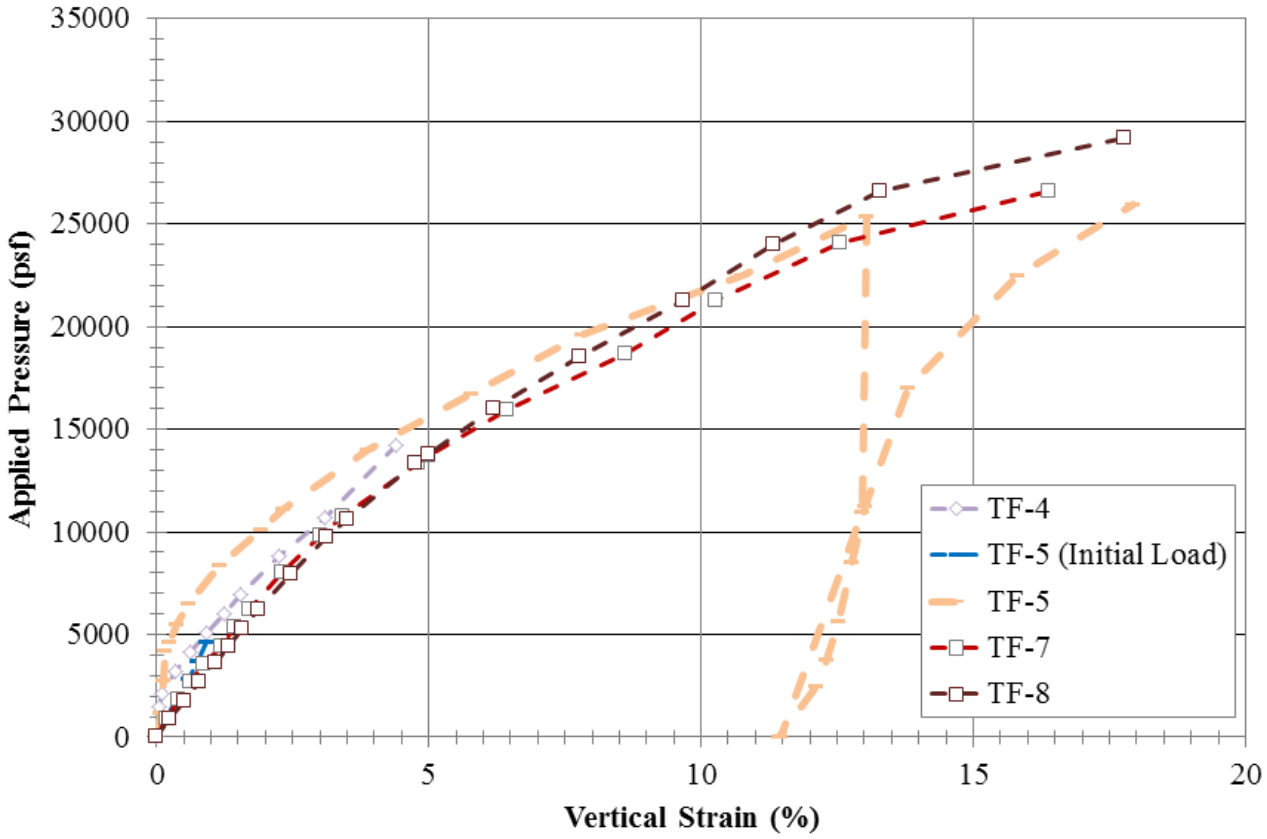

Figure 33. Graph. Repeatability of PT at TFHRC.

Figure 34. Photo. TF-11 at failure with S_v = 3-13/16 inches, T_f = 1,400 lb/ft, and 21A material.

Figure 35. Photo. TF-3 at failure with S_v = 7⅝ inches, T_f = 2,400 lb/ft, and 21A material.

Figure 36. Photo. TF-13 at failure with S_v = 11¼ inches, T_f = 3,600 lb/ft, and 21A material.

Figure 37. Photo. TF-10 at failure with S_v = 15¼ inches, T_f = 4,800 lb/ft, and 21A material.

The same diagonal shear failure mechanism could also be seen through forensic examination of the geotextile after testing the PTs with facing elements. For example, figure 38 shows the rupture pattern in each layer of reinforcement for TF-6 ($q_{ult,emp}$ = 43,828 psf); the lowest layer of reinforcement (near the base of the GRS composite) is in the foreground of the figure with subsequent layers laid out above. A distinct rupture pattern follows a diagonal path through the depth of the specimen; rupture around the connections is also seen in the middle layers.

Rupture at the connections occurred due to extreme downdrag of the reinforced fill behind the block whereby the differential settlement between the fill and the block caused tension (and ultimately rupture) in the reinforcement at the connection. For example, at failure, TF-6 experienced a total maximum vertical strain of 15.7 percent, equating to about 1 ft of settlement; considering the reinforcement layers are spaced every 0.64 ft, the total settlement extended below one layer of the GRS composite. Note that even with the rupture at the connections, only some cracking of the facing blocks was observed (figure 39).

Figure 38. Photo. Rupture pattern for geotextiles in TF-6 ($q_{ult,emp}$ = 43,828 psf); the lowest layer of reinforcement is the closet fabric in the picture.

Figure 39. Photo. Post-test picture of TF-6 (S_v = 7⅝ inches, T_f = 4,800 lb/ft).

5. COMPARISON TO PLANE STRAIN CONDITIONS

Both vertical capacity and stiffness are impacted by the boundary effects related to testing. Considering the application of PTs to bridge abutments, the relationship between the more plane stress conditions of a columnar PT and the plane strain (PS) conditions of an abutment was investigated.

5.1 CAPACITY

A PT with no facing can be considered a type of unconfined compression test; its state of stress at failure can be represented by the Mohr-Coulomb equation (figure 40).

$$\tau = c + \sigma tan\phi$$

Figure 40. Equation. Mohr-Coulomb shear strength.

Where τ = shear strength, σ = applied normal stress, c = cohesion and ϕ = friction angle. Note that when applying figure 40 to a GRS composite, c and ϕ represent the shear strength parameters of the GRS composite (c_{GRS} and ϕ_{GRS} , respectively) and not of the backfill soil alone. In an unconfined compression PT, where the facing element has been removed, the ultimate capacity of the GRS column ($q_{ult,PT}$) can be approximated using figure 41.

$$q_{ult,PT} = 2c_{GRS}$$

Figure 41. Equation. Ultimate capacity of an unconfined GRS PT.

For the PS condition, the bearing capacity of a footing supporting the bridge superstructure can be estimated using Meyerhof's (1957) solution for a rough strip footing bearing on top of a slope (figure 42):[24]

$$q_{ult,PS} = c_{GRS}N_{cq} + 0.5\gamma_{GRS}bN_{\gamma q}$$

Figure 42. Equation. Ultimate capacity of a strip footing on slope.

Where $q_{ult,PS}$ = ultimate capacity of strip footing under PS conditions, c_{GRS} is the cohesion of the GRS composite, γ_{GRS} = unit weight of the GRS composite, b = footing width, and N_{cq} and $N_{\gamma q}$ = bearing capacity factors for a strip footing with a rough base (given by Meyerhof, 1957). The bearing capacity factor $N_{\gamma q}$ approaches zero when the slope angle (β_s) is 90°; thus, figure 42 reduces to figure 43 for a vertical GRS abutment.

$$q_{ult,PS} = c_{GRS}N_{cq}$$

Figure 43. Equation. Ultimate capacity of a strip footing on a vertical GRS abutment.

The ratio of the bearing capacity of a strip footing on top of a GRS abutment to that of a GRS column is therefore calculated according to figure 44.

$$\frac{q_{ult,PS}}{q_{ult,PT}} = \frac{N_{cq}}{2}$$

Figure 44. Equation. Ratio of plane strain capacity to PT capacity.

For a surface footing (i.e., no embedment depth) on top of a vertical GRS abutment, the value of N_{cq} varies with the footing offset from the edge of the wall face (a), wall height (H), footing width (b), and stability factor (N_s), mathematically shown in figure 45 and graphically shown in figure 46. To use figure 46, the effective cohesion of the GRS composite is required to calculate the stability factor, N_s; this can be obtained from laboratory or numerical experiments.

$$N_s = \frac{\gamma_{GRS} H}{c_{GRS}}$$

Figure 45. Equation. Stability Factor.

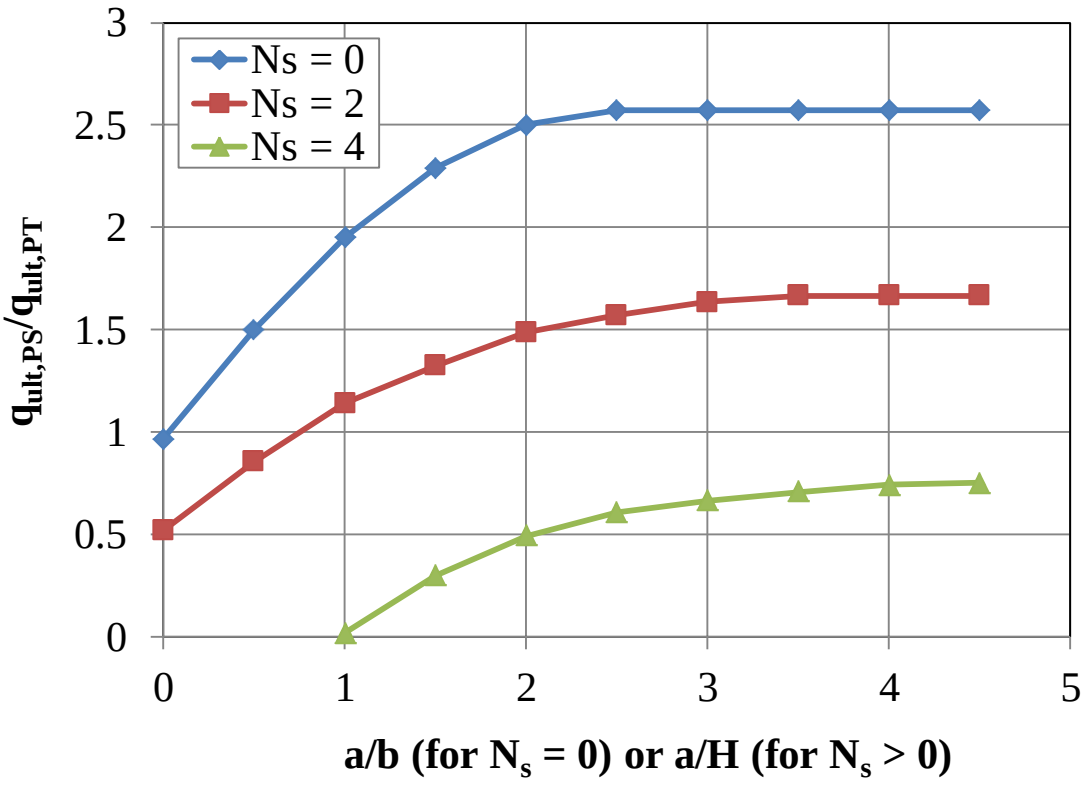

Figure 46. Graph. Ratio of plane strain capacity to PT capacity for different stability factors.

Pham (2009) conducted five plane strain generic soil-geosynthetic composite (GSGC) tests: two of the tests were identical except one was unconfined (0 psi) and the other test had a uniform confining stress of 5 psi.[25] The GRS composite consisted of a granular A-1-a backfill (soil

classification = GW-GM, unit weight, γ = 153.7 lb/ft^3, cohesion, c = 1,480 psf and friction angle, ϕ = 50º) and a 4,800 lb/ft geotextile reinforcement spaced at 7⅝ inches. The corresponding failure stresses were about 42,450 psf and 70,957 psf for the 0 and 5 psi confining stresses, respectively. These failure stresses are calculated as the ratio of applied vertical load to the area of the top load pad (i.e. footing) on the GSGC mass for each test. Note that Pham (2009) reported failure stresses as the ratio of applied vertical load to the total area of the GSGC mass.[25]

The results of these tests can be used to determine the strength properties (cohesion and friction angle) of a particular GRS composite. The Mohr-Coulomb failure circles for the two Pham (2009) tests are shown in figure 47; the resulting cohesion and friction angle for the GRS composite tested is 3,342 psf and 72º, respectively; the stability factor (figure 45) is 0.29. Based on this stability factor, the ratio of plane strain capacity to column (PT) capacity varies with *a*/*H* (figure 48). The correction factor to convert from the PT to a plane strain condition for a typical GRS abutment with the setback (a) equal to 8 inches and height from 10 to 30 ft (i.e., *a*/*H* = 0.02 to 0.07) ranges between 0.92 and 0.97 for this particular GRS composite, close to unity. Therefore, the failure of the PT is approximately representative of an in-service PS condition for well-graded gravels, meaning the PT results can be directly used to estimate the strength limit for capacity in design. Note that the strength properties of the foundation soil underneath in-service GRS abutments would still need to be verified separately.[1]

Note that there are some limitations to the formulation above. The relationship between the bearing capacity of the strip footing and the performance tests requires the cohesion and friction angle of the GRS composite, which are not easy parameters to determine. Additional work is required to develop relationships between the composite shear strength parameters and the soil shear strength parameters, with respect to reinforcement spacing and strengths.

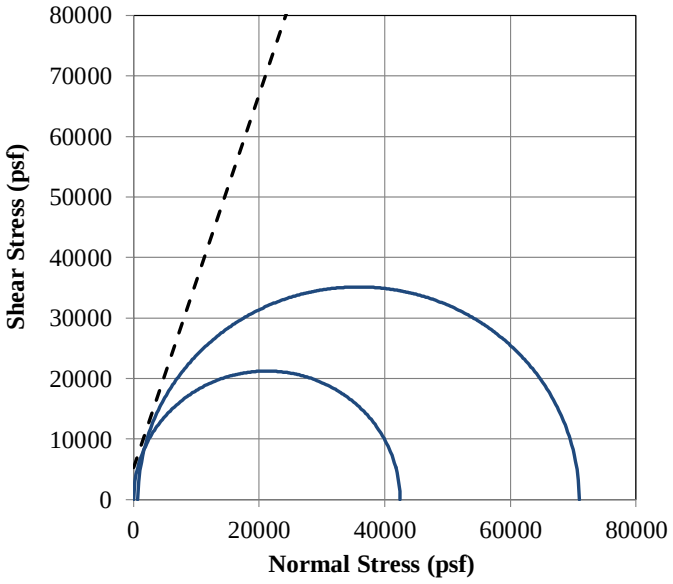

Figure 47. Graph. Mohr-Coulomb failure envelope for Pham (2009) plane strain GSGC tests.

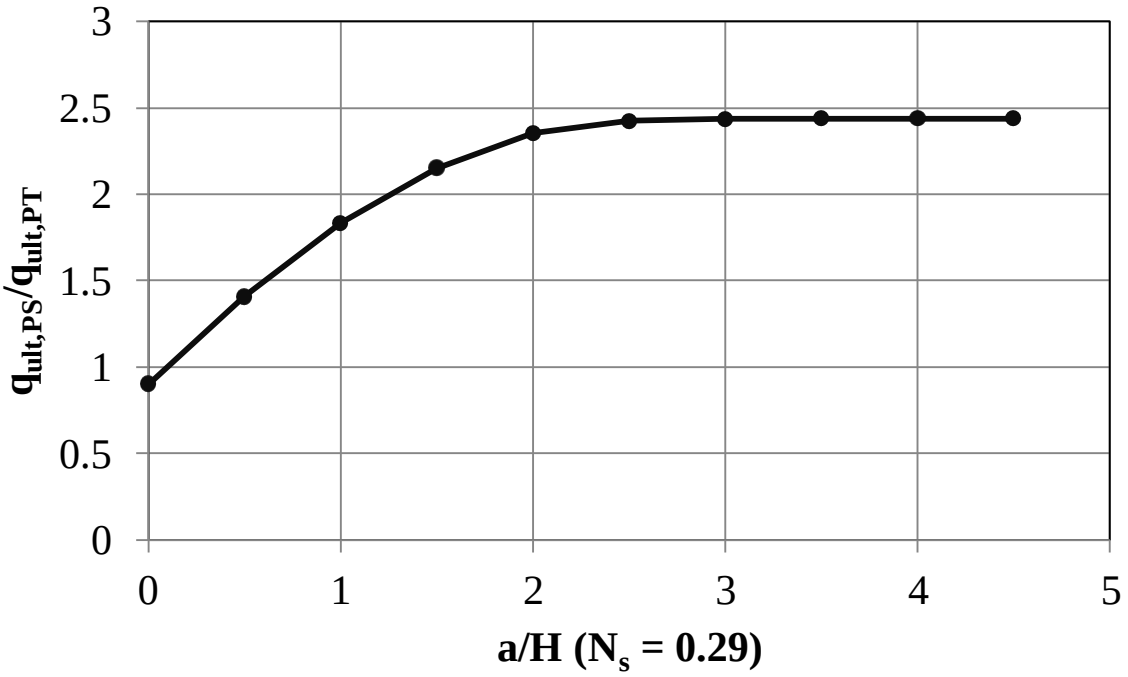

Figure 48. Graph. Plane strain capacity to PT capacity for a stability factor of 0.29.

5.2 STIFFNESS

The GRS PTs have a height to width ratio of about 2 (table 7); the stiffness of the unconfined GRS column (S_{PT}) can therefore be taken as equal to the Young's modulus of the GRS composite (E_{GRS}). In contrast, if a performance test was conducted on an infinitely long unconfined GRS abutment (i.e., plane strain conditions), having a finite width as shown in figure 49, the stiffness of this GRS mass is represented according to figure 50.

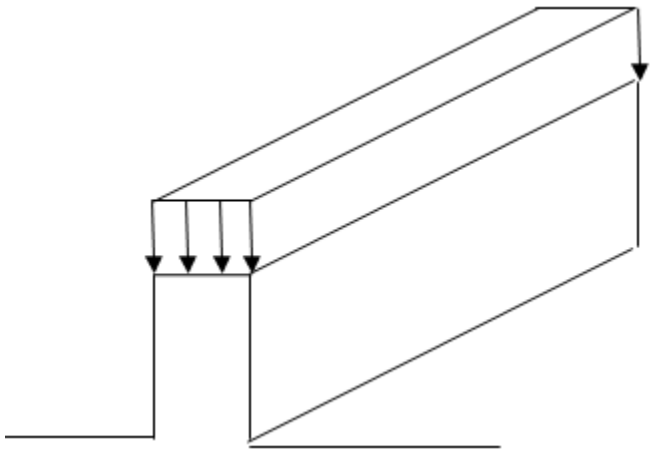

Figure 49. Illustration. Infinitely Long Unconfined GRS abutment.

$$\frac{q}{\varepsilon_v} = \frac{\mathbf{E_{GRS}}}{(1 + \nu_{GRS})(1 - \nu_{GRS})}$$

Figure 50. Equation. Stiffness of an Infinitely Long Unconfined GRS abutment.

Where q = applied stress, ε_v = vertical strain, E_{GRS} = Young's modulus of the GRS and ν_{GRS} = Poisson's ratio of the GRS. Assuming ν_{GRS} is equal to 0.5, this infinitely long GRS strip will be 1.33 times stiffer than a square GRS column.[2] In reality, the width is not finite in the direction perpendicular to a GRS abutment, as shown on the left of figure 51. To date, typical L/b ratios for in-service GRS abutments range between 7 and 14, depending on load requirements, where L is the length and b is the width of the bearing area. NAVFAC (1986) considers L/b ratios > 5 to be plane strain while current FHWA practice considers L/b ratios > 10 to be plane strain conditions; therefore, most GRS abutments can be idealized as plane strain.[26]

In the context of elastic theory, the bridge footing on a GRS abutment can be considered a strip running parallel to the edge of the wall at an offset, as shown on the left side of figure 51. Considering the response at low strain levels is close to elastic conditions, the stiffness of such a strip surface footing can be estimated using elastic theory, in particular the solution for a strip footing on a linear elastic half space.[27,28] Since the conditions are not a linear elastic half space for abutment applications, the solution for a strip footing on top of a wall is obtained by doubling the solution for a strip footing on a linear elastic half space, as shown on the right side of figure 51. Note that this assumes zero lateral deformations along the wall height, which is not strictly correct for GRS abutments since the CMU facing is free to displace laterally; however, it is the best available method to date to estimate vertical settlement.

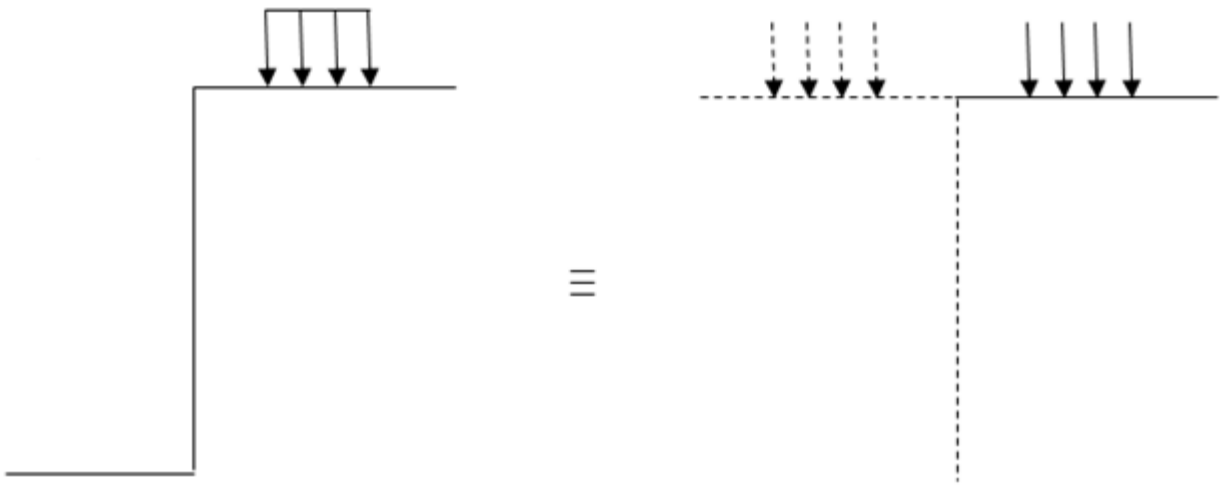

Figure 51. Illustration. Solution for strip footing on top of a wall.

For a material with a Poisson's ratio of 0.5, Gibson (1967) provided solutions for the relative displacement between the center of the strip footing and any arbitrary point assuming a constant stiffness with depth.[27] If the arbitrary point is selected to be the bottom of the GRS wall, the expression for settlement without doubling the load is shown in figure 52.

$$\rho = \frac{3qb}{4\pi E_{GRS}}\left[\frac{1}{2}\left(1+\frac{a+\frac{b}{2}}{\frac{b}{2}}\right)ln\left(\frac{H^2+(a+\frac{b}{2})^2}{(\frac{b}{2})^2}\right)+\frac{1}{2}\left(1-\frac{a+\frac{b}{2}}{\frac{b}{2}}\right)ln\left(\frac{H^2+a^2}{(\frac{b}{2})^2}\right)+\frac{H}{a}tan^{-1}\left(\frac{a+b}{H}\right)+\frac{H}{a}tan^{-1}\left(\frac{-b}{H}\right)\right]$$

Figure 52. Equation. Vertical displacement of a GRS abutment with a strip footing.

Where q = applied stress, b is the footing width, E_{GRS} is the Young' modulus of the GRS composite, a is the setback distance between the face of the wall and the applied load, and H is the height of the abutment. The corresponding vertical strain (ε_V) is given by figure 53.

$$\varepsilon_v = \frac{\rho}{H}$$

Figure 53. Equation. Vertical strain.

Where ρ is the vertical displacement (figure 52) and H is the height of the wall.

The stiffness of a GRS abutment supporting a surface strip footing (S_{GRS}) can be related to the applied stress ($2q$, due to doubling of the load) and the vertical strain (ε_V) (figure 54).

$$S_{GRS} = \frac{2q}{\varepsilon_v} = \frac{2qH}{\rho}$$

Figure 54. Equation. Stiffness of a GRS abutment supporting a strip footing.

The ratio between this stiffness and the stiffness from a performance test ($S_{GRS} = E_{GRS}$) can then be calculated according to figure 55. The variation of stiffness ratio with b/H is plotted in figure 56. It was found that this ratio is essentially independent of the value of a/b.

$$\frac{S_{GRS}}{S_{PT}} = \frac{2qH}{\rho E_{GRS}} = \frac{8\pi H}{3b\left[\frac{1}{2}\left(1+\frac{a+\frac{b}{2}}{\frac{b}{2}}\right)ln\left(\frac{H^2+(a+\frac{b}{2})^2}{(\frac{b}{2})^2}\right)+\frac{1}{2}\left(1-\frac{a+\frac{b}{2}}{\frac{b}{2}}\right)ln\left(\frac{H^2+a^2}{(\frac{b}{2})^2}\right)+\frac{H}{a}tan^{-1}\left(\frac{a+b}{H}\right)+\frac{H}{a}tan^{-1}\left(\frac{-b}{H}\right)\right]}$$

Figure 55. Equation. Vertical displacement of a GRS abutment with a strip footing.

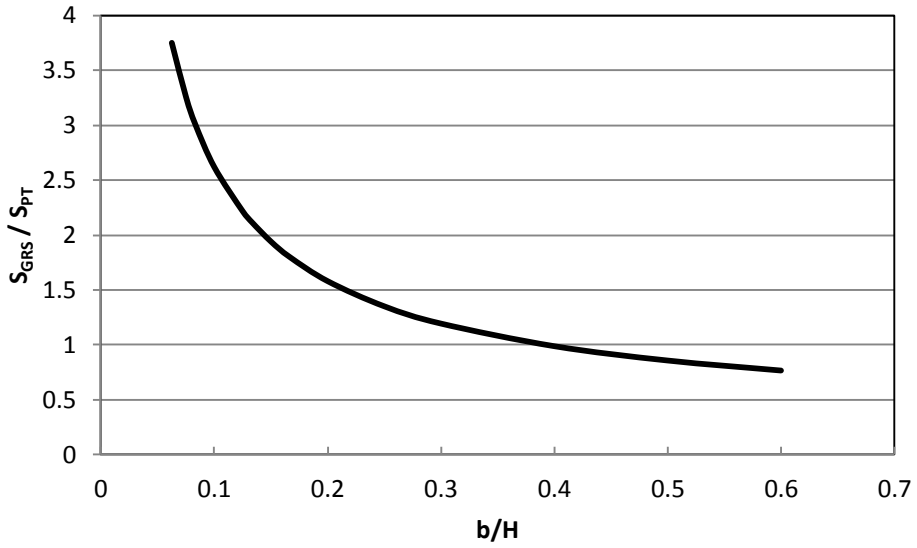

Figure 56. Graph. Ratio of plane strain stiffness of a strip footing on top of a wall (S_{GRS}) to that of a PT (S_{PT}) for the case of constant stiffness with depth.

For GRS abutments, *b* is a minimum of 2.5 ft for bridge spans larger than 25 ft and has been as large as 4.5 ft for the Tiffin River Bridge; *H* typically ranges from 10 to 30 ft; *b*/*H* is therefore between about 0.08 and 0.45.[(5)] From figure 56, the ratio of plane strain stiffness of a strip footing on top of a wall (S_{GRS}) to that of a PT (S_{PT}) ranges between 0.92 and 3 suggesting that the stiffness reported from a PT will be conservative (up to a factor of three times) compared to what a GRS abutment might experience in-service.

Note that further research should be conducted on the stiffness of GRS abutments, and the corresponding equivalency to a GRS PT, since the above formulations are simplistic and do not consider the effects of the facing element (e.g., CMUs) on the capacity and stiffness of a GRS composite. The effect of compaction-induced stresses and related shakedown is also ignored. Compaction-induced stresses increase the locked-in lateral stress especially in the upper reaches of the GRS; associated with an increase in confinement is an increase in stiffness and its effects should be investigated.

6. PARAMETRIC ANALYSIS

The combined series of tests performed in Defiance County and at TFHRC make up a parametric study where the following parameters were investigated: (1) aggregate type, (2) compaction, (3) gradation, (4) bearing bed reinforcement, (5) reinforcement strength, (6) similar ratios of reinforcement strength to spacing, (T_f/S_v), and (7) facing.

6.1 EFFECT OF AGGREGATE TYPE

The aggregate selected has a large impact on the performance and composite behavior of GRS; both the size (i.e., d_{max}) and the strength (i.e., c, ϕ) of the backfill selected are important. In PTs, it is very difficult to isolate one backfill variable over another to determine the individual contributions to GRS performance. Instead, general conclusions based on aggregate classification and angularity can be drawn using PT results; however, advanced computer modeling is a potential avenue to better understand the component contributions of particular fill materials.

The majority of GRS- Integrated bridge systems (IBSs) built across the country use an open-graded aggregate for the abutment backfill. Commonly, an AASHTO No. 89 has been employed; an early performance test performed in Defiance County shows the behavior of a GRS composite with this backfill and 4,800 lb/ft reinforcement spaced at 7⅝ inches.[1] To create a database of PT results with alternate aggregate types, while providing an opportunity to demonstrate the construction of a PT to FHWA Division Offices, Federal Lands Highway Division, and the Resource Center through the EDC GRS-IBS Validation Sessions, a series of tests were conducted in this study (table 9). Note that since these PTs were conducted as demonstration piers, the level of compaction control on each lift was not consistent or uniform.

Table 9. Parametric study on aggregate size.

Test No.	Backfill				Reinforcement		Facing
	Type	ϕ (°)	c (psf)	d_{max} (inch)	T_f (lb/ft)	S_v (in.)	
DC-1	8	54	0	½	4,800	7⅝**	CMU
DC-2	8P*	46	0	¾	4,800	7⅝**	CMU
DC-3	57	52	0	1	4,800	7⅝**	CMU
DC-4	9	49	0	⅜	4,800	7⅝**	CMU

ϕ = the peak friction angle, c = the cohesion, T_f = the MARV value of the wide width tensile strength, and S_v = the spacing.
*Rounded pea-gravel angularity.
**Two courses of bearing bed reinforcement placed at the top of the PT.

Based on the results (table 10), no relationship can be determined with respect to the strength limit for open-graded aggregates since there are only two PTs conducted to failure of the GRS composite. The largest aggregate tested, the No. 57 stone, had the lowest service limit of all the tests, indicating more deformation under an applied load. In addition, the rounded pea gravel had a lower strength and service limit than the more angular aggregate meeting the same gradation specifications for an AASHTO No. 8 material.

Table 10. Effect of aggregate type results.

	Maximum Tested		Strength Limit	Design Limit		Service Limit
Test No.	q_{max} (psf)	ε_{max} (%)	$q_{ult,emp}$ (psf)	$q_{@\varepsilon\leq5\%}$ (psf)	V_{allow} = $q_{@\varepsilon\leq5\%}$ /3.5 (psf)	$q_{@\varepsilon=0.5\%}$ (psf)
DC-1	23,310	7.95	23,310	19,983	5,709	3,065
DC-2	22,709	7.07	22,709	19,399	5,543	2,171
DC-3	18,447	5.82	N/A	16,182	4,623	1,324
DC-4	26,730	7.64	N/A	17,350	4,957	2,212

q_{max} = the maximum applied pressure during testing, ε_{max} = the maximum recorded vertical strain, $q_{ult,emp}$ = the measured failure pressure, $q_{@\varepsilon=5\%}$ = the applied stress at 5-percent vertical strain, $V_{allow,emp}$ = the total allowable pressure on the GRS,[(1)] $q_{@\varepsilon=0.5\%}$ = the applied stress at 0.5-percent vertical strain.

6.2 EFFECT OF COMPACTION

The effect of compaction for open-graded materials was investigated through two PTs conducted in Defiance County, OH (table 11). The testing conditions were identical except for the compaction effort. DC-1 was compacted to non-movement while DC-5 involved no compaction effort beyond end dumping the material and leveling for each lift of fill. The results show a similar vertical capacity (23,310 psf versus 21,539 psf for DC-1 and DC-5, respectively); however, the higher strength for DC-1 is likely due to the increased locked-in stresses induced due to compaction. Note that the friction angle of both composites is reported as the same; however, the degree of compaction may have a small impact for open-graded aggregates (larger for well-graded backfills). This effect is currently being investigated.

While the capacity of the specimens was similar, the deformation response was different (figure 57). As expected, Test DC-5 had a softer response resulting from not being compacted. The modulus of the primary settlement portion of the curve for the uncompacted composite (DC-5) is about 270 ksf while the modulus for the compacted composite (DC-1) is 430 ksf (table 11).

Table 11. Parametric study on compaction.

Test No.	Backfill			Reinforcement		Facing	E_o (ksf)	$q_{ult,emp}$ (psf)
	Type	ϕ (°)	c (psf)	T_f (lb/ft)	S_v (in.)			
DC-1	8	54	0	4,800	7⅝**	CMU	430	23,310
DC-5	8***	54	0	4,800	7⅝**	CMU	270	21,539

ϕ = the peak friction angle, c = the cohesion, T_f = the MARV value of the wide width tensile strength, S_v = the spacing, E_o = the initial stress-strain ratio, and $q_{ult,emp}$ = the measured vertical capacity.
**Two courses of bearing bed reinforcement placed at the top of the PT.
***Uncompacted sample.

At the service limit state of 0.5 percent vertical strain, the allowable stress is limited to 316 psf for the uncompacted GRS composite, but 3,065 psf for the same composite compacted to non-movement (table 8); however, if negating the initial immediate settlement resulting from the first load increment, before the onset of primary deformation of the uncompacted sample, the allowable stress is about 1,345 psf (figure 58).

The ratio of strain for the uncompacted (DC-5) and compacted (DC-1) GRS composite ($\varepsilon_{v,uncompact}/\varepsilon_{v,compact}$), accounting for the immediate deformation related to the uncompacted composite (DC-5), decreases with increasing applied pressure (figure 59). For the particular GRS composite tested (table 11, figure 58), at an in-service dead load of 4,000 psf, an uncompacted abutment will experience about 3 times the strain as a compacted abutment; however, near failure, at about 20,000 psf, an uncompacted abutment will experience about 1.7 times the strain as a compacted abutment. Note that in the evaluation of tolerable settlements for highway bridge design, FHWA recommends the construction-point concept, whereby the settlements between critical construction points (such as between application of dead load and opening to traffic) are evaluated.[29]

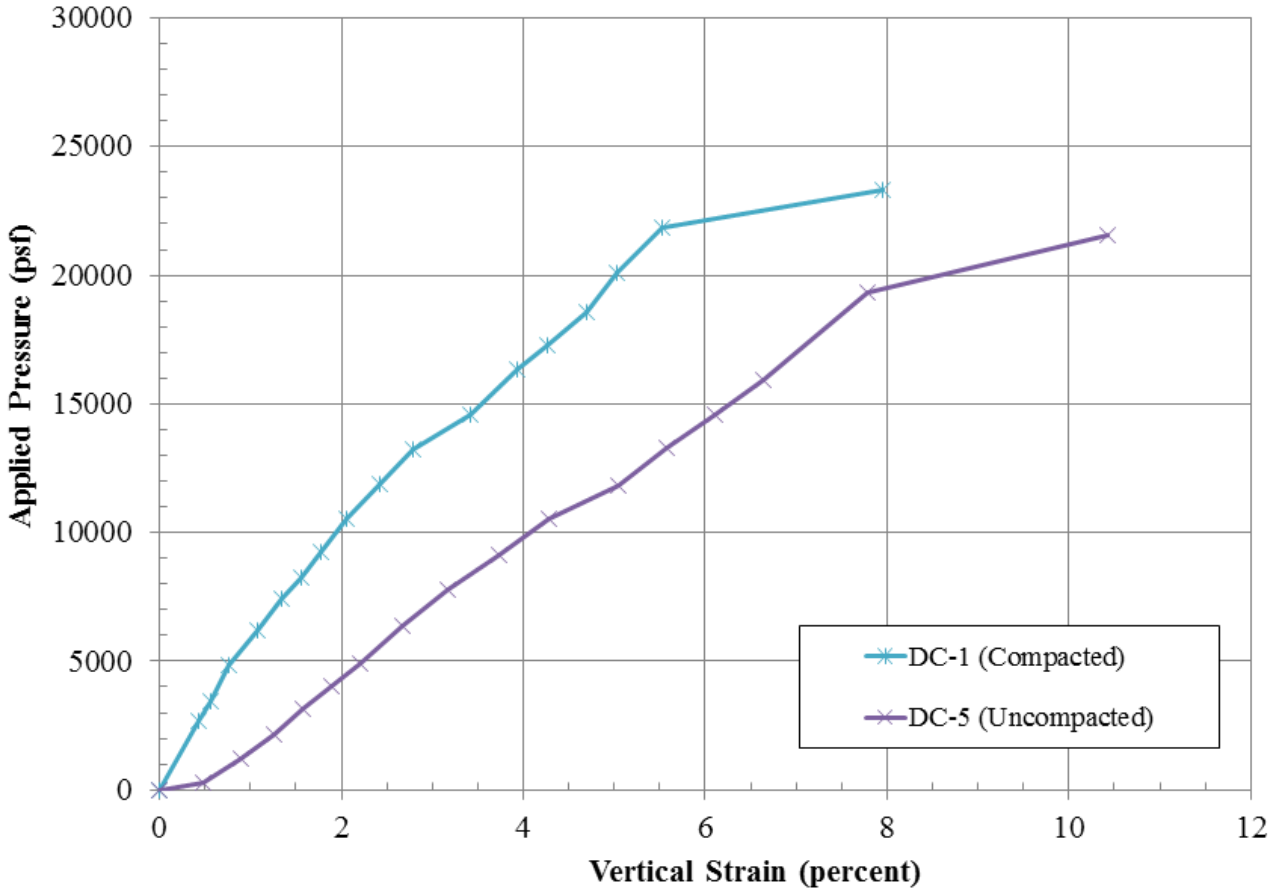

Figure 57. Graph. Comparison between compacted and uncompacted GRS composites.

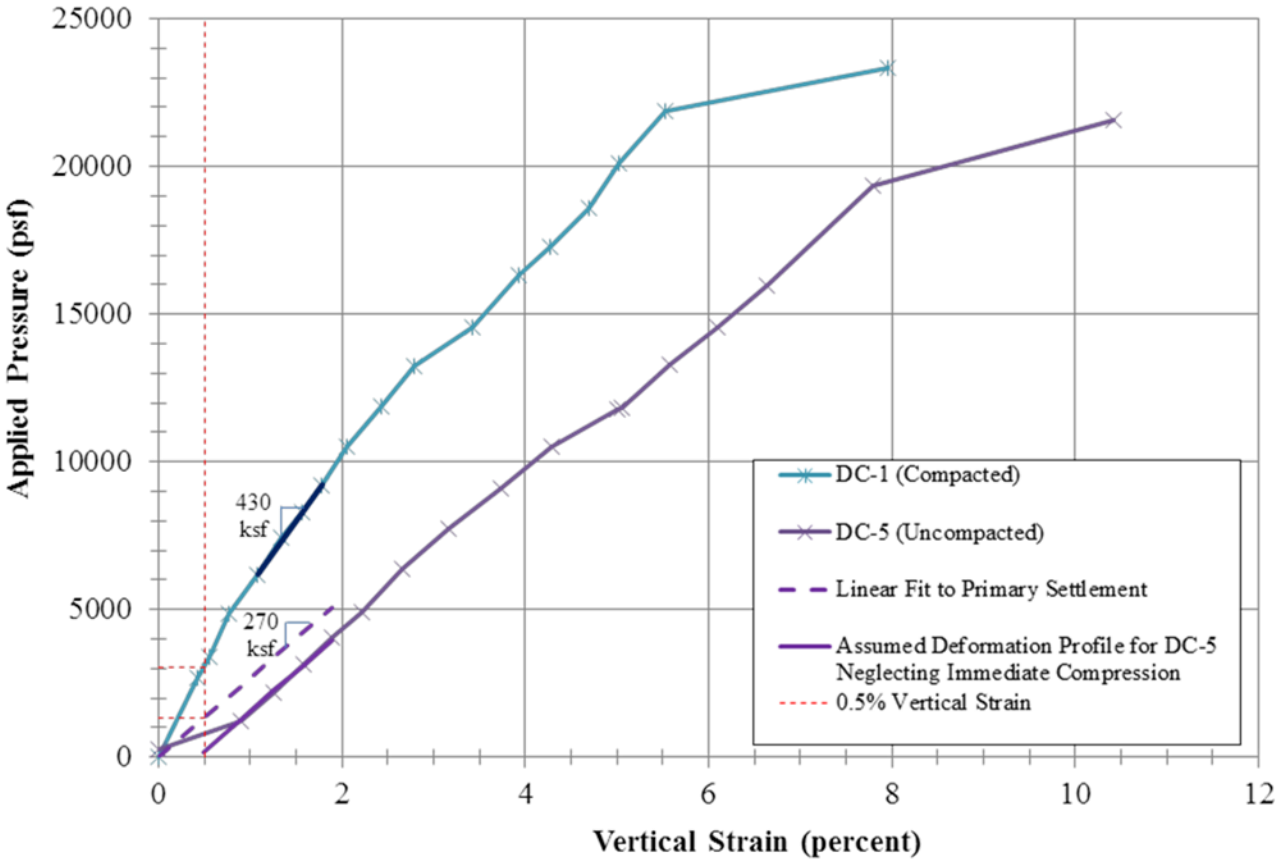

Figure 58. Design service limit for uncompacted sample DC-5.

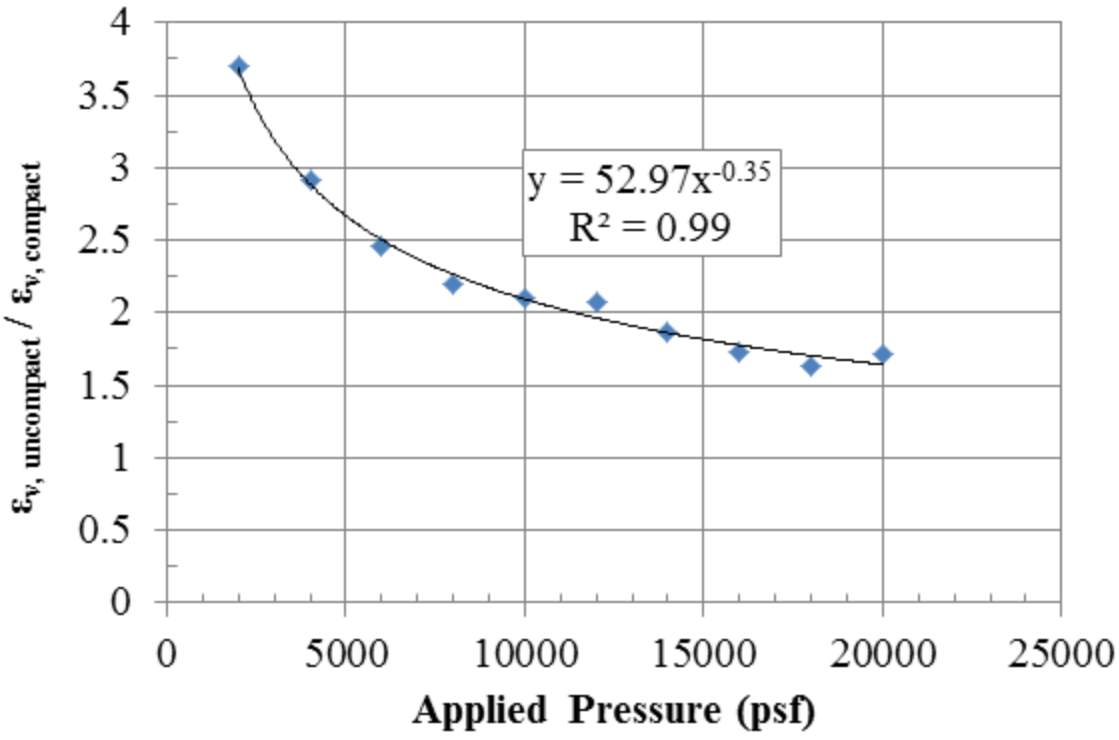

Figure 59. Graph. Comparison of compacted and uncompacted strains between the DC-1 and DC-5 tests.

6.3 EFFECT OF BEARING BED REINFORCEMENT

Bearing bed reinforcement, where the reinforcement is spaced at half the primary spacing, is recommended in at least the top five courses of CMU facing elements for GRS abutments to aid in serviceability.[(1)] To investigate the impact of the bearing bed, two PTs were conducted with identical parameters, except one (TF-8) had two courses of bearing bed reinforcement, as recommended in the empirical design procedure using performance testing by Adams et al. 2011a (table 12); the other (TF-7) had no bearing bed reinforcement.[(1)] The axial behavior results indicate that the bearing bed provides some added vertical capacity; however, vertical deformation is not improved at low strain levels (figure 60). The modulus for primary compression is similar whether or not the bearing bed is present (table 12).

Table 12. Parametric study on bearing bed reinforcement.

Test No.	Backfill				Reinforcement		Facing	E_o (ksf)	$q_{ult,emp}$ (psf)
	Type	ϕ(°)	c (psf)	d_{max} (in.)	T_f (lb/ft)	S_v (in.)			
TF-7	21A	53	115	1	4,800	7⅝	no CMU	320	26,546
TF-8	21A	53	115	1	4,800	7⅝**	no CMU	320	29,134

ϕ = the peak friction angle, c = the cohesion, T_f = the MARV value of the wide width tensile strength, S_v = the spacing, E_o = the initial stress-strain ratio, and $q_{ult,emp}$ = the measured vertical capacity.
**Two courses of bearing bed reinforcement placed at the top of the PT.

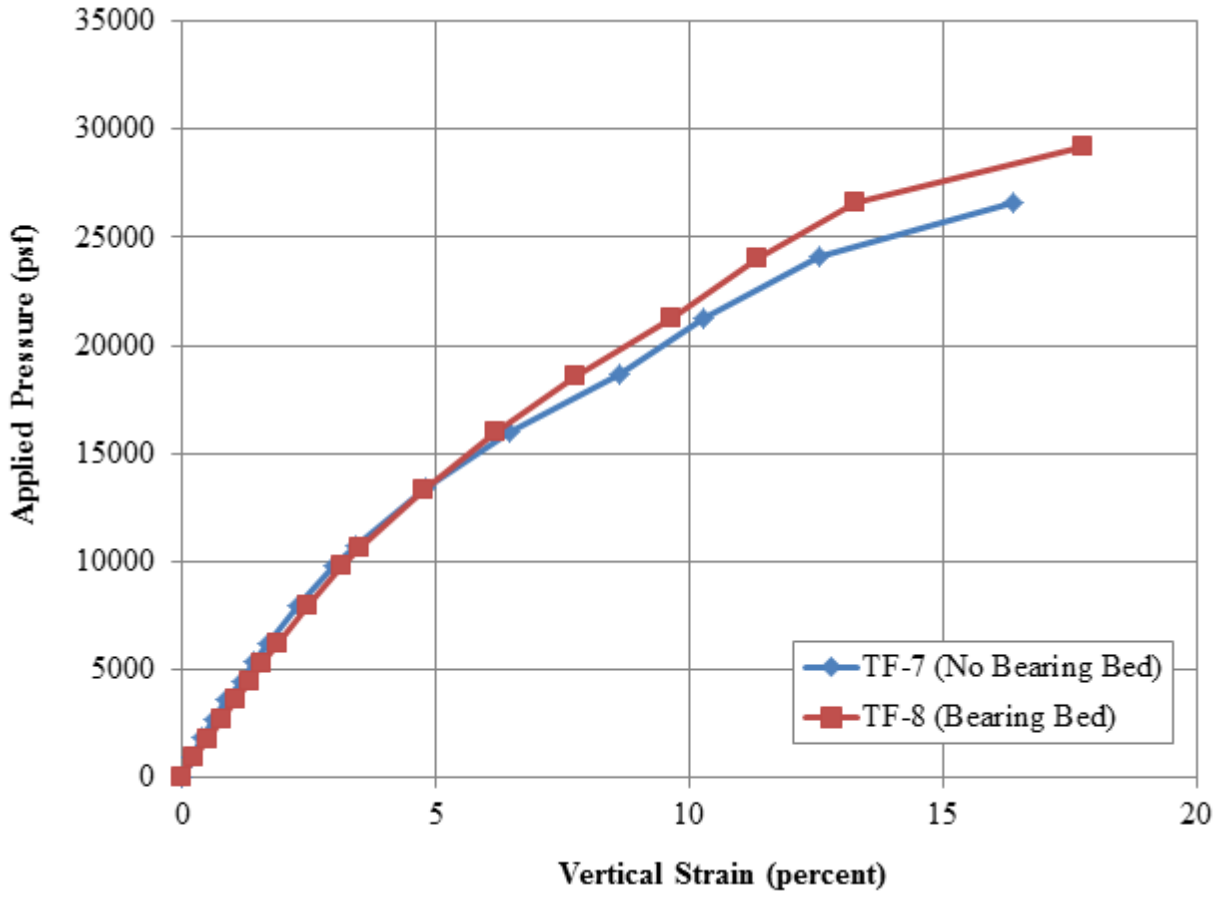

Figure 60. Graph. Effect of bearing bed reinforcement for TF-7 and TF-8.

Looking at the lateral deformation characteristics for both tests at an applied stress of about 3,600 psf, typical of bridge loads (figure 61), the bearing bed reinforcement serves to limit deformation in the zone of its placement. The approximate location of the bearing bed reinforcement is illustrated with red dashed lines in figure 61. At considerably higher loads, around 26,600 psf, the same effect is observed (figure 62). Note that the LVDT located at the bottom of the PT for the TF-7 test was damaged during testing due to sloughing of the fill

material so no values were recorded in the later stages of the test; the full lateral displacement curves for all of the PTs will be presented in a separate report.

At service loads, when bearing bed reinforcement is present (TF-8), the maximum lateral deformation is lower and occurs at about mid-height (38⅛ inches from the top) whereas when bearing bed reinforcement is excluded (TF-7), the maximum lateral deformation occurs near the top (7⅝ inches from the top). The lateral deformation at 7⅝ inches below the top of the GRS PT is 0.16 inches for TF-7 (no bearing bed) and 0.07 inches for TF-8 (with bearing bed reinforcement); the bearing bed reduced the lateral deformation by about half at 3,600 psf applied vertical pressure. At larger loads, the difference in the measured lateral deformation between including a bearing bed and not diminishes considerably at the top of wall. Note that since the results are based on only two PTs, additional testing is required to verify the conclusions for different aggregate and reinforcement materials and to investigate the depth of influence for the bearing bed.

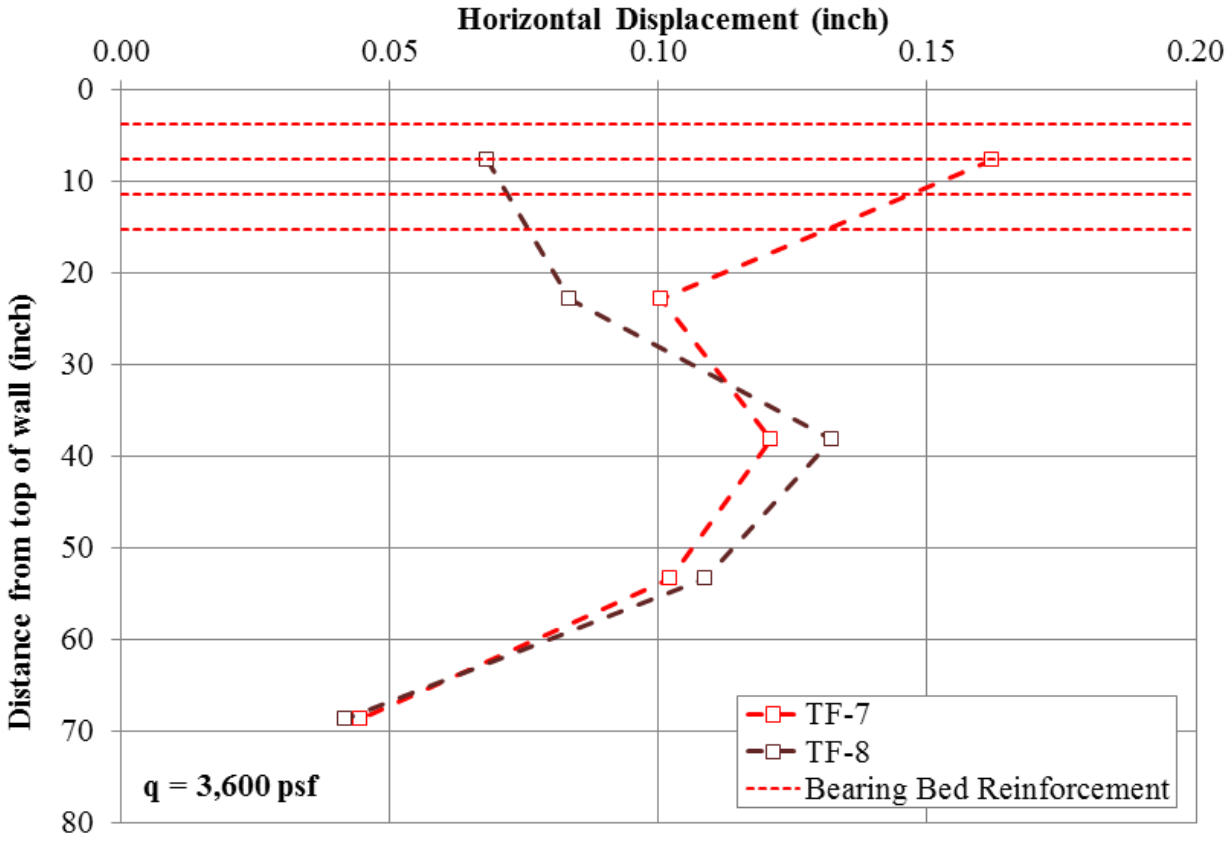

Figure 61. Graph. Measured lateral deformation at 3,600 psf applied stress for TF-7 (no bearing bed reinforcement) and TF-8 (2 courses of bearing bed reinforcement).

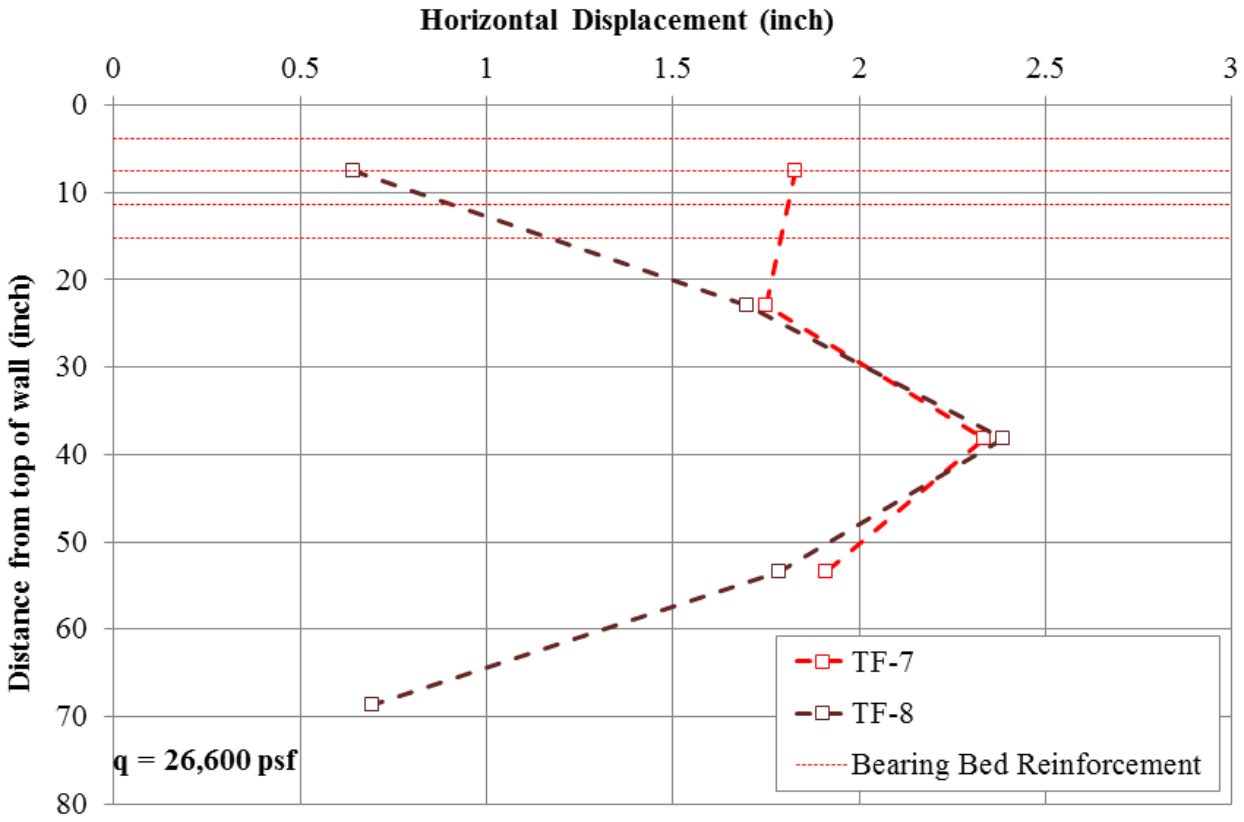

Figure 62. Graph. Measured lateral deformation at 26,600 psf applied stress for TF-7 (no bearing bed reinforcement) and TF-8 (2 courses of bearing bed reinforcement).

6.4 Effect of Gradation

For the GRS-IBS, both open-graded and well-graded materials that meet the specifications in the Interim Implementation Guide are acceptable for use in the GRS abutment; however, there are advantages and disadvantages of both.[1] Open-graded materials are free draining, easier to work with, and their use in construction is independent of weather conditions; however, they are less stiff than well-graded materials, which can achieve greater density under the same compactive effort. In addition, the classical bell-shaped Proctor curves cannot be attained with open-graded materials. The primary disadvantage of working with well-graded fill is compaction control and maintaining the optimum moisture content for efficient compaction.

PTs TF-1 and TF-2 are identical except for the backfill material type; TF-1 used an open-graded AASHTO No. 8 while TF-2 used a well-graded AASHTO A-1-a backfill (table 13). The friction angle for both tests were similar (55° versus 53° for TF-1 and TF-2, respectively), but the well-graded material (TF-2) had cohesion of 115 psf. The corresponding soil shear strengths at a given applied stress (figure 40) are therefore only 5 percent different, with TF-2 having slightly higher shear strength.

Table 13. Parametric study on gradation (T_f = 2,400 lb/ft, S_v = 7⅝ inches).

Test No.	Backfill				Reinforcement		Facing	E_o (ksf)	$q_{ult,emp}$ (psf)
	Type	ϕ(°)	c (psf)	d_{max} (inch)	T_f (lb/ft)	S_v (inch)			
TF-1++	8	55	0	½	2,400	7⅝	CMU	320	20,487
TF-2	21A	53	115	1	2,400	7⅝	CMU	710	25,260

ϕ = the peak friction angle, c = the cohesion, T_f = the MARV value of the wide width tensile strength, S_v = the spacing, E_o = the initial stress-strain ratio, and $q_{ult,emp}$ = the measured vertical capacity.

++Technical difficulties resulted in unloading/reloading of the composite.

The resulting load-deformation profiles are shown in figure 63. The well-graded material is considerably stiffer than the open-graded material. At an applied pressure of 4,000 psf, the vertical strain is about 1.1 percent for TF-1 (open-graded) and 0.4 percent for TF-2 (well-graded). The modulus of the composite tested in TF-1 is 320 ksf (table 13) compared to 710 ksf for the composite tested in TF-2; TF-1 (open-graded) is 55 percent less stiff than TF-2 (well-graded). In terms of bearing capacity, TF-1 was 20 percent less strong than TF-2. The results indicate that the gradation, and perhaps cohesion, impacts the stiffness more so than strength, indicating that well-graded fills have an advantage with respect to serviceability. As previously discussed in section 6.1, isolating the effect of cohesion on the performance is difficult using PTs, although based on the soil-geosynthetic capacity equation (figure 8), it will serve to improve capacity, although its contribution should not be considered in design.

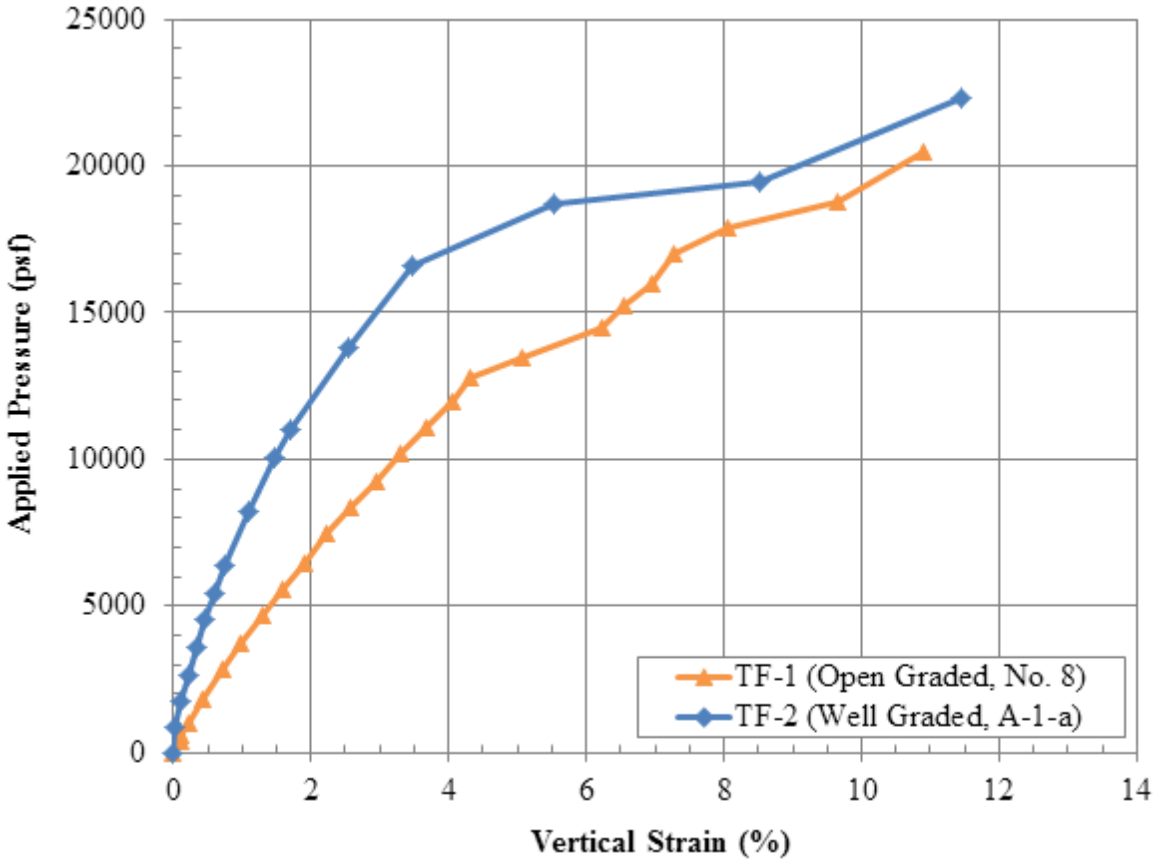

Figure 63. Graph. Comparison of open-graded and well-graded backfills for TF-1 and TF-2.

Comparing DC-1 and TF-6 also provides similar insight into the modulus difference between open-graded and well-graded composites, respectively (table 14). Note that DC-1 included two courses of bearing bed reinforcement; however, it was previously shown that the bearing bed reinforcement does not impact the modulus at low strain levels, but the capacity is slightly improved with the two additional layers of reinforcement at the top. The modulus of the composite with open-graded backfill (DC-1) was 430 ksf, whereas the modulus of the composite with well-graded backfill (TF-6) was 750 ksf. Both are slightly larger than the measured modulus of similar composites with lower reinforcement strengths (table 13).

Table 14. Parametric study on gradation (T_f = 4,800 lb/ft, S_v = 7⅝ inches.)

Test No.	Backfill				Reinforcement		Facing	E_o (ksf)	$q_{ult,emp}$ (psf)
	Type	ϕ(°)	c (psf)	d_{max} (inch)	T_f (lb/ft)	S_v (inch)			
DC-1	8	54	0	½	4,800	7⅝**	CMU	430	23,310
TF-6++	21A	53	115	1	4,800	7⅝	CMU	750	43,763

ϕ = the peak friction angle, c = the cohesion, T_f = the MARV value of the wide width tensile strength, S_v = the spacing, E_o = the initial stress-strain ratio, and $q_{ult,emp}$ = the measured vertical capacity.
**Two courses of bearing bed reinforcement placed at the top of the PT.
++Technical difficulties resulted in unloading/reloading of the composite.

6.5 EFFECT OF REINFORCEMENT STRENGTH

The impact of reinforcement strength on the behavior of a GRS composite was investigated for both open-graded (table 15) and well-graded aggregates (table 16).

Table 15. Parametric study on reinforcement strength with open-graded aggregates.

Test No.	Backfill				Reinforcement		Facing	E_o (ksf)	$q_{ult,emp}$ (psf)
	Type	ϕ (°)	c (psf)	d_{max} (inch)	T_f (lb/ft)	S_v (inch)			
DC-1	8	54	0	½	4,800	7⅝**	CMU	430	23,310
TF-1++	8	55	0	½	2,400	7⅝	CMU	320	20,487

ϕ = the peak friction angle, c = the cohesion, T_f = the MARV value of the wide width tensile strength, S_v = the spacing, E_o = the initial stress-strain ratio, and $q_{ult,emp}$ = the measured vertical capacity.
**Two courses of bearing bed reinforcement placed at the top of the PT.
++Technical difficulties resulted in unloading/reloading of the composite.

Table 16. Parametric study on reinforcement strength with well-graded aggregates.

Test No.	Backfill				Reinforcement		Facing	E_o (ksf)	$q_{ult,emp}$ (psf)
	Type	ϕ (°)	c (psf)	d_{max} (inch)	T_f (lb/ft)	S_v (inch)			
TF-2	21A	53	115	1	2,400	7⅝	CMU	710	25,260
TF-6++	21A	53	115	1	4,800	7⅝	CMU	750	43,763

ϕ = the peak friction angle, c = the cohesion, T_f = the MARV value of the wide width tensile strength, S_v = the spacing, E_o = the initial stress-strain ratio, and $q_{ult,emp}$ = the measured vertical capacity.
++Technical difficulties resulted in unloading/reloading of the composite.

DC-1 and TF-1 both tested similar open-graded aggregates (AASTHO No. 8s) at the same reinforcement spacing of 7⅝ inches, but DC-1 used a 4,800 lb/ft geotextile while TF-1 used a 2,400 lb/ft geotextile (table 15). The response indicates that the higher reinforcement strength

(4,800 lb/ft) produces a stiffer and stronger response than the lower reinforcement strength (2,400 lb/ft) for open-graded backfill. By doubling the reinforcement strength, the results indicate an increase by a factor of 1.14 for capacity and 1.34 for the initial stress-strain ratio.

Comparing the effect of reinforcement strength with a well-graded AASHTO A-1-a aggregate, with and without facing, it was found that increasing the ultimate reinforcement strength (MARV) by a factor of two from 2,400 lb/ft (TF-2) to 4,800 lb/ft (TF-6) at the same reinforcement spacing (S_v = 7⅝ inches) results in an increase in the measured capacity and initial stress-strain ratio by a factor of 1.73 and 1.06, respectively for CMU facing (table 16). When no facing is present, the same increase in reinforcement strength from 2,400 lb/ft (TF-3) to 4,800 lb/ft (TF-7) at a spacing of 7⅝ inches results in an increase in the measured capacity by a factor of 1.5. For open-graded aggregates, the percent increase in capacity is less than for the well-graded material tested which may be due to the increased cohesion and maximum density of the well-graded material, thus leading to higher soil shear strengths and increased stiffness properties.

6.6 EFFECT OF THE RELATIONSHIP BETWEEN REINFORCEMENT STRENGTH AND SPACING

The current AASHTO LRFD Bridge Design Specifications (2012) do not distinguish between MSE technology and closely-spaced GRS technology.[30] In AASHTO (2012), reinforcement spacing is linearly proportional to the reinforcement strength, leading engineers to prefer larger spaced systems with proportionally greater reinforcement strengths.[10] Research on closely spaced systems, however, indicates that reinforcement spacing plays a significantly larger role than the reinforcement strength.[5,11,25,31]

To investigate the relationship between the MARV wide width reinforcement tensile strength (T_f) and spacing (S_v), several PTs were designed to keep the same T_f/S_v ratios, both with (table 17) and without facing elements (table 18). The strength of the reinforcement was assumed to be the manufacturer supplied MARV (table 6). Within the data set of this study, there are three pairs of tests (with and without facing) at a constant T_f/S_v ratio (table 19). For a T_f/S_v ratio of 3,800 lb/ft^2, the load-test curves for the tests with facing are presented in figure 64 and the load-test curves for the tests without facing are presented in figure 65.

Table 17. Parametric study for 3,800 lb/ft^2 T_f/S_v ratio (with facing).

Test No.	Backfill				Reinforcement		Facing	E_o (ksf)	$q_{ult,emp}$ (psf)
	Type	ϕ (°)	c (psf)	d_{max} (in.)	T_f (lb/ft)	S_v (in.)			
TF-2	21A	53	115	1	2,400	7⅝	CMU	710	25,260
TF-9	21A	53	115	1	4,800	15¼	CMU	550	22,310
TF-14	21A	53	115	1	3,600	11¼	CMU	460	23,562

ϕ = the peak friction angle, c = the cohesion, T_f = the MARV value of the wide width tensile strength, S_v = the spacing, E_o = the initial stress-strain ratio, and $q_{ult,emp}$ = the measured vertical capacity.

Table 18. Parametric study for 3,800 lb/ft^2 T_f/S_v ratio (with no facing).

Test No.	Backfill				Reinforcement		Facing	E_o (ksf)	$q_{ult,emp}$ (psf)
	Type	ϕ (°)	c (psf)	d_{max} (in.)	T_f (lb/ft)	S_v (in.)			
TF-3	21A	53	115	1	2,400	7⅝	no CMU	330	17,491
TF-10	21A	53	115	1	4,800	15¼	no CMU	260	10,330
TF-13	21A	53	115	1	3,600	11¼	no CMU	260	12,960

ϕ = the peak friction angle, c = the cohesion, T_f = the MARV value of the wide width tensile strength, S_v = the spacing, E_o = the initial stress-strain ratio, and $q_{ult,emp}$ = the measured vertical capacity.

Table 19. T_f/S_v ratios for each PT.

No.	T_f/S_v					
	3,800 lb/ft^2		4,400 lb/ft^2		7,600 lb/ft^2	
	CMU Facing	No Facing	CMU Facing	No Facing	CMU Facing	No Facing
1	TF-2	TF-3	TF-12	TF-11	TF-6	TF-7
2	TF-9	TF-10				TF-8
3	TF-14	TF-13			DC-1	
4	TF-1				DC-2	
5					DC-3	
6					DC-4	
7					DC-5	

Note: The table shows which sets of tests were performed at a particular T_f/S_v ratio, thus some cells are blank.

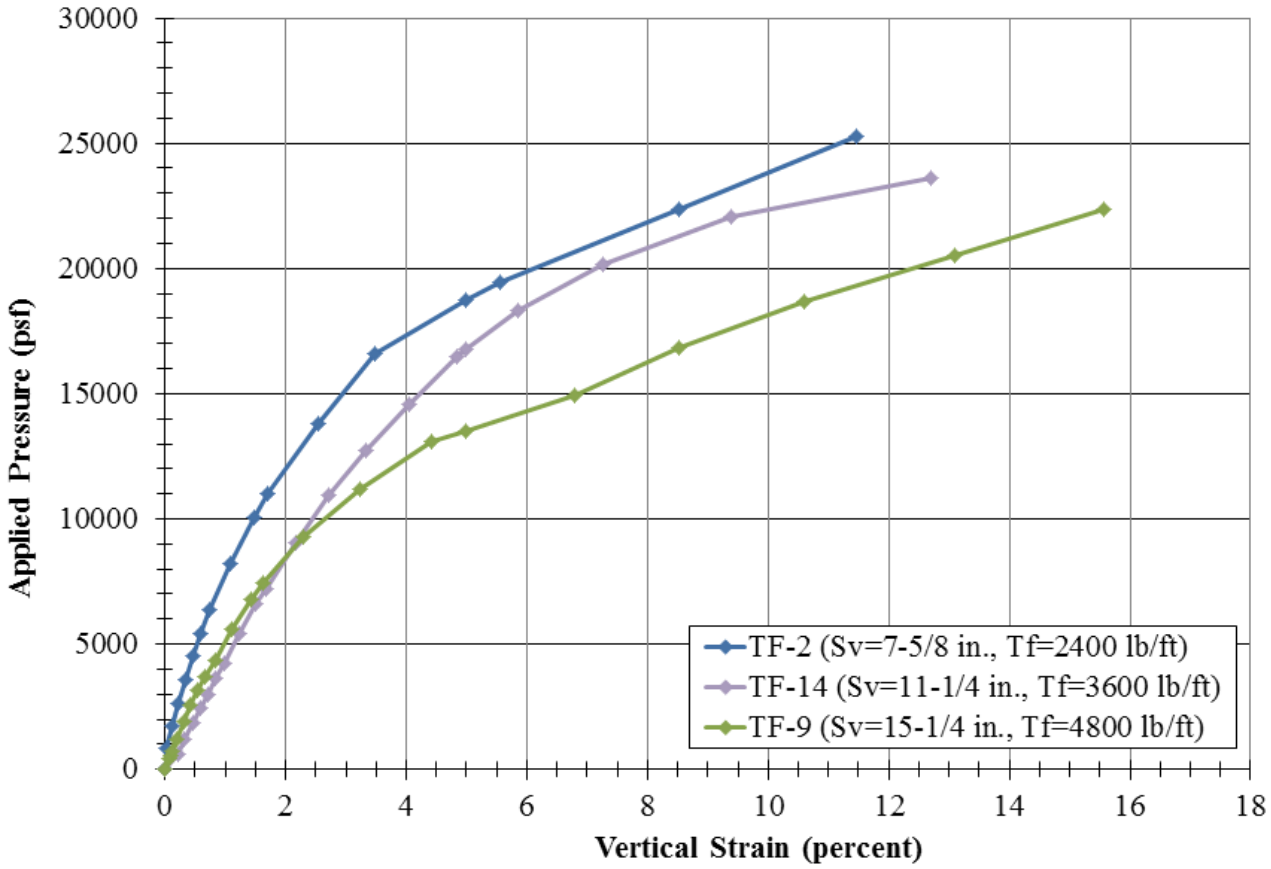

Figure 64. Graph. Stress-strain curves for PTs with CMUs at T_f/S_v = 3,800 psf

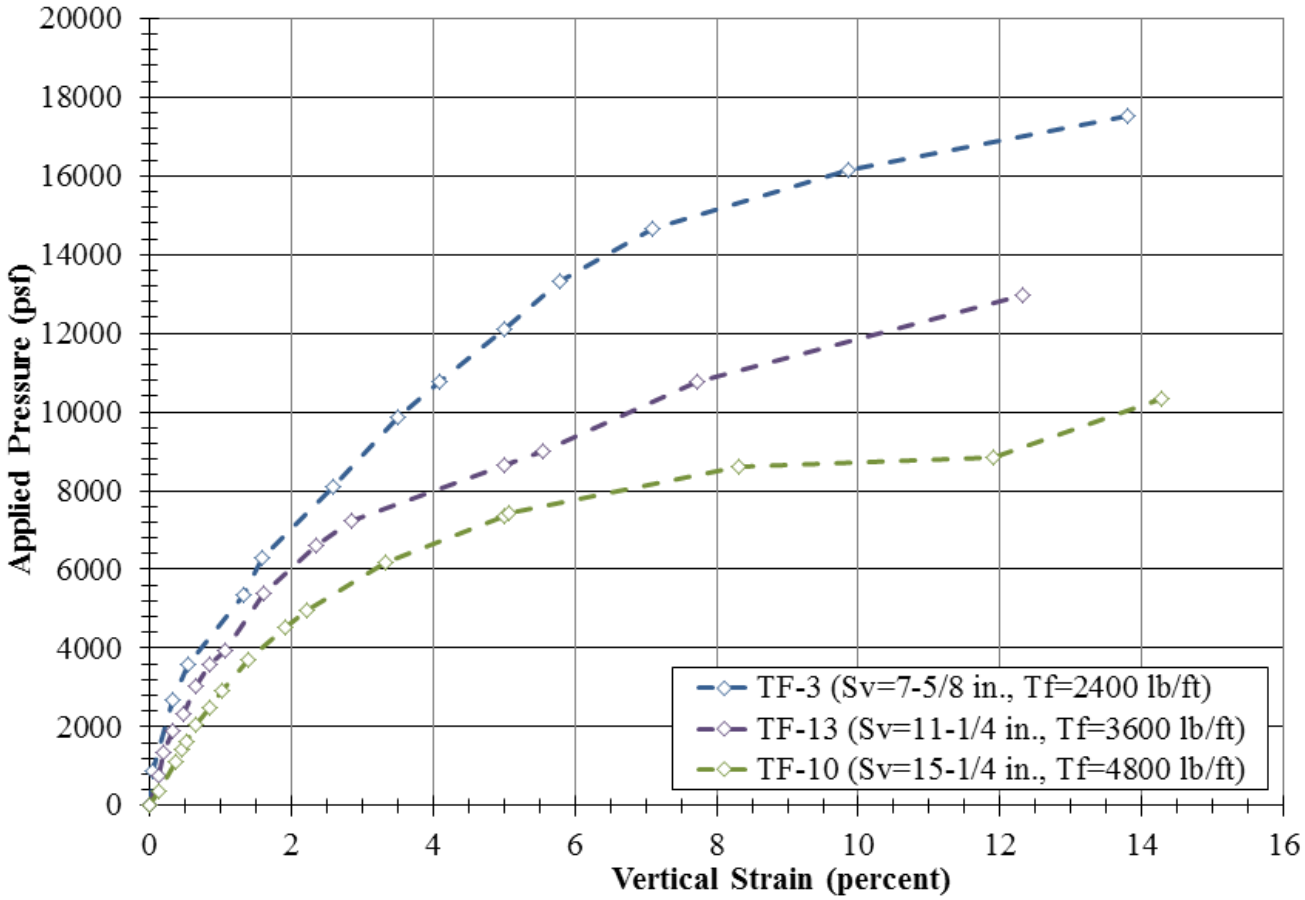

Figure 65. Graph. Stress-strain curves for PTs with no CMU facing at T_f/S_v = 3,800 psf.

For a T_f/S_v ratio of 3,800 lb/ft^2, as the reinforcement spacing increased, the vertical capacity decreased for the same T_f/S_v ratio, whether a CMU facing was absent (figure 66) or present (figure 67). Contrary to MSE design theory, as reinforcement strength increased, while increasing the spacing proportionally, the vertical capacity decreased, whether a CMU facing was absent (figure 68) or present (figure 69).

This suggests that the relationship between reinforcement strength and spacing is not proportional to capacity as outlined in current MSE design; a GRS abutment with a given T_f and S_v will not have the same strength figure as a GRS abutment with twice the strength ($2T_f$) and reinforcement spacing ($2S_v$).

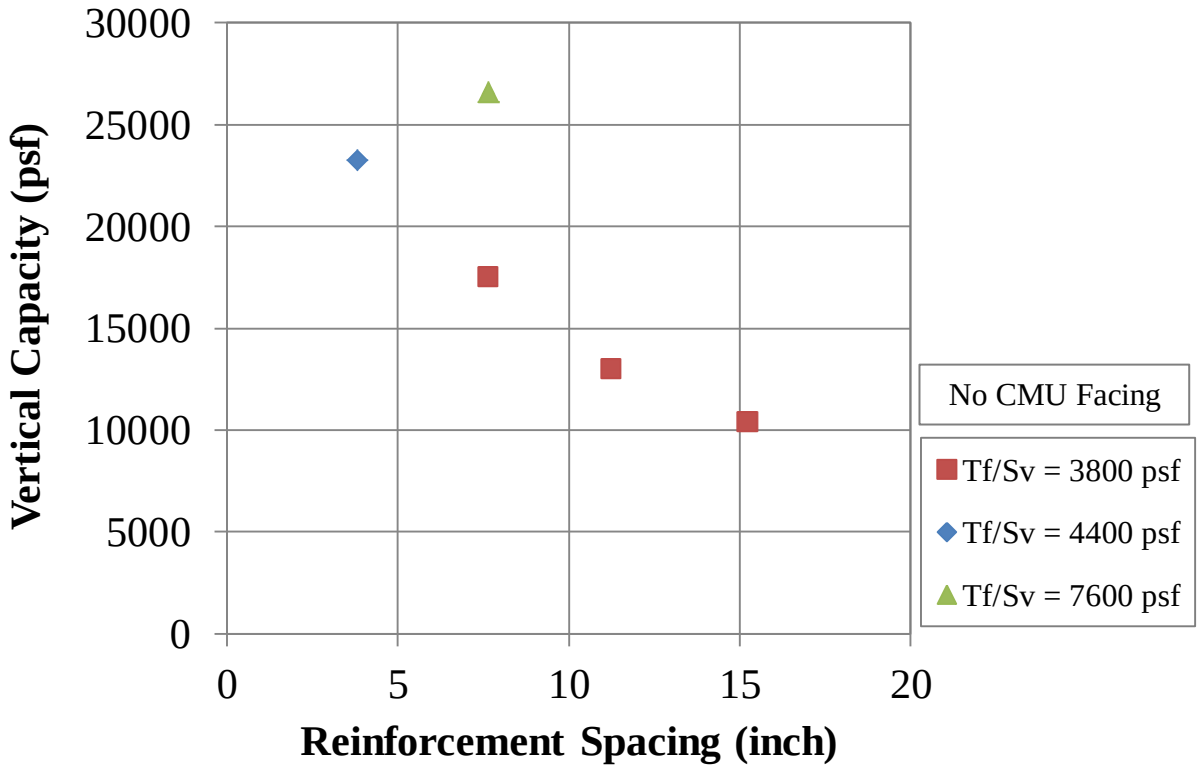

Figure 66. Graph. Capacity of GRS with no CMU facing at various reinforcement spacing for different T_f/S_v ratios.

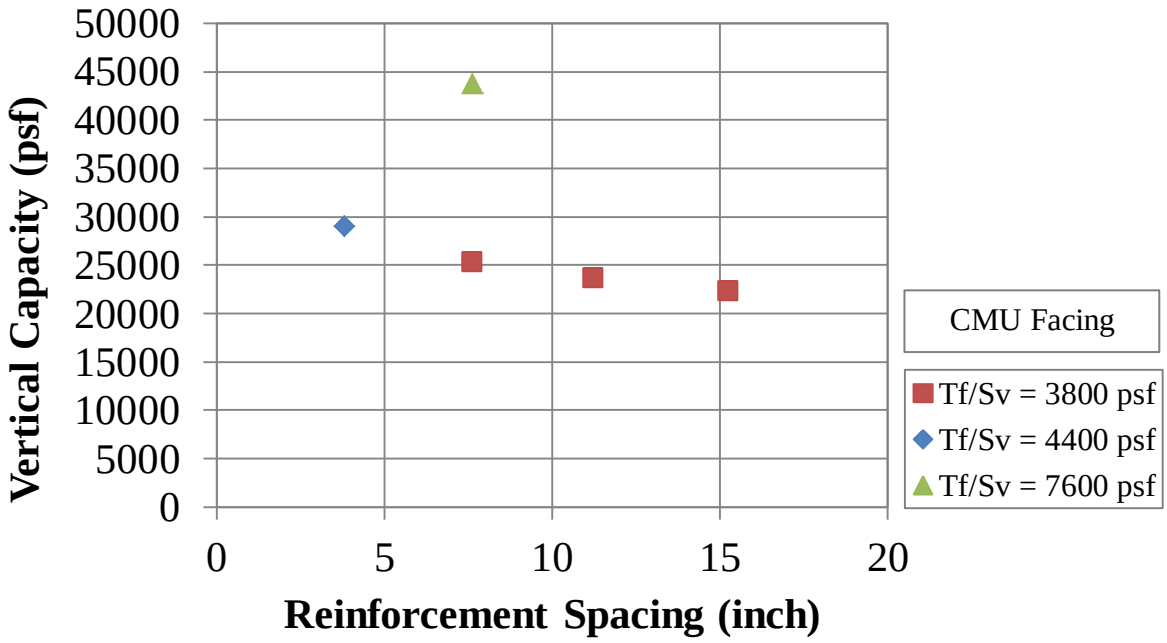

Figure 67. Graph. Capacity of GRS with CMU facing at various reinforcement spacing for different T_f/S_v ratios.

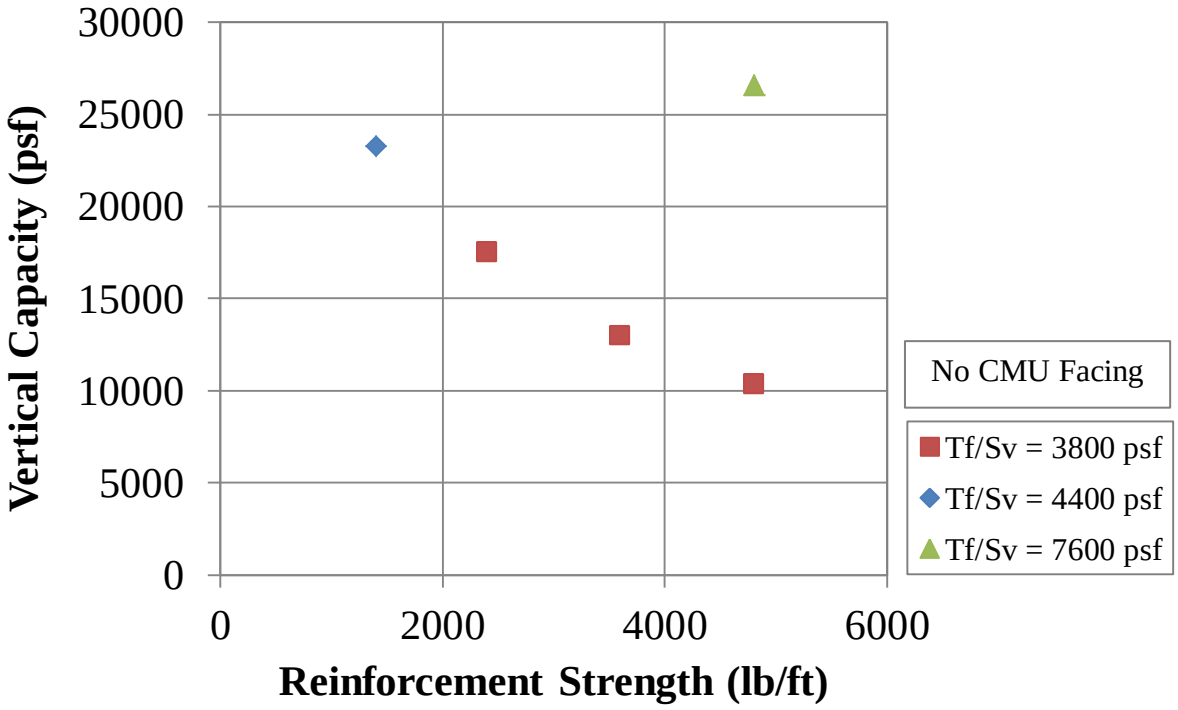

Figure 68. Graph. Capacity of GRS with no CMU facing at various reinforcement strength for different T_f/S_v ratios.

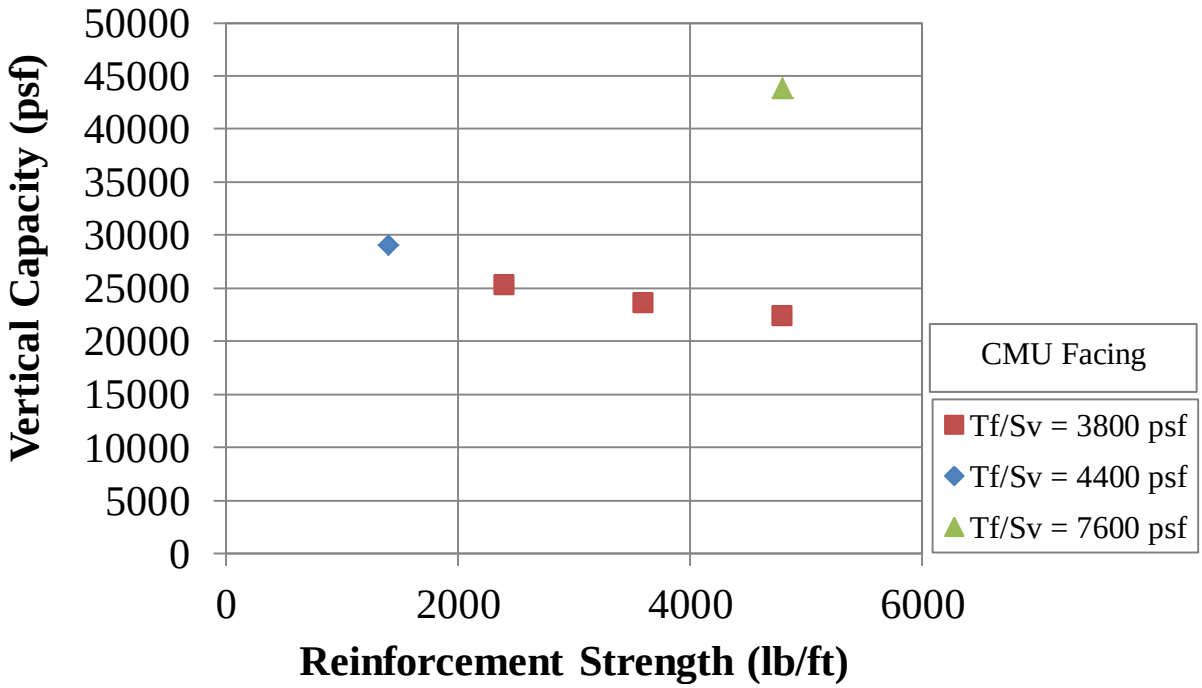

Figure 69. Graph. Capacity of GRS with CMU facing at various reinforcement strength for different T_f/S_v ratios.

At the same T_f/S_v ratio of 3,800 lb/ft^2, increasing the reinforcement spacing and reinforcement strength by a factor of two from 7⅝ to 15¼ inches and 2,400 to 4,800 lb/ft, respectively, resulted in a reduction of the capacity by a factor of 0.9 and 0.6 for CMU facing and no facing, respectively. According to the design theory employed by AASHTO (2012), there would be no reduction in capacity.[10] The relationship between reinforcement strength and spacing is therefore not directly proportional. The results are similar to those reported by Pham (2009).[25]

6.7 EFFECT OF FACING

In the GRS-IBS Interim Implementation Guide, the effect of the facing is ignored in determining the capacity of a GRS composite (i.e., confining stress is equal to zero in figure 8).[1] The PTs provide insight on the magnitude of the impact CMU facing elements have on the performance of GRS composites. Of the nineteen tests included in this study, there were five pairs of identical GRS composites constructed with the well-graded aggregate; each pair consisted of one test with a frictionally connected CMU facing and another test without the CMU facing (table 21). The stress-strain response for each pair is shown in figure 70 through figure 74.

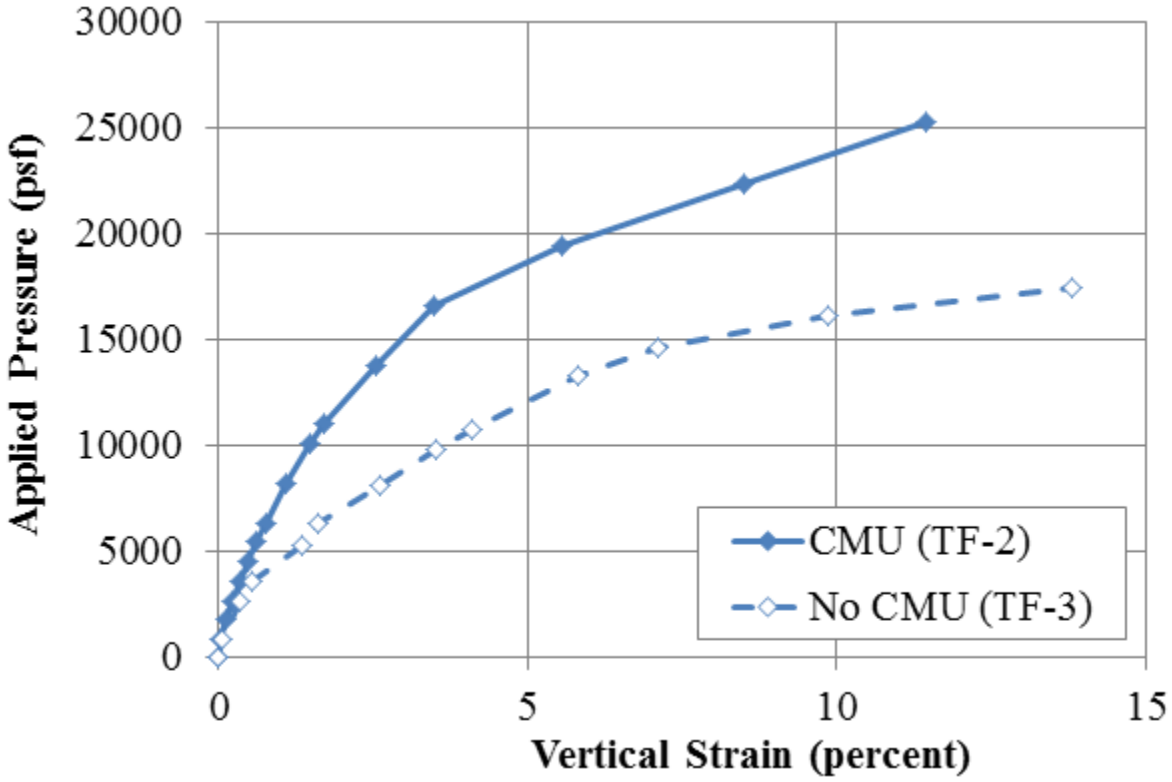

Figure 70. Graph. Stress-strain response for TF-2 (CMU facing) and TF-3 (no CMU facing) with S_v = 7⅝ inches and T_f = 2,400 lb/ft.

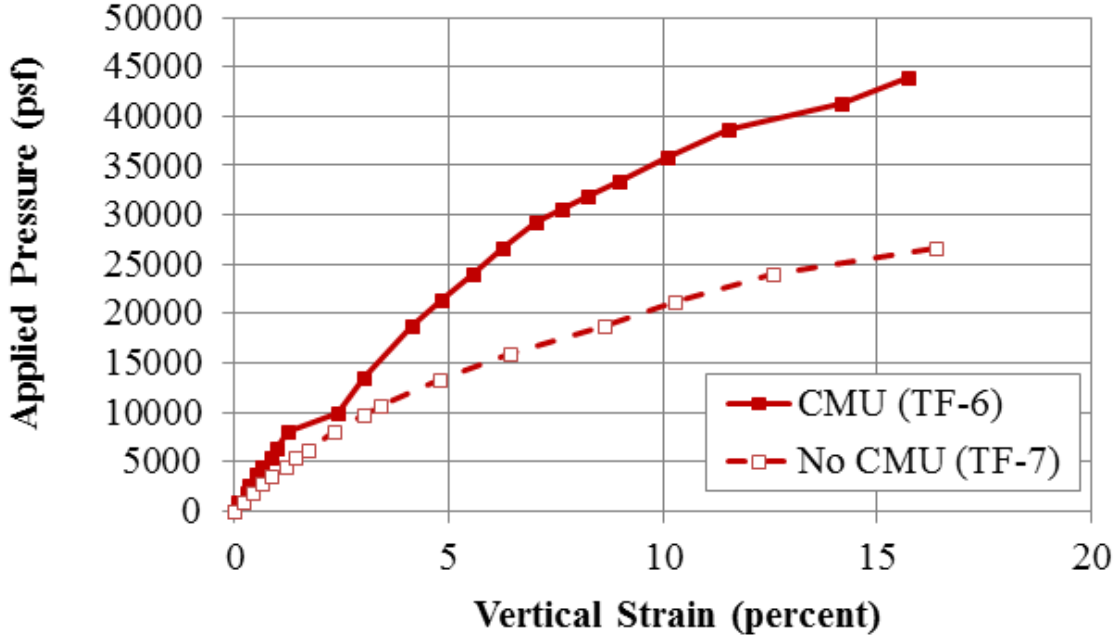

Figure 71. Stress-strain response for TF-6 (CMU facing) and TF-7 (no CMU facing) with S_v = 7⅝ inches and T_f = 4,800 lb/ft.

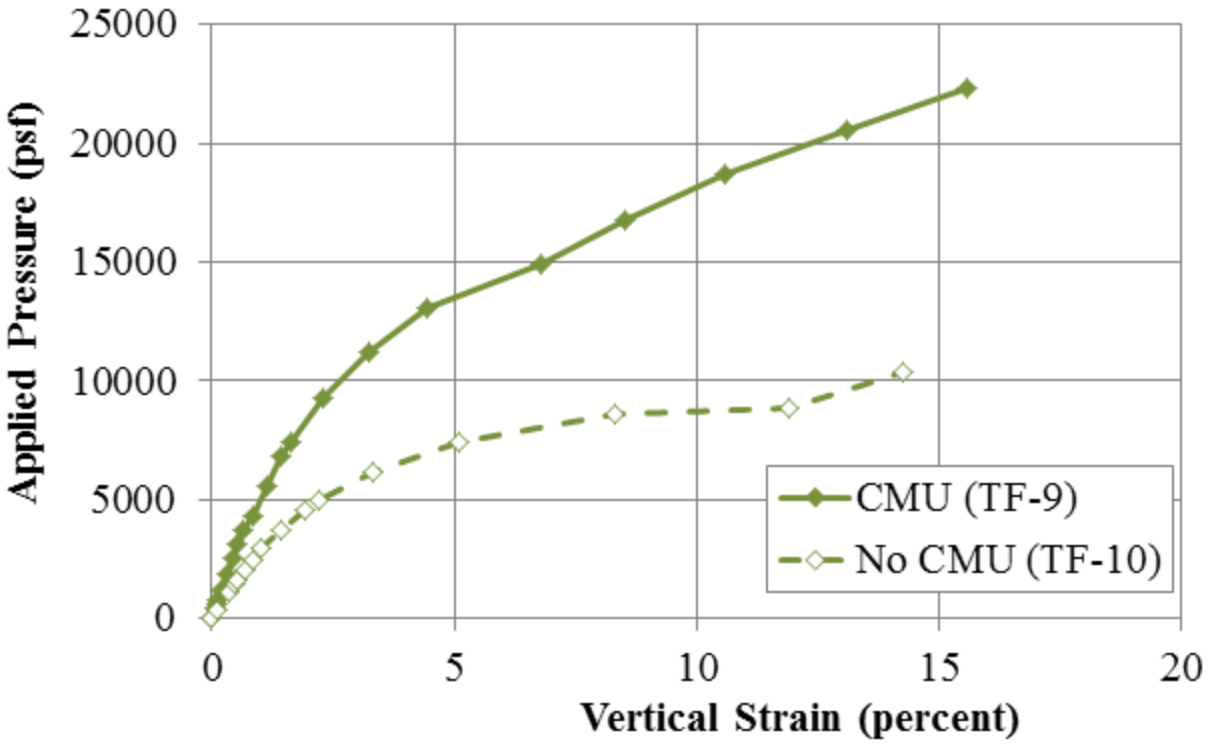

Figure 72. Graph. Stress-strain response for TF-9 (CMU facing) and TF-10 (No CMU facing) with S_v = 15¼ inches and T_f = 4,800 lb/ft.

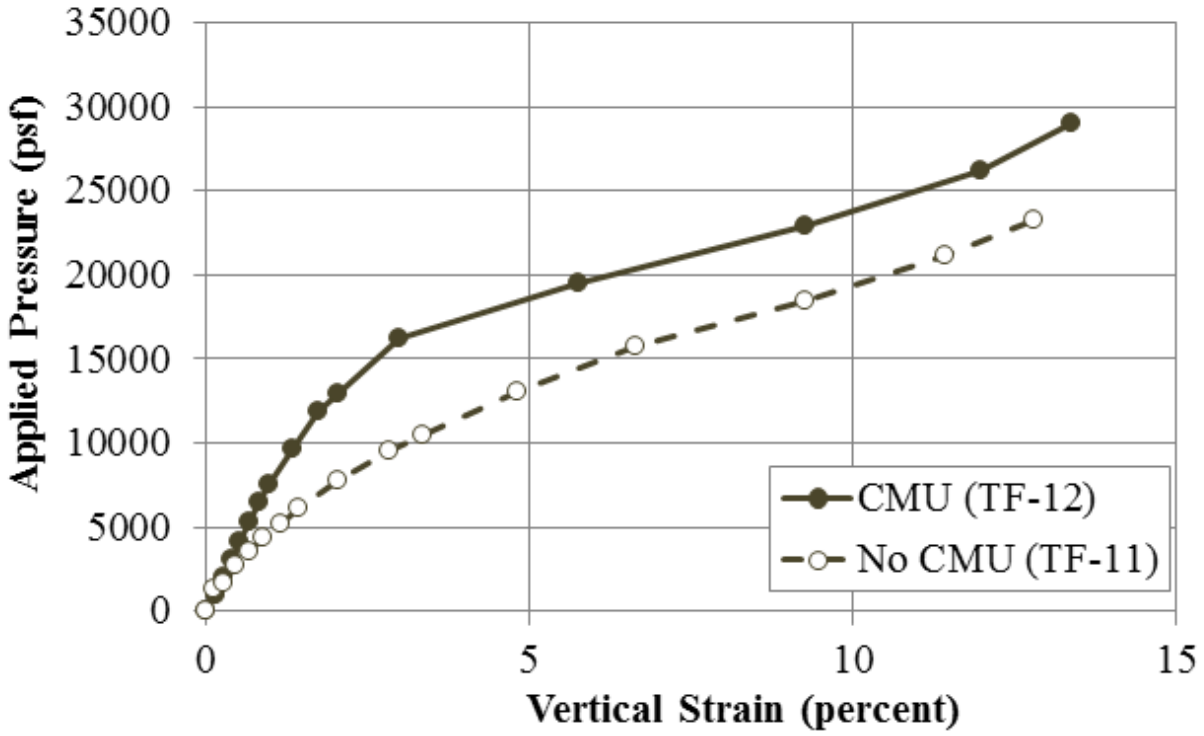

Figure 73. Graph. Stress-strain Response for TF-12 (CMU facing) and TF-11 (no CMU facing) with S_v = 3-13/16 inches and T_f = 1,400 lb/ft.

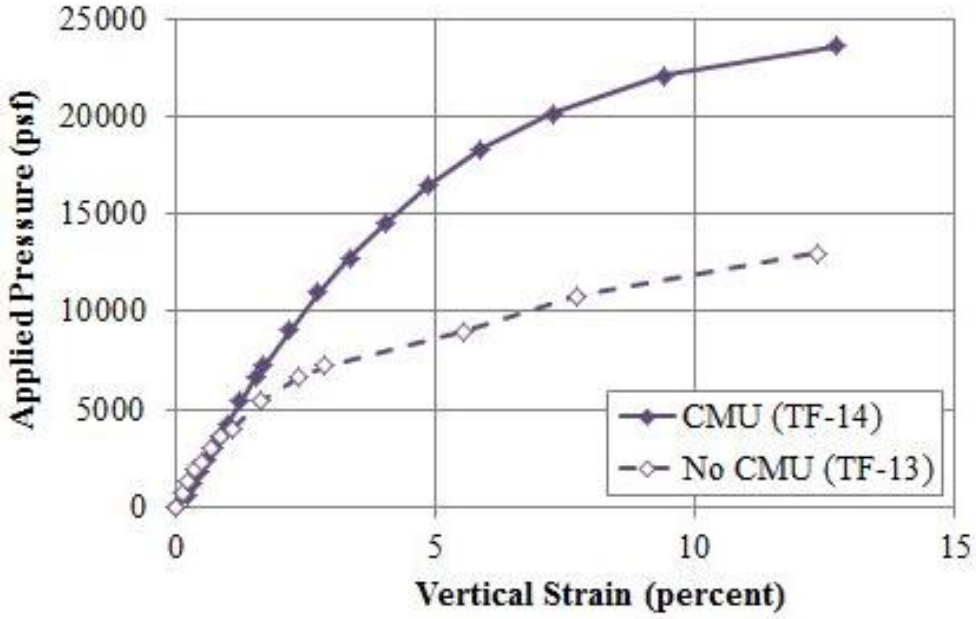

Figure 74. Graph. Stress-strain response for TF-14 (CMU facing) and TF-13 (no CMU facing) with S_v = 11¼ inches and T_f = 3,600 lb/ft.

The frictionally connected CMU facing has an impact on the performance of GRS; it provides confinement, leading to a stiffer response and an increased capacity compared to a GRS composite with no facing element (table 20). In addition, at the current service stress limit (applied stress, q, of 4,000 psf), the ratio of service vertical strain with no facing to service vertical strain with a CMU facing ranges from 1.2 to 2.2 (table 21). The largest impact was for the 15⅝-inch spaced GRS composite (TF-9 and TF-10). At ultimate failure, the ratio is considerably closer, ranging from 0.8 to 1.2.

Table 20. Effect of CMU facing on stiffness and capacity.

Test	Facing	S_v (inch)	T_f/S_v (psf)	Eo (ksf)	$\frac{E_{o,CMU}}{E_{o,no\ CMU}}$	$q_{ult,emp}$ (psf)	$\frac{q_{ult,\ emp\ CMU}}{q_{ult,\ emp\ no\ CMU}}$
TF-2	CMU	7⅝	3,800	710	2.15	25,260	1.44
TF-3	None			330		17,491	
TF-6	CMU	7⅝	7,600	750	2.34	43,763	1.65
TF-7	None			320		26,546	
TF-9	CMU	15¼	3,800	550	2.12	22,310	2.16
TF-10	None			260		10,330	
TF-12	CMU	3-13/16	4,400	810	2.08	29,030	1.25
TF-11	None			390		23,249	
TF-14	CMU	11¼	3,800	460	2.09	23,562	1.82
TF-13	None			220		12,960	

S_v = the reinforcement spacing, T_f = the MARV value of the wide width tensile strength, E_o = the initial stress-strain ratio, $E_{o,CMU}$ = the initial stress-strain ratio for tests with CMU facing, $E_{o,\ no\ CMU}$ = the initial stress-strain ratio for tests without any facing, $q_{ult,emp}$ = the measured vertical capacity, $q_{ult,emp\ CMU}$ = the measured failure pressure for tests with CMU facing, and $q_{ult,emp\ no\ CMU}$ = the measured failure pressure for tests without any facing.

Table 21. Effect of CMU facing on strain.

Test	Facing	S_v (inch)	T_f/S_v (psf)	$\varepsilon_{@q=4000psf}$ (%)	$\frac{\varepsilon_{@q=4000psf,\ no\ CMU}}{\varepsilon_{@q=4000psf,\ CMU}}$	$\varepsilon_{@qult}$ (%)	$\frac{\varepsilon_{@qult,\ no\ CMU}}{\varepsilon_{@qult,\ CMU}}$
TF-2	CMU	7⅝	3,800	0.39	1.84	11.46	1.20
TF-3	None			0.73		13.80	
TF-6	CMU	7⅝	7,600	0.55	1.86	15.70	0.80
TF-7	None			1.02		12.50	
TF-9	CMU	15¼	3,800	0.74	2.16	15.60	0.91
TF-10	None			1.59		14.27	
TF-12	CMU	$3^{13}/_{16}$	4,400	0.50	1.59	13.37	0.96
TF-11	None			0.79		12.79	
TF-14	CMU	11¼	3,800	0.93	1.17	12.69	0.97
TF-13	None			1.09		12.32	

S_v = the reinforcement spacing, T_f = the MARV value of the wide width tensile strength, $\varepsilon_{@q=4000psf}$ = the measured strain at an applied load of 4,000 psf, and $\varepsilon_{@qult}$ = the measured strain at failure.

From table 20, the facing more than doubles the initial stress-strain ratio as compared to the PTs without any facing. In terms of capacity, the facing plays the biggest and smallest role for the largest spaced (S_v = 15¼ inches) and the closest spaced ($S_v = 3^{13}/_{16}$ inches) system tested, respectively. The design assumption to not include the effect of confinement from the face in determining the capacity and required reinforcement strength is therefore conservative.[(1)]

While the magnitude of strain at failure is similar for a given GRS composite tested with or without a facing (table 21), the ultimate capacity is increased when a facing element is present (table 20 and figure 75). For the five pairs of tests conducted at TF (table 21), including the CMU facing produced an improved ultimate capacity between 1.25 and 2.2 times greater than the GRS composite without any facing (a similar trend to the strain at the current 4,000 psf service limit).

For the same T_f/S_v ratio of 3,800 lb/ft^2, there is a linear relationship between the reinforcement spacing (S_v) and the ratio of capacity with CMU facing ($q_{ult,emp\ CMU}$) to the capacity without a facing ($q_{ult,emp\ no\ CMU}$) (figure 75). Similarly, there is a linear relationship with reinforcement strength (figure 76). To further investigate this, additional tests should be conducted at other T_f/S_v ratios (4,400 and 7,600 psf) and at larger reinforcement spacing.

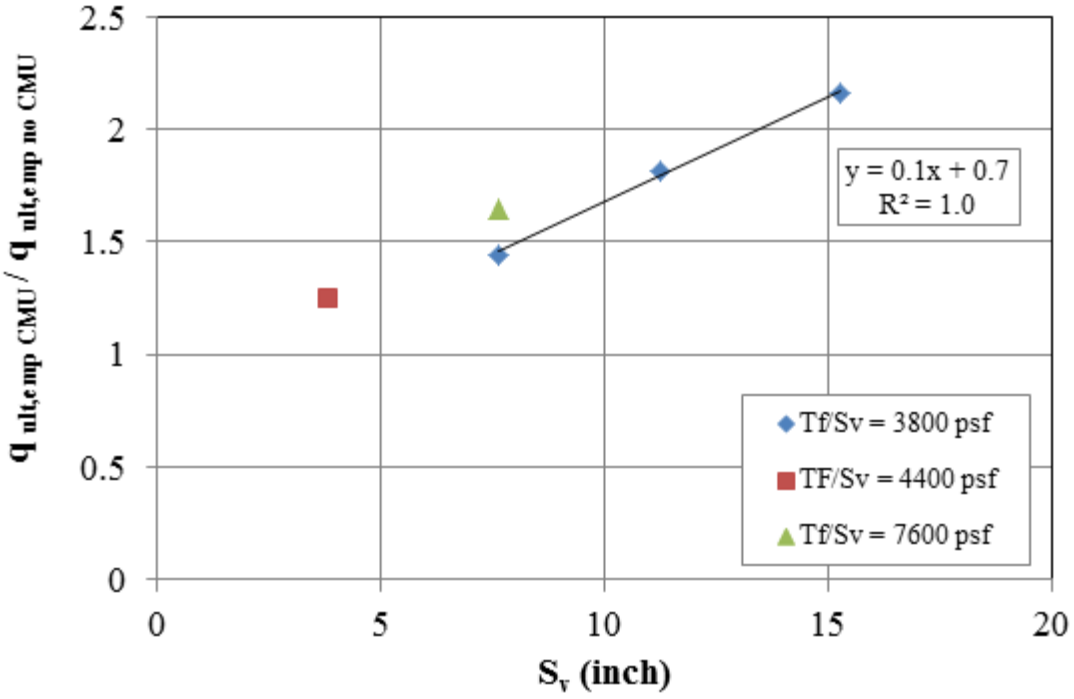

Figure 75. Graph. Effect of CMU facing on ultimate capacity as a function of reinforcement spacing.

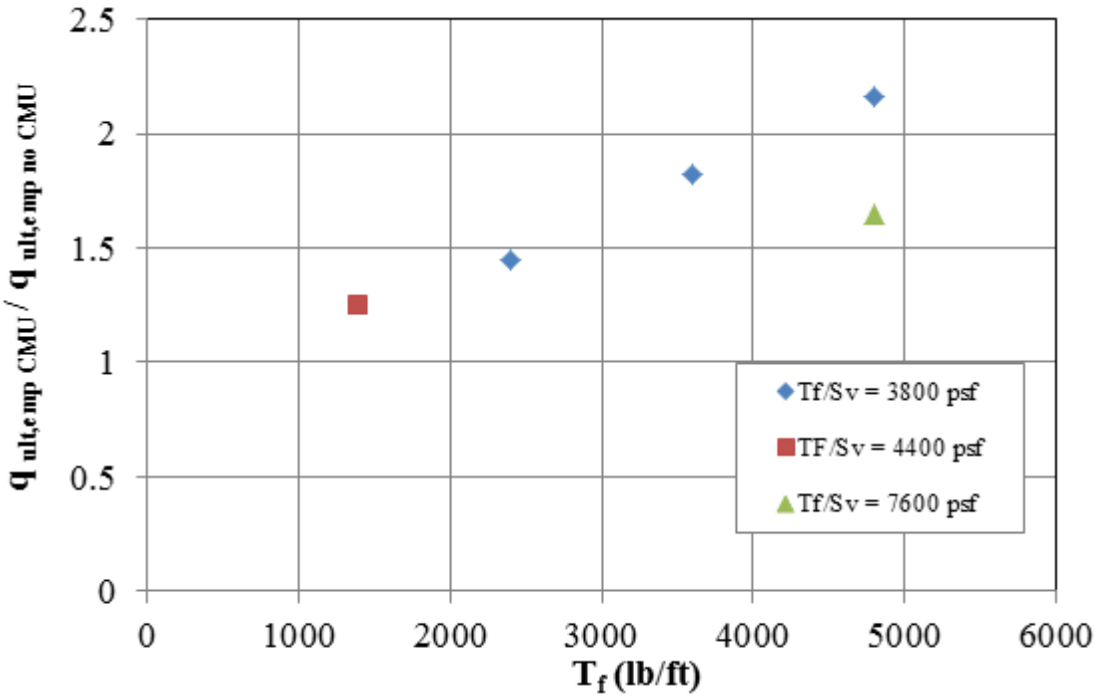

Figure 76. Graph. Effect of CMU facing on ultimate capacity as a function of reinforcement strength.

Using figure 8, the confining stress due to the facing elements can be back-calculated using the measured ultimate capacity from the PTs (figure 77). The results indicate that as reinforcement spacing increases, the effect of the facing element on the capacity is more pronounced. Note that the confining stress changes throughout the PT with applied pressure; figure 77 represents only the back-calculated confining stress at failure.

Using the equation developed by Wu et al. (2010) (figure 11), the estimated confining stress for the CMU blocks is about 72 psf, lower than that estimated at failure (figure 77).[11] The bulk unit weight and depth of the CMU is 150 pcf and 7⅝ inches, respectively; the interface friction angle between the geotextile and the CMU block was assumed equal to 37°, based on connection strength testing performed at TFHRC.[32] This simple method of determining the confining stress was used when comparing the measured capacity for each test to the estimated capacity for each test using figure 8.

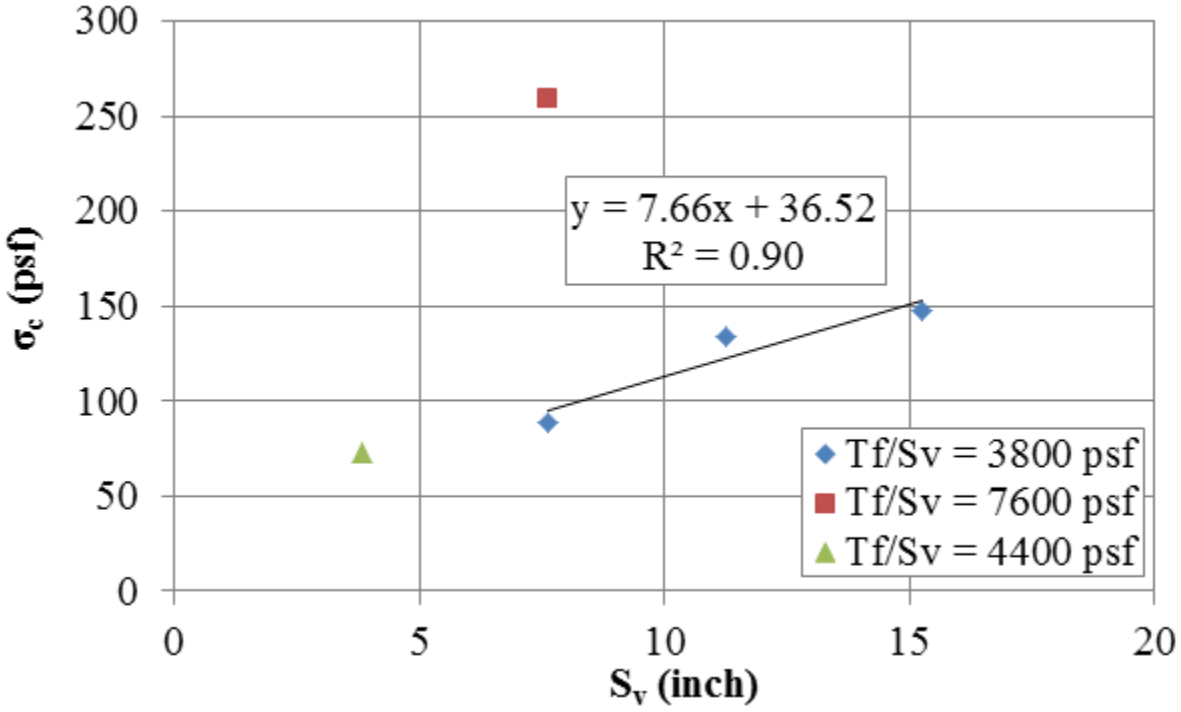

Figure 77. Graph. Calculated confining pressure due to CMU facing at the ultimate capacity.

7. APPLICATIONS OF PERFORMANCE TESTING TO DESIGN

The load test results from GRS performance testing have been used in the design of GRS abutments. Designers can use the empirical results to estimate capacity (strength limit) and deformation (service limit) of the GRS abutment, needed in the internal stability design.[1] In addition, the database of results can be used to validate the GRS capacity equation (figure 8) and calibrate a more accurate LRFD resistance factor.

7.1 DESIGN DATABASE

The results indicate that, based on the current limitations set forward by FHWA for GRS abutments of a 4,000-psf service pressure and a 0.5-percent vertical deformation service limit, seven GRS composites tested in this study may meet the strength and service limits (table 22).[1] The service limit pressure at a vertical strain of 0.5 percent is for the dead load only since live loads have not been found to impact the total strain for in-service GRS-IBS structures.[5] Note that only three GRS composites tested in this study meet both the design limits and the material specifications ($T_f \geq$ 4,800 lb/ft, $d_{max} \geq$ ½ inches); however, based on the results of this study, consideration should perhaps be given to amend the criteria in future design guidance.

Table 22. PTs meeting GRS strength and service limit design criteria.

	GRS Composite				Design Strength Limit			Service Limit
					ASD		LRFD	
Test No.	ϕ (°)	d_{max} (inch)	S_v (inch)	T_f (lb/ft)	$q_{@\varepsilon=5\%}$ (psf)	$q_{@\varepsilon=5\%}$ /FS (psf)	Φ_{cap} ($q_{@\varepsilon=5\%}$) (psf)	$q_{@\varepsilon=0.5\%}$ (psf)
DC-1	54	½	7⅝	4,800	19,983	5,709	8,992	3,065
DC-2	46	¾	7⅝	4,800	19,399	5,543	8,730	2,171
DC-4	49	1	7⅝	4,800	17,350	4,957	7,808	2,212
TF-2	53	⅜	7⅝	2,400	18,711	5,346	8,420	4,759
TF-6	53	½	7⅝	4,800	22,007	6,288	9,903	3,704
TF-12	53	½	$3^{13}/_{16}$	1,400	18,573	5,307	8,358	4,028
TF-14	53	½	$3^{13}/_{16}$	1,400	16,748	4,785	7,537	2,037

ϕ = the peak friction angle, d_{max} = the maximum aggregate size, S_v = the reinforcement spacing, T_f = the MARV value of the wide width tensile strength, $q_{@\varepsilon=5\%}$ = the stress at 5-percent vertical strain from a corresponding PT, FS = the factor of safety (equal to 3.5), Φ_{cap} = the resistance factor for capacity (equal to 0.45), $q_{@\varepsilon=0.5\%}$ = the service stress at 0.5-percent vertical strain from a corresponding PT, ASD = Allowable Stress Design, and LRFD = load and resistance factor design.

7.2 STRENGTH LIMIT

7.2.1 Analytical

PT results can be used to validate the ultimate capacity equation (figure 8). Figure 78 illustrates the comparison between the measured capacity from various PTs and the calculated capacity from figure 8. Note that figure 78 includes results from additional sources of research.[1,4,8,11,33,34] Based on the results of the PTs presented in this report and plotting the bias against the standard normal variable (figure 79 and table 23), the mean bias is 0.88 (i.e., the bias at a standard normal variable of zero) with a coefficient of variation (COV) of about 35 percent. Including other results from the literature, the average bias is 0.95 with a COV of about 32 percent (figure 80 and table 24).

The mean bias values near unity and low COV values for all of the GRS composite tests (table 24) indicate good agreement between the GRS capacity equation (figure 8) and the measured results. Note that the measured results used for comparison were taken at failure of the composite, not at a design limit of 5 percent vertical strain, as will be discussed later in the empirical method of design (see section 7.2.2). This may change the level of reliability between the analytical method and the empirical method of design, since both have equal factors of safety of 3.5.[1] A full LRFD calibration needs to be conducted to determine a more reliable resistance factor for each strength limit design method.

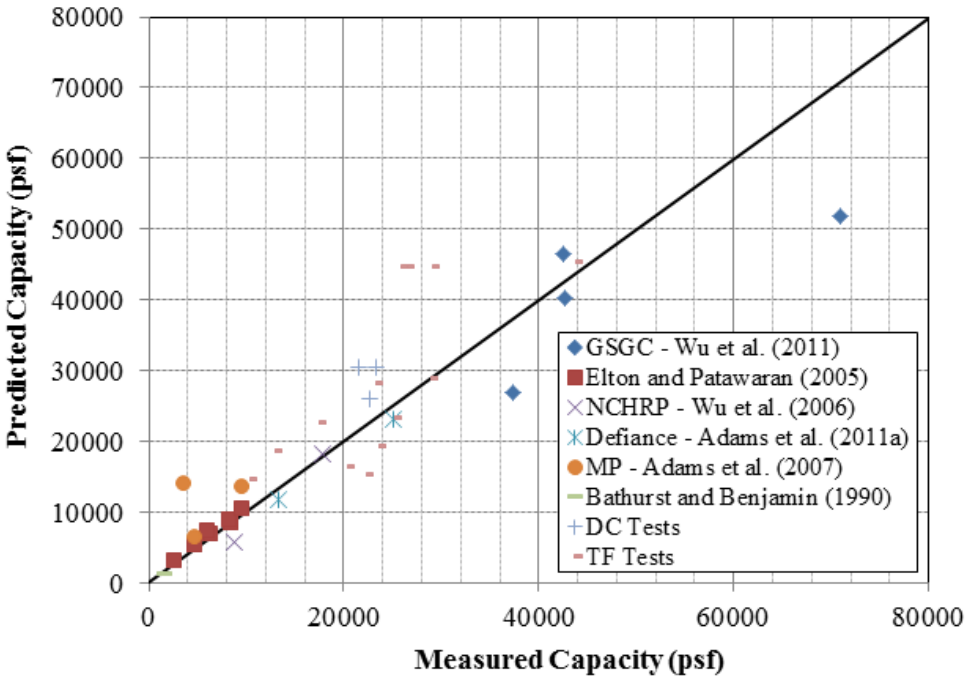

Figure 78. Graph. Comparison of predicted capacity and measured capacity.

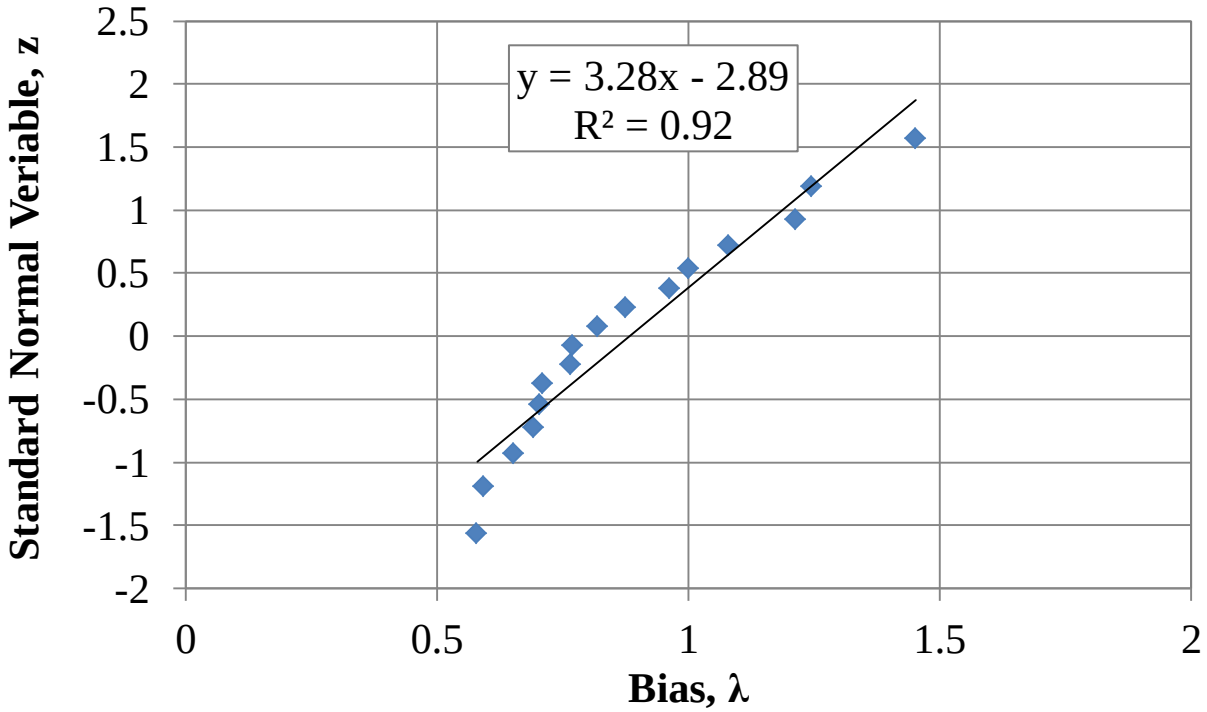

Figure 79. Graph. Cumulative distribution function plot for DC and TF PTs.

Table 23. Predicted and measured vertical capacity for DC and TF PTs.

Test	Measured $q_{ult,emp}$ (psf)	Predicted $q_{ult,an,c}$ (psf)	Bias, λ Measured / Predicted	Standard Normal Variable, z
DC-1	23,310	30,439	0.77	-0.32
DC-2	22,709	25,952	0.88	0.16
DC-3	N/A	40,812	N/A	N/A
DC-4	N/A	17,078	N/A	N/A
DC-5	21,539	30,439	0.71	-0.49
TF-1	20,487	16,447	1.25	1.15
TF-2	25,260	23,403	1.08	0.67
TF-3	17,491	22,741	0.77	-0.16
TF-4	N/A	44,786	N/A	N/A
TF-5	25,920	44,786	0.58	-1.56
TF-6	43,763	45,448	0.96	0.38
TF-7	26,546	44,786	0.59	-1.19
TF-8	29,134	44,786	0.65	-0.93
TF-9	22,310	15,369	1.45	1.56
TF-10	10,330	14,707	0.70	-0.54
TF-11	23,249	28,348	0.82	0.07
TF-12	29,030	29,001	1.00	0.54
TF-13	12,960	18,764	0.69	-0.72
TF-14	23,562	19,426	1.21	0.93
			Mean Bias	0.88
			Standard Deviation	0.30
			Coefficient of Variation (percent)	0.35

N/A = Not applicable, did not fail the composite.

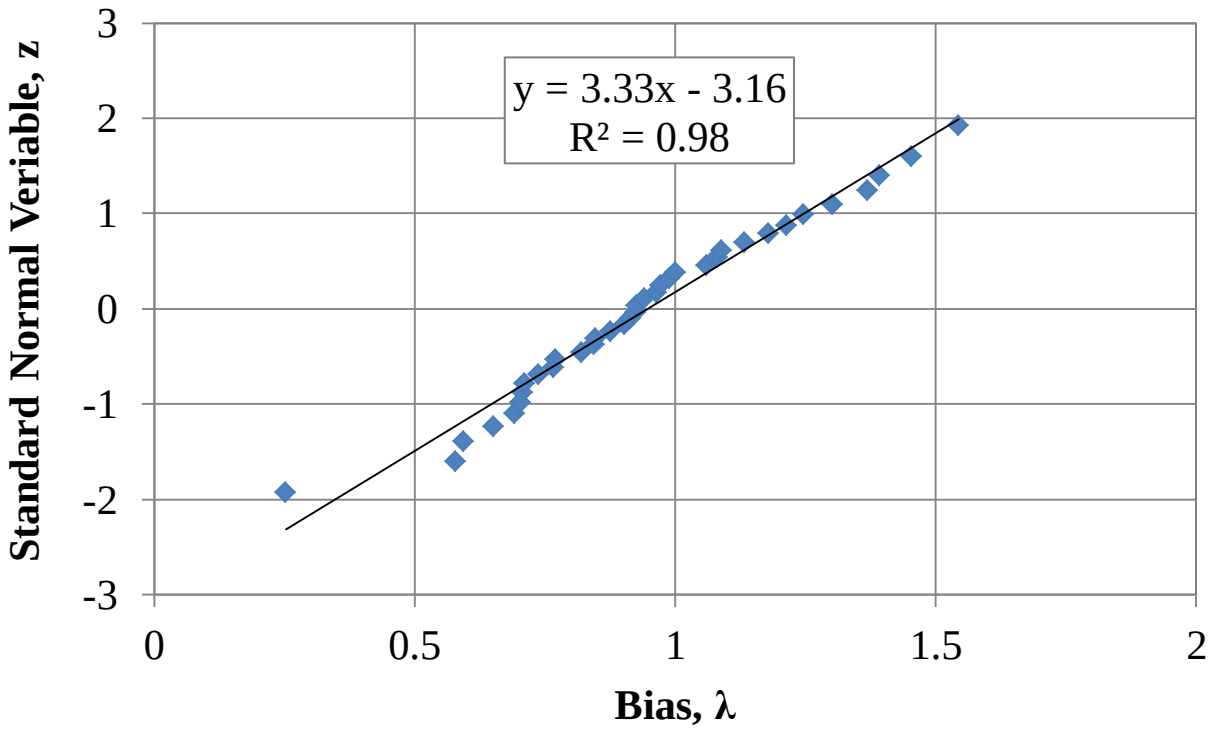

Figure 80. Graph. Cumulative distribution function plot for all GRS composite tests.

Table 24. Predicted and measured vertical capacity for all GRS composite tests.

Test	Measured $q_{ult,emp}$ (psf)	Predicted $q_{ult,an,c}$ (psf)	Bias, λ Measured / Predicted	Standard Normal Variable, z	Reference No.
GSGC 2	70,957	51,841	1.37	1.24	11
GSGC 3	42,574	40,207	1.06	0.46	
GSGC 4	37,252	26,795	1.39	1.40	
GSGC 5	42,449	46,485	0.91	-0.10	
Elton 1	4,805	5,324	0.90	-0.17	8
Elton 2	2,695	3,178	0.85	-0.31	
Elton 3	6,392	6,909	0.93	0.03	
Elton 4	6,100	7,226	0.84	-0.38	
Elton 5	8,398	8,495	0.99	0.31	
Elton 6	8,293	8,812	0.94	0.10	
Elton 7	9,589	10,397	0.92	-0.03	
NCHRP 1	8,356	5,685	1.54	1.93	33
NCHRP 2	17,757	18,287	0.97	0.24	
Defiance 1	13,370	11,797	1.13	0.70	1
Defiance 2	25,068	23,030	1.09	0.61	
Bathurst	1,670	1,283	1.30	1.10	34

MP A	4,696	6,371	0.74	-0.70	4
MP B	3,548	14,044	0.25	-1.93	
MP C	9,600	13,493	0.71	-0.79	
DC-1	23,310	30,439	0.77	-0.32	N/A
DC-2	22,709	25,952	0.88	0.16	
DC-5	21,539	30,439	0.71	-0.49	
TF-1	20,487	16,447	1.25	1.15	
TF-2	25,260	23,403	1.08	0.67	
TF-3	17,491	22,741	0.77	-0.16	
TF-5	25,920	44,786	0.58	-1.56	
TF-6	43,763	45,448	0.96	0.38	
TF-7	26,546	44,786	0.59	-1.19	
TF-8	29,134	44,786	0.65	-0.93	
TF-9	22,310	15,369	1.45	1.56	
TF-10	10,330	14,707	0.70	-0.54	
TF-11	23,249	28,348	0.82	0.07	
TF-12	29,030	29,001	1.00	0.54	
TF-13	12,960	18,764	0.69	-0.72	
TF-14	23,562	19,426	1.21	0.93	
			Mean Bias	0.95	
			Standard Deviation	0.30	
			Coefficient of Variation (percent)	0.32	

N/A = not applicable, no reference number is associated with a test since results are being reported for the first time in this report.

7.2.2 Empirical

The strength design limit for capacity is defined as the stress at which the GRS composite fails (meaning it cannot sustain any additional load) or strains 5 percent vertically, whichever occurs first. To relate this to the ultimate capacity and to non-dimensionalize the results, the stress-strain curves were normalized by the ultimate capacity of the particular GRS composite for all of the PTs taken to failure (figure 81). The 5-percent vertical strain limit can significantly reduce the allowable stress placed on a GRS composite; figure 82 shows that at 5-percent strain, the applied pressure is between 50 and 85 percent of the measured ultimate capacity (table 8).

Along with the additional factor of safety of 3.5, using 5-percent vertical strain as a design strength limit for the empirical internal stability design is a conservative measure; however, it accounts for the resources available at most laboratory institutions so that PTs can be terminated at a reasonable, yet achievable, strain limit. The more important design limit for GRS walls and abutments is the service limit.

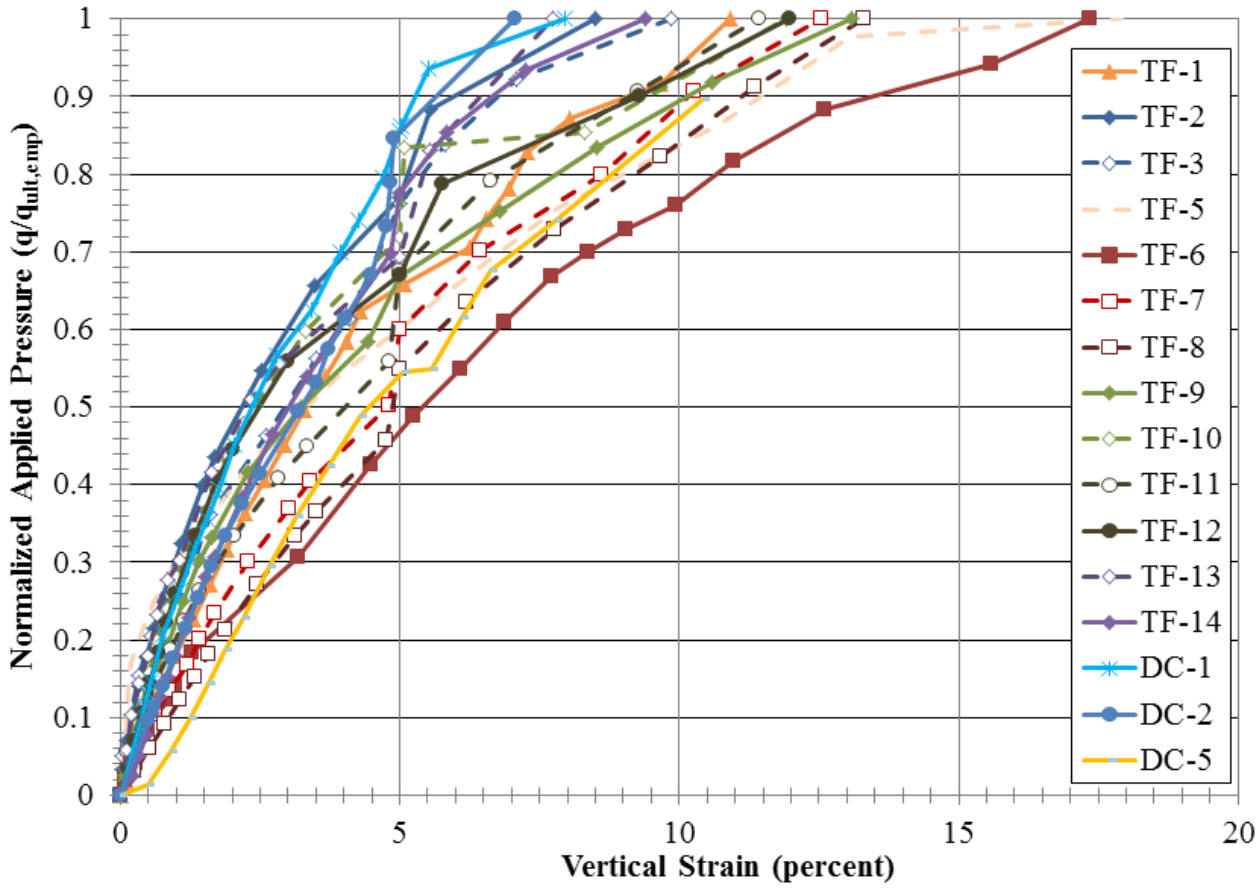

Figure 81. Graph. Normalized applied stress versus strain for all PT.

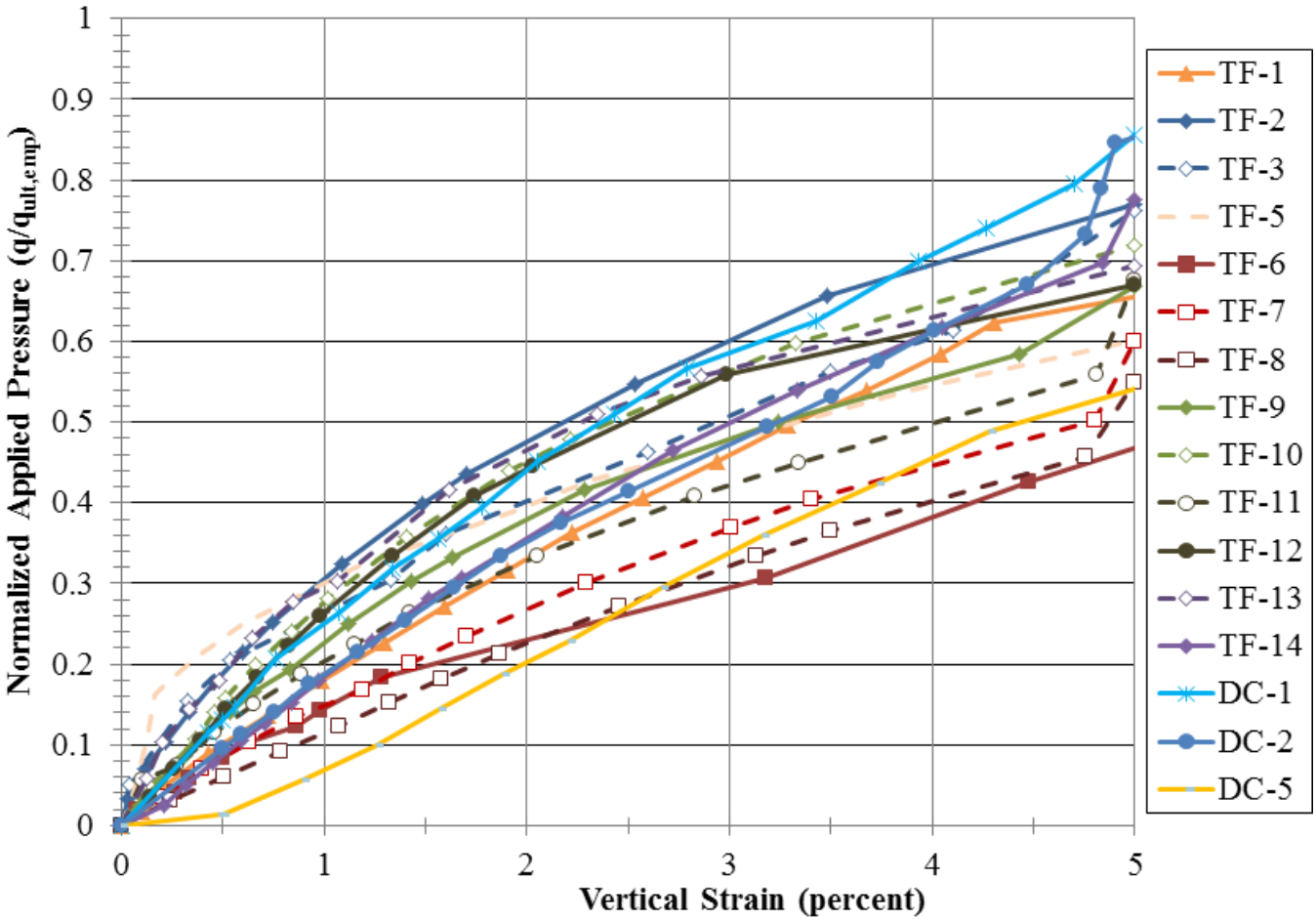

Figure 82. Graph. Normalized load-deformation behavior for the DC and TF PTs up to 5-percent vertical strain.

7.3 SERVICE LIMIT

FHWA guidance currently recommends a service limit of 4,000 psf applied vertical stress (dead plus live load, with load factors = 1.0) with a target of 0.5-percent vertical strain for GRS abutments, measured by using only dead load, unless the engineer decides to permit additional load and/or deformation.[1] For a 20-ft-tall wall, the initial compression of the GRS composite would therefore be limited to 1.2 inches. Note that the majority of compression within a GRS abutment occurs shortly after placement of dead load, with little post-construction settlement, if constructed as outlined by FHWA.[5]

The stress-strain curve generated by the PT can immediately be used to estimate deformation. By knowing the applied dead load, the resulting strain can be found from the PT results. Alternatively, using a corresponding PT for the particular GRS composite would yield the amount of dead load (unfactored) that can be placed on the abutment to limit the deformation to the tolerable amount. For the range of tests conducted in this study (compacted only), the allowable applied stress is between 1,324 and 6,016 psf (table 8 and figure 84).

Using the normalized load test curves (figure 85), the service stress to meet the 0.5-percent vertical strain limit is 6 to 23 percent of the ultimate stress, with an average of 13 percent for all tests. For only the tests with a CMU facing, as would be typical in the field, the range is slightly narrower, between 8 and 19 percent with an average of 12 percent; for the tests without a facing element, the average is 15 percent.

When looking strictly at the PTs that meet the current FHWA specifications for a GRS abutment, the allowable applied stress at low strain levels (i.e., at in-service conditions) ranges between about 8 percent and 13 percent of the ultimate stress (figure 86), with an average of 10 percent.[1] By estimating an ultimate stress using the GRS capacity equation (figure 8), ignoring the effects of cohesion and confining stress as indicated by Adams et al. (2011a) for design of GRS abutments, and assuming 10 percent of the ultimate capacity, the maximum service stress (unfactored dead load only) to limit short-term vertical strain to 0.5 percent can be predicted (table 25).[1]

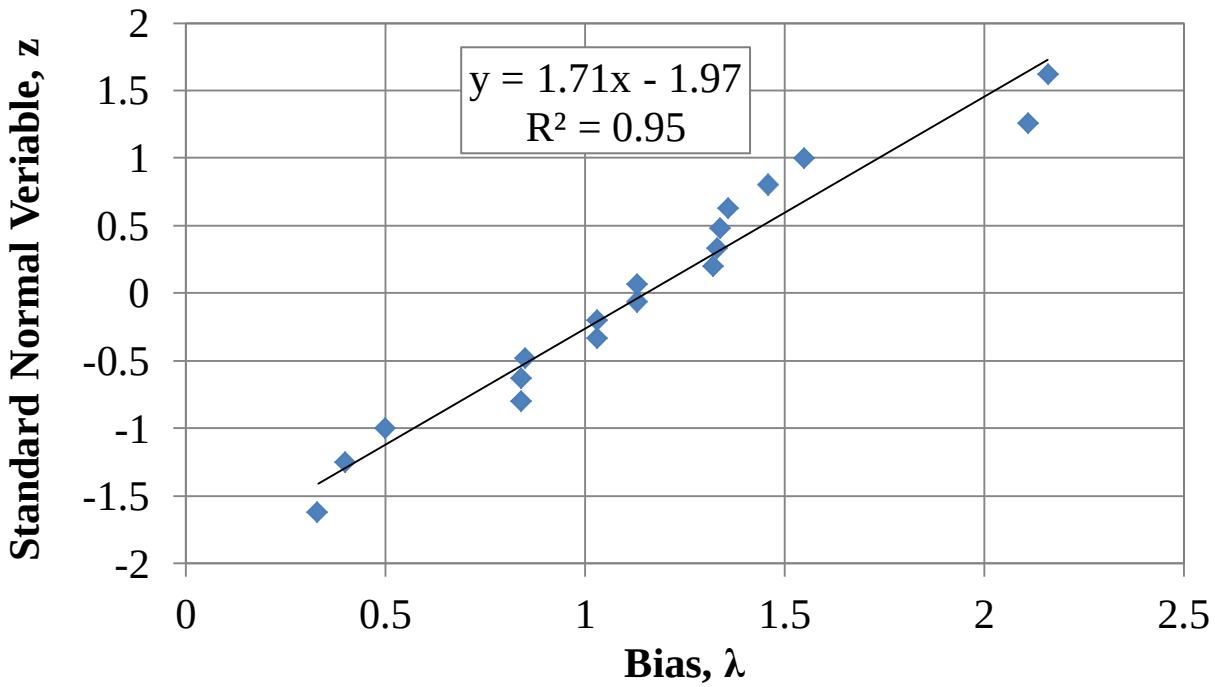

Figure 83. Graph. Cumulative distribution function for proposed service limit pressure.

Table 25. Estimation of allowable dead load to limit vertical strain to 0.5 percent using the GRS capacity equation.

Test	Measured		Predicted	Bias, λ	Standard Normal Variable, z
	$q_{ult,emp}$ (psf)	$q_{@\varepsilon=0.5\%}$(psf)	$q_{@\varepsilon=0.5\%,\ predicted}$ = 10% of $q_{ult,an}$ (psf)	Measured / Predicted	
DC-1	23,310	3,065	2,974	1.03	-0.34
DC-2	22,709	2,171	2,551	0.85	-0.48
DC-3	N/A	1,324	4,021	0.33	-1.62
DC-4	N/A	2,212	1,655	1.34	0.48
TF-1	20,471	2,068	1,570	1.32	0.20
TF-2	25,260	4,759	2,204	2.16	1.62
TF-3	17,491	3,417	2,204	1.55	1.00
TF-4	N/A	3,705	4,409	0.84	-0.80
TF-5	25,920	6,016	4,409	1.36	0.63
TF-6	43,763	3,704	4,409	0.84	-0.63
TF-7	26,546	2,224	4,409	0.50	-1.00
TF-8	29,134	1,753	4,409	0.40	-1.25
TF-9	22,310	2,955	1,401	2.11	1.25
TF-10	10,330	1,586	1,401	1.13	-0.07
TF-11	23,249	2,839	2,765	1.03	-0.20
TF-12	29,030	4,028	2,765	1.46	0.80
TF-13	12,960	2,398	1,807	1.33	0.34
TF-14	23,562	2,037	1,807	1.13	0.07
				Mean Bias	1.15
				Standard Deviation	0.58
				Coefficient of Variation (percent)	0.51

N/A = Not applicable, did not fail the composite.

The results indicate that by using 10 percent of the predicted design capacity, the mean bias between the measured results from this series of PTs and the predicted allowable stress at 0.5-percent vertical strain is 1.15 with a COV of 0.51 (table 25). This is on the conservative side and offers another tool to estimate deformation in lieu of conducting a performance test on a particular GRS composite.

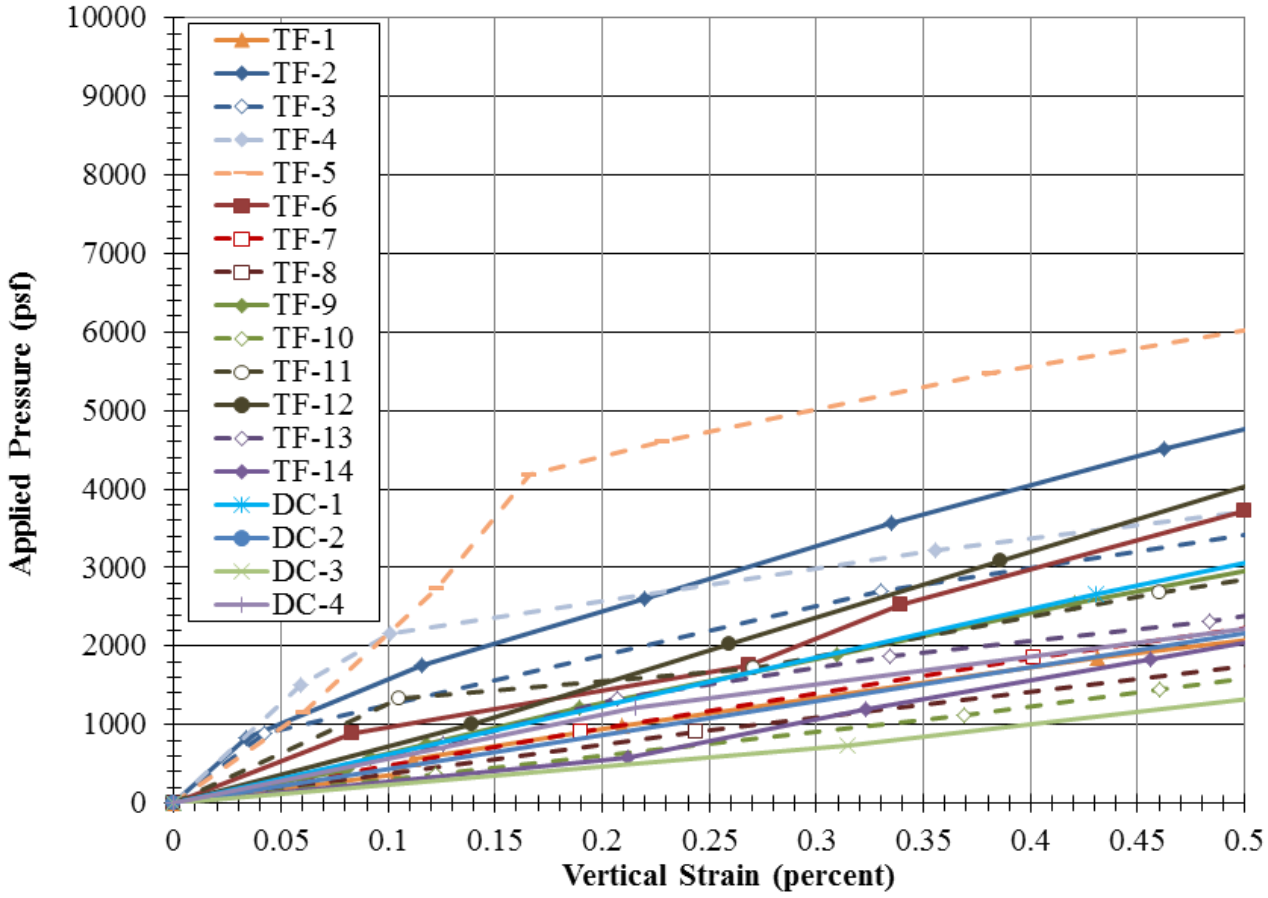

Figure 84. Graph. Load-deformation behavior for the Turner Fairbank PTs at low strain levels.

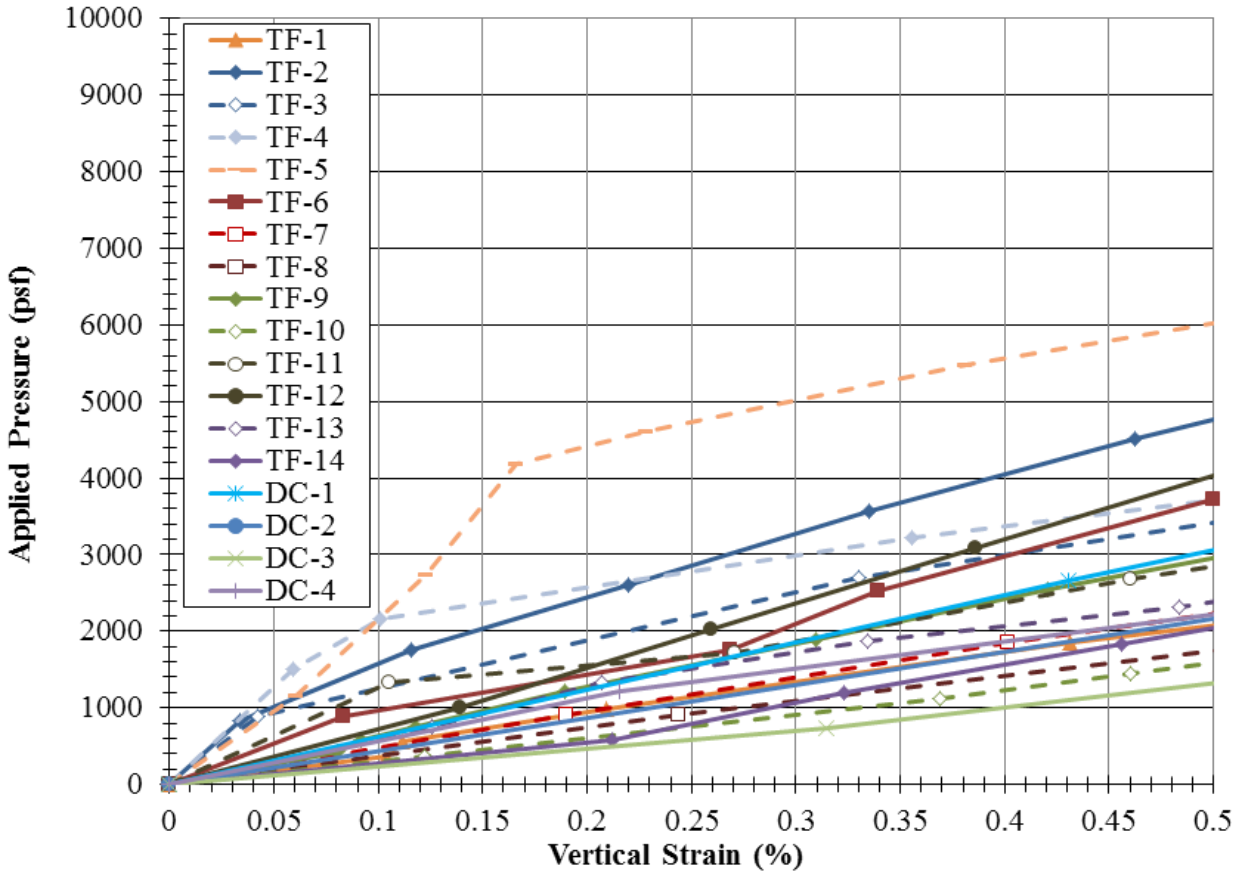

Figure 85. Graph. Normalized load-deformation behavior for the DC and TF PTs up to 0.5-percent vertical strain.

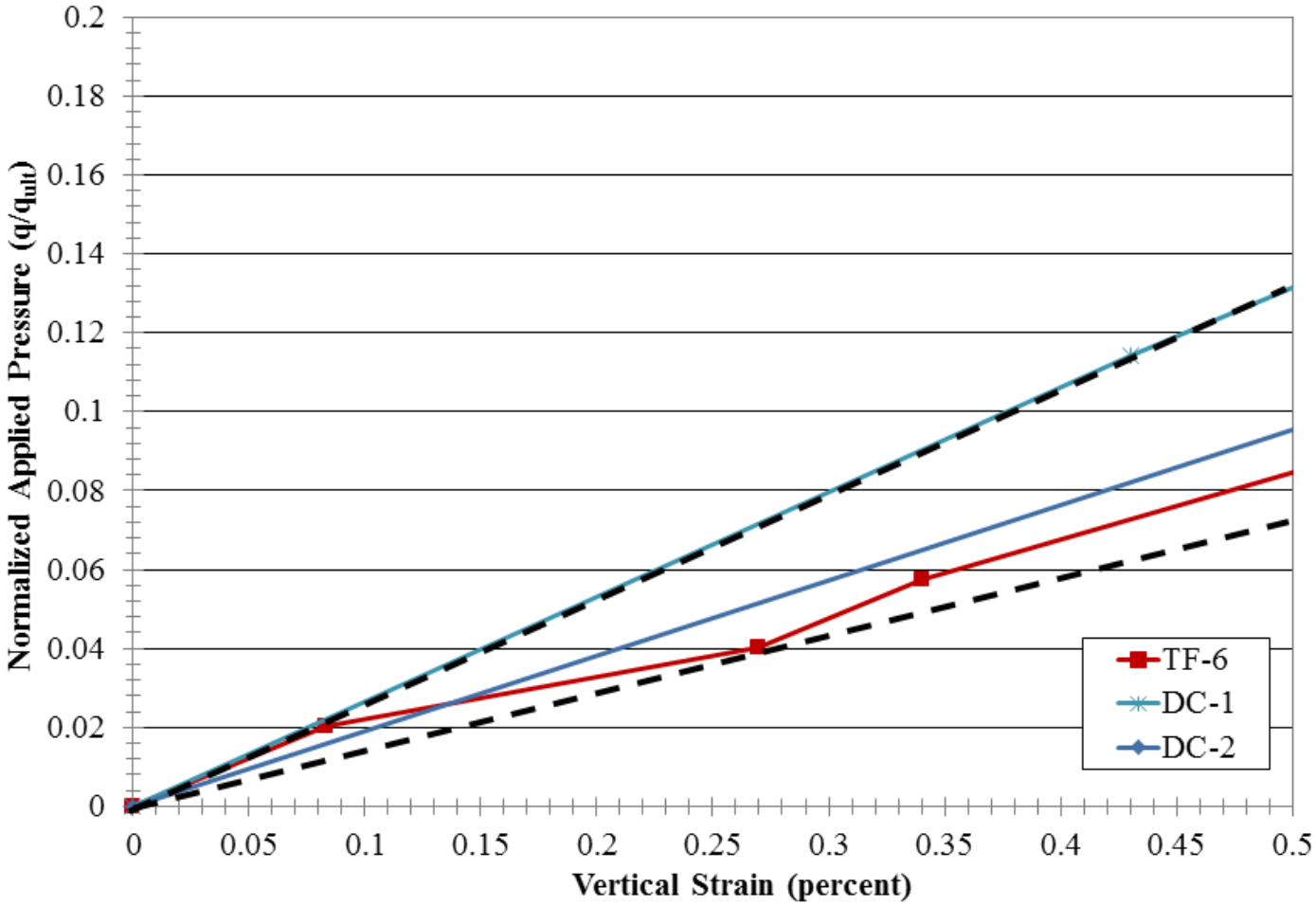

Figure 86. Graph. PTs strictly meeting FHWA GRS abutment design specifications.

7.4 LRFD CALIBRATION FOR STRENGTH LIMIT

In the United States, bridges that receive federal funding for construction must be designed in accordance with the AASHTO LRFD Bridge Design Specifications. AASHTO first adopted a load factor design (LFD) in 1977 for certain portions of the bridge superstructure. In the mid-1990s, the AASHTO Specifications adopted LRFD in geotechnical engineering design based on the work of Barker et al. (1991).[35] Since then, LRFD research has extended to more and more aspects of geotechnical structures.

LRFD in geotechnical design of bridge and building foundations has the following benefits:

1. Efficiency in design effort can be achieved when using the same factored loads for both superstructure and sub-structure design.
2. More consistent margins of safety can be realized in both superstructure and sub-structure design.
3. More economical use of materials can be accomplished when a more rational basis for setting the margin of safety is provided.

A methodology for calibrating the load bearing capacity (strength limit state) of bridge foundations on a GRS abutment is described and presented. Calibration for serviceability limit state is just as, if not more important, since most shallow foundation designs are governed more by serviceability rather than the ultimate limit state; however, the scope of this report is limited to only the strength limit state.[10]

7.4.1 Background

Code calibration is the process of determining values of load and resistance factors. While load factors have already been well established in the AASHTO code, resistance factors for newer types of geotechnical structures must be obtained by calibration. Resistance factors can be calibrated using the following approaches:

1. Judgment.
2. Fitting with Allowable Stress Design (ASD).
3. Reliability theory.

Calibration by judgment was the first approach at arriving code parameters, but it suffers from non-uniform margins of safety. Calibration by fitting with ASD essentially results in the LRFD code mimicking the ASD code. It does not necessarily result in more uniform margins of safety or economy. Calibration by fitting was performed for the internal stability design of GRS abutments.[1] The approach adopted herein to calibrate the load bearing capacity of GRS composites is based on reliability theory, which offers a rational process for optimizing the value of resistance factor. The results are then compared with those from calibrating by fitting with ASD.

In general, there are three approaches to estimating resistance factors using reliability analysis: (1) first order second moment (FOSM); (2) advanced first order second moment (AFOSM) and (3) Monte Carlo simulation (MCS). FOSM is the simplest and results in resistance factors that

are marginally lower (more conservative) than the AFOSM method, which requires programming of an optimization routine. MCS is only accurate if the load and resistance distributions are correctly modeled. According to Paikowsky (2010), if the statistical parameters are not well-defined, the resulting resistance factor using MCS will not be correct; moreover, if the load and resistance distribution is assumed to be lognormal, MCS will theoretically produce the same results as the FOSM method.[36] Thus, the simpler FOSM approach is adopted in this report.

In the reliability-based approach, the load (Q) and resistance (R) are considered random variables, which can be described by their own probability density functions. One form of margin of safety can be expressed by the difference R – Q where failure occurs when R – Q < 0. In the FOSM approach, R and Q are assumed to have a lognormal distribution; hence a limit state function can be written (figure 87) which is also lognormal. Failure occurs when R/Q is less than 1 or when g(R,Q) is less than 0. The probability density function of figure 87 is shown in figure 88.

$$g(R,Q) = ln(R/Q)$$

Figure 87. Equation. Limit state function for FOSM approach.

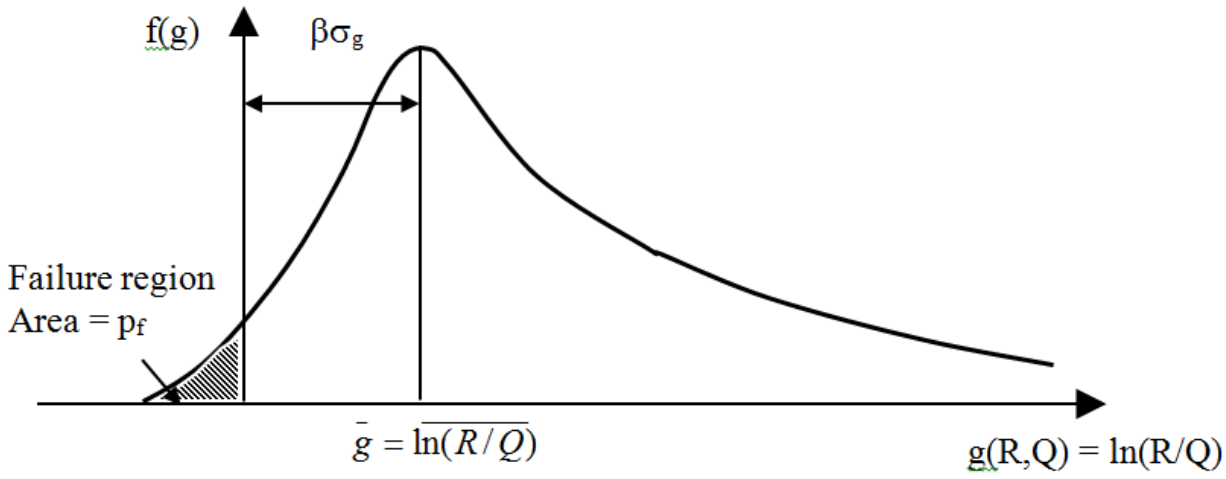

Figure 88. Graph. Reliability index for lognormal R and Q.

The reliability index (β) is the number of standard deviations between the mean safety margin (ḡ) and failure, where g(R,Q) = 0. According to Paikowsky (2010), many shallow foundations supporting bridge elements have been designed with a target reliability index (β_T) between 3.0 and 3.5, which corresponds to a probability of failure of 0.135 percent and 0.023 percent, respectively.[36] Note that these target reliability indices are for foundations on natural soil whereas GRS is an engineered fill.

7.4.2 Reliability Analysis: FOSM

In LRFD, the factored resistance must be greater than or equal to the factored loads (figure 89).

$$\Phi R \geq \sum_{i=1}^{n} \gamma_i Q_i$$

Figure 89. Equation. LRFD format.

Where Φ = resistance factor, γ_i = load factor for load component i, R = resistance and Q_i = load component i (e.g., dead load or live load). Many load combinations exist in the AASHTO code; however, resistance factors herein are calibrated using the Strength I load combination only. With only dead and live loads considered, it can be shown that the resistance factor based on FOSM can be calculated according to figure 90.

$$\Phi = \frac{\lambda_r \left(\gamma_D \left[\left(\frac{Q_D}{Q_D + Q_L}\right) / \left(1 - \frac{Q_D}{Q_D + Q_L}\right)\right] + \gamma_L\right)}{\left(\gamma_D \left[\left(\frac{Q_D}{Q_D + Q_L}\right) / \left(1 - \frac{Q_D}{Q_D + Q_L}\right)\right] + \gamma_L\right) \sqrt{\frac{1 + V_R^2}{1 + V_Q^2}}\, e^{\left(\beta_T \sqrt{ln\left[\left(1+V_R^2\right)\left(1+V_Q^2\right)\right]}\right)_i}}$$

Figure 90. Equation. Resistance factor using FOSM.

Where λ_R , λ_D , and λ_L are bias factors for resistance, dead load and live load, respectively, γ_D and γ_L are the dead (1.25 for AASHTO assuming Strength I load combination and assuming dead load of structural components and non-structural attachments only; dead load due to the wearing surface is not considered as it usually represents only a small fraction of the total dead weight) and live (1.75 for AASHTO assuming Strength I load combination) load factors, respectively, and V_R and V_Q are the coefficients of variation (COV) of the resistance and loads, respectively. The bias factor, λ, is the ratio of the measured to the nominal or calculated value; if the variable tends to be over-predicted, then the bias factor will be less than 1. Note that the COV for a variable that is related to several statistically independent variables is merely the square root of the sum of the squares of the various coefficients of variation. For example, figure 91 shows that the COV for factored load (V_Q) is equal to the sum of the squares of the COV for dead load (V_D) and live load (V_L).

$$V_Q = \sqrt[2]{V_D^2 + V_L^2}$$

Figure 91. Equation. Coefficient of variation for factored load.

It can be seen that in the FOSM method to estimate the resistance factor (figure 90), the random variables are characterized by their first two moments, namely the mean and the standard deviation (which is equal to the product of the coefficient of variation and the mean). Therefore, it is essential to compile the statistics of the load and resistances prior to calibration.

Load Statistics

In the final report to the National Cooperative Highway Research Program (NCHRP) Project No. 20-7/186, Kulicki et al. (2007) provided bias factors and COVs for dead and live loads (table 26).[37] Thus, from (figure 91) and table 26, the COV for factored load is equal to 15.6 percent.

Table 26. Statistics for dead and live loads.

	Dead Load[1]	Live Load[2]
Bias Factor	$\lambda_D = 1.05$	$\lambda_L = 1.14$
COV	$V_D = 10\%$	$V_L = 12\%$

[1]Assumes cast-in-place concrete elements only.
[2]Assumes HL-93 loading for shear and an average daily truck traffic (ADTT) of 1,000 for two loaded lanes.[10,37]

Resistance Statistics

The variables in the soil-geosynthetic capacity equation (figure 8) and the required reinforcement strength equation (figure 10) include the maximum aggregate size (d_{max}), the reinforcement strength (T_f) and the passive earth pressure coefficient (K_{pr}); it is reasonable to assume that the reinforcement spacing (S_v) is not a random variable, therefore the associated fabrication factor is assumed to be unity. Therefore, the COV of the resistance (V_R) can be expressed according to figure 92.

$$V_R = \sqrt[2]{V_{dmax}^2 + V_{T_f}^2 + V_{K_p}^2 + V_M^2}$$

Figure 92. Equation. Coefficient of variation for resistance.

Where V_{dmax}, V_{Tf}, V_{Kp} and V_M are the COVs of d_{max}, T_f, K_p and the capacity model, respectively.

Note that the ultimate reinforcement strength is usually measured in the laboratory under unconfined conditions; however, it should ideally be measured under confinement to replicate actual in-service conditions. Benjamin et al. (2008) performed numerous measurements of reinforcement strength for woven and non-woven geotextiles in the ground and found the COV for reinforcement strength (V_{Tf}) of woven geotextiles was 2.3 and 4.25 percent for the cross-machine and machine directions, respectively.[38] Since woven geotextiles were used in the PTs and are the most commonly used geosynthetic in GRS abutments and IBSs, a V_{Tf} value of 4 percent is utilized in this study. For the COV for the passive earth pressure coefficient (V_{Kp}), NCHRP Report 651 recommended a value of 15 percent when measuring friction angles with lab tests.[36] The COV for maximum aggregate size (V_{dmax}) has not yet been investigated, but it is expected to be small; for one reason, the quarries will set their crushers to a given maximum grain size with a high degree of certainty. A value of $V_{dmax} = 5$ percent is therefore assumed in this calibration. Additionally, the mean bias factor for the capacity prediction model, using only the data produced in this study, is 0.88 with a COV of about 35 percent (table 23). The resulting COV for resistance (V_R) is estimated at 39 percent.

7.4.3 Resistance Factor

The database of results from this study consists of sixteen cases taken to failure of the GRS composite, four with open-graded backfill (DC-1, DC-2, DC-5, and TF-1) and twelve with well-graded backfill material (TF-2, TF-3, and TF-5 to TF-14). Because the number of cases with open-graded backfill is limited, the present strategy is to arrive at one value for the resistance factor that is applicable to all conditions. With additional testing in the future, separate resistance factors can be calibrated for each soil type, if necessary.

The resistance factor for GRS capacity, calculated according to figure 90, is presented as a function of the ratio of dead load to total load, $Q_D/(Q_D + Q_L)$, and the target reliability index (β_T) in figure 93. Note that a $Q_D/(Q_D + Q_L)$ of 0.5 corresponds approximately to a bridge span of about 60 ft, whereas a $Q_D/(Q_D + Q_L)$ of 0.2 corresponds to a bridge span of approximately 250 ft.[39] The bridge span for a GRS-IBS is currently limited to 140 ft (Adams et al. 2011); therefore the resistance factors of interest correspond to $Q_D/(Q_D + Q_L)$ greater than about 0.32. Over this range, the resistance factor varies from 0.26 to 0.28 for β_T = 3.5, from 0.32 to 0.34 for β_T = 3.0, and from 0.40 to 0.41 for β_T = 2.5 using FOSM.

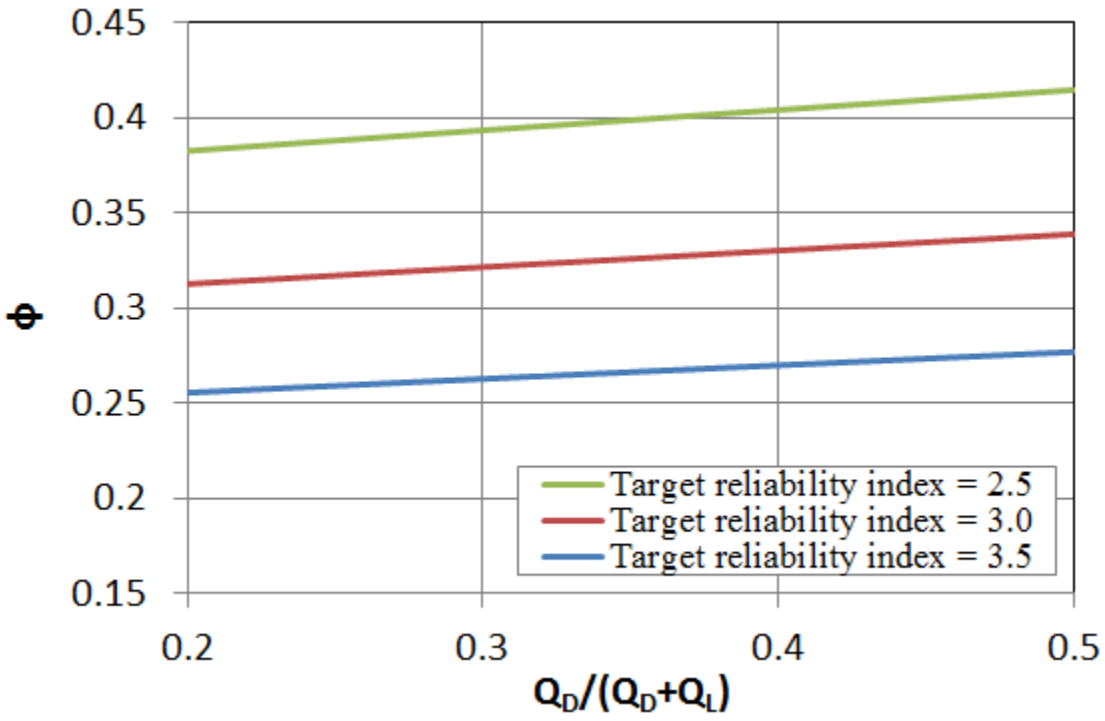

Figure 93. Graph. Resistance factor for footings on GRS composites for different dead to dead plus live load ratios and target reliability indices based on PT series.

Similarly, a reliability analysis was performed using the results of all prior GRS composite testing with a mean bias of 0.95 and a COV for the model of 32 percent (table 24). This slightly increases the resistance factor for the same target reliability indices (figure 94); for the range of $Q_D/(Q_D + Q_L)$ greater than 0.32, the resistance factor varies from 0.31 to 0.33 for β_T = 3.5, from 0.38 to 0.39 for β_T = 3.0, and from 0.46-0.48 for β_T = 2.5 using FOSM.

The resistance factors found through the reliability analysis using the standard reliability indices of 3.0 and 3.5 for bridge foundations are lower than the resistance factor found through calibration by fitting to ASD. For a factor of safety (FS) of 3.5, a resistance factor of 0.45 was estimated for the soil-geosynthetic capacity equation.[1] Through back-calculation, this equates to a reliability index (β) of about 2.5.

In NCHRP Report 507, Paikowsky et al. (2004) suggested that for redundant foundation systems (such as pile groups), a reliability index of 2.3 was appropriate.[40] With the frequency of the reinforcement spacing, GRS composites can be considered a redundant foundation system as well, with no catastrophic collapse observed at failure for any of the PTs. In addition, Bathurst et al. (2008) suggest that a reliability index of 2.3 is appropriate for the internal stability of reinforced soil walls.[41] This leads to the conclusion that the currently used resistance factor of 0.45, having a reliability index of 2.5, is reasonable for design.

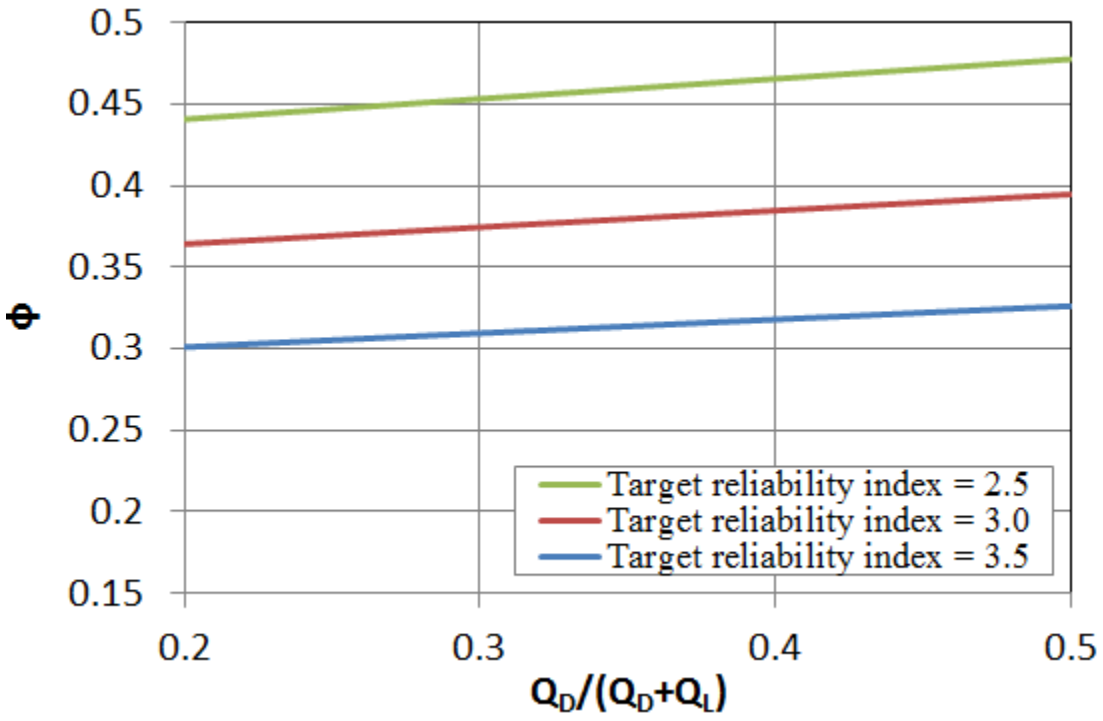

Figure 94. Graph. Resistance factor for footings on GRS composites for different dead to dead plus live load ratios and target reliability indices based on all testing to date.

8. CONCLUSIONS

The results of the PT research performed on GRS composites leads to several important conclusions. General conclusions include the following:

1. The performance test can be used to model the load-deformation behavior of a particular GRS composite and is repeatable. Based on equivalency comparisons, the ratio of the measured vertical capacity in a PT to that of the same GRS in plane strain is near unity, and the stiffness of what a plane strain GRS composite might experience (such as an abutment) is up to 3 times higher (on the conservative side) compared to what is measured in a GRS PT (section 5).
2. A two-post frame with single hydraulic jacks produces more even load distribution than a two bolted channel beams in combination with four hydraulic jacks.

The load-deformation relationship of GRS composites depends on several parameters including preloading, aggregate angularity, compaction level, presence of bearing bed reinforcement, and facing confinement.

- Figure 32 indicates that preloading of the GRS composite (TF-6 with S_v = 7⅝ inches, T_f = 4,800 lb/ft, 21A material, CMU facing) resulted in strain hardening to produce a stiffer response during two unload-reload cycles. The reload response is similar during both cycles, with a ratio of stress to strain equal to approximately 3,000 ksf, compared to the ratio for the initial, virgin loading equal to approximately 750 ksf, an increase by a factor of four. Similar results were found for an open-graded material as well (TF-1 with S_v = 7⅝ inches, T_f = 2,400 lb/ft, AASHTO No. 8 material, CMU facing), as shown in figure 30. The effect of preloading was not explored for other reinforcement spacing in this study.
- Angularity impacts the strength (e.g., friction angle) of the backfill used and therefore the GRS composite. The GRS composite using a rounded pea gravel aggregate (DC-2) had both a lower ultimate strength ($q_{ult,emp}$) and service limit capacity ($q_{@\varepsilon=0.5\%}$) than that using the more angular aggregate (DC-1) meeting the same gradation specifications for an AASHTO No. 8 material (table 10).
- The results indicate a similar ultimate vertical capacity ($q_{ult,emp}$) between an uncompacted (DC-5) and compacted (DC-1) GRS composite, but a much softer response with no compactive effort. For the particular GRS composite tested (table 11 and figure 58), at an in-service dead load of 4,000 psf, an uncompacted abutment will experience an initial strain about three times more than a compacted abutment; however, near failure, at about 20,000 psf, an uncompacted abutment will experience about 1.7 times the strain as a compacted abutment.
- The results indicate that the bearing bed provides some added vertical capacity; however, vertical deformation is not improved at low strain levels (figure 60). The modulus for primary compression is similar whether the bearing bed is present or not (table 12). At both low and high applied normal stresses, representing bridge loads (figure 61) and near failure loads (figure 62), respectively, the bearing bed reinforcement serves to limit lateral deformation in the zone of its placement.

- The frictionally connected CMU facing has an impact on the performance of GRS; it provides confinement, leading to a stiffer response and an increased capacity compared to a GRS composite with no facing element. From table 20, the facing more than doubles the initial stress-strain ratio as compared to the PTs without any facing. In terms of capacity, the facing plays the biggest and smallest role for the largest spaced (S_v = 15¼ inches) and the closest spaced ($S_v = 3^{13}/_{16}$ inches) system tested, respectively. For the 5 pairs of tests conducted at TF, including the CMU facing produced an improved ultimate capacity between 1.2 and 2.2 times greater than the GRS composite without any facing (table 21). A similar trend to the strain at the current 4,000-psf service limit is also found. The design assumption to not include the effect of confinement from the face in determining the capacity and required reinforcement strength is therefore conservative.[(1)]
- In addition, at the current service stress limit (applied stress, *q*, of 4,000 psf), the ratio of service vertical strain with no facing to service vertical strain with a CMU facing ranges from 1.2 to 2.2 (table 21). The largest impact was for the 15⅝-inch spaced GRS composite (TF-9 and TF-10). At ultimate failure, the ratio is considerably closer, ranging from 0.8 to 1.2.
- For the same T_f/S_v ratio of 3,800 lb/ft^2, there is a linear relationship between the reinforcement spacing (S_v) and the ratio of capacity with CMU facing ($q_{ult,emp\ CMU}$) to the capacity without facing ($q_{ult,emp\ no\ CMU}$) (figure 75). Similarly, there is a linear relationship with reinforcement strength (figure 76).

Both open-graded and well-graded aggregates can be used as the reinforced backfill in GRS composites; each has their advantages and disadvantages. The PT results further distinguished the effect aggregate selection can have on the behavior of GRS.

- The well-graded material is considerably stiffer than the open-graded material. At an applied pressure of 4,000 psf, the vertical strain is about 1.1 percent for TF-1 (open-graded) and 0.4 percent for TF-2 (well-graded). The modulus of the composite tested in TF-1 is 320 ksf (table 13) compared to 710 ksf for the composite tested in TF-2; TF-1 (open-graded) is 55 percent less stiff than TF-2 (well-graded). In terms of bearing capacity, TF-1 was 20 percent less strong than TF-2. The results indicate that the gradation, and perhaps cohesion (at the same friction angle), impacts the modulus more so than the strength, giving indication that well-graded fills have an advantage with respect to serviceability.
- As discussed in section 6.1, isolating the effect of cohesion and other soil parameters on the performance of GRS is difficult using PTs, although based on the soil-geosynthetic capacity equation (figure 8), it will serve to improve capacity, although its contribution should not be considered in design.
- The response indicates that the higher reinforcement strength (4,800 lb/ft) produces a stiffer and stronger response than the lower reinforcement strength (2,400 lb/ft) for open-graded backfill (table 15); the same is true for the composites with no facing element. By doubling the reinforcement strength, the results indicate an increase of measured capacity by a factor of 1.14 for capacity and 1.34 for the initial stress-strain ratio.
- For the well-graded aggregate, increasing the reinforcement strength increases the capacity by a factor of 1.5 and 1.7 for no facing and CMU facing (table 16), respectively, but does not significantly impact the stiffness.

The relationship between reinforcement strength and spacing was investigated through a series of PTs with the same T_f/S_v ratio.

- The response for experiments conducted with a T_f/S_v ratio of 3,800 lb/ft^2 showed that as reinforcement spacing increased, the vertical capacity decreased for the same T_f/S_v ratio, whether a CMU facing was absent (figure 66) or present (figure 67). This suggests that the relationship between reinforcement strength and spacing is not proportional to capacity as outlined in current MSE design (AASHTO 2012); a GRS abutment with a given T_f and S_v will not have the same strength as a GRS abutment with twice the strength ($2T_f$) and reinforcement spacing ($2S_v$).
- At the same T_f/S_v ratio of 3,800 lb/ft^2, increasing the reinforcement spacing by a factor of two from 7⅝ to 15¼ inches and the reinforcement strength by a factor of two from 2,400 to 4,800 lb/ft, resulted in a reduction of the capacity by a factor of 0.9 and 0.6 for CMU facing and no facing, respectively. The relationship is therefore not directly proportional, as indicated for MSE design (AASHTO 2012).

The primary purpose of PTs is to provide a designer with the unique stress-strain properties of a particular GRS composite for use in design. There is an empirical method and an analytical method currently available for GRS by FHWA.[(1)]

- Note that only 3 GRS composites tested in this study meet both the design limits and the material specifications (e.g., $T_f \geq 4{,}800$ lb/ft, $d_{max} \geq$ ½ inches) for GRS abutments; however, based on the results of this study, perhaps the criteria can be amended to reduce the reinforcement strength limitation, provided the reinforcement strength meets internal stability design requirements.[(1)]
- Based on the results of the PTs presented in this report, the average bias for the capacity equation is 0.88 with a COV of about 35 percent (table 23). Including the results from other sources in the literature, the average bias is 0.95 with a COV of about 32 percent. These numbers indicate relatively good agreement between figure 8 and the measured ultimate capacity (table 24).
- The 5-percent vertical strain limit can significantly reduce the allowable stress placed on a GRS composite; figure 82 shows that at 5-percent strain, the applied pressure is between 50 and 85 percent of the measured ultimate capacity (table 8).
- The results indicate that by using 10 percent of the predicted design capacity (figure 8), the 0.5-percent vertical strain as required by FHWA for the service limit of GRS abutments can largely be satisfied. The mean bias of the ratio between the measured results at 0.5-percent vertical strain from this series of PTs and the predicted allowable stress at 10 percent of the design capacity is 1.15 with a COV of 0.51 (table 25). This is on the conservative side yet offers another tool to estimate deformation in lieu of conducting a performance test on a particular GRS composite.

Finally, a reliability analysis for the soil-geosynthetic capacity equation (figure 8) was performed on the 16 PTs taken to failure in this study, along with previous results from additional GRS testing found from the literature.

- A target reliability index of 2.5 is reasonable for the strength limit models for GRS composites designed according to Adams et al. (2011). A lower target reliability index is warranted for closely-spaced GRS composites because of the redundancy in the reinforcement and because no catastrophic collapse was observed in any of the performance tests at failure. In addition, Bathurst et al. (2008) suggest that a reliability index of 2.3 is appropriate for the internal stability of reinforced soil walls.[1,41]
- Performing a reliability analysis using the FOSM approach produces a resistance factor around 0.45, similar to that found through calibration by fitting to ASD methods.

APPENDIX A. SOIL TESTING DATA

SIEVE ANALYSIS DATA

Table 27. AASHTO No. 8 sieve analysis (DC tests).

Sieve No.	Sieve Size (inch)	Mass of Soil + Pan (g)	Mass of Pan (kg)	Mass of soil (kg)	Percent Retained	Percent Passing
0.75	0.75	0	1,393.3	0	0.00	100.00
0.50	0.5	0	1,087.9	0	0.00	100.00
0.375	0.375	1,314.4	1,102.7	211.7	3.01	96.99
4	0.187	6,469.6	1,515	4,954.6	70.49	26.50
8	0.0937	2,666.2	1,129	1,537.2	21.87	4.63
16	0.0469	1,105.3	910.2	195.1	2.78	1.85
50	0.0117	807.6	741.5	66.1	0.94	0.91
100	0.0059	820.1	809.4	10.7	0.15	0.76
200	0.0029	924.1	916.4	7.7	0.11	0.65
Pan	—	715.4	669.8	45.6	0.65	0.00

Table 28. AASHTO No. 8 pea gravel sieve analysis (DC tests).

Sieve No.	Sieve Size (inch)	Mass of Soil + Pan (kg)	Mass of Pan (kg)	Mass of soil (kg)	Percent Retained	Percent Passing
0.75	0.75	0	0	0	0.00	100.00
0.50	0.5	1.115	1.085	0.03	0.43	99.57
0.375	0.375	1.38	1.1	0.28	3.99	95.58
4	0.187	6.7	1.015	5.685	80.98	14.60
8	0.0937	1.665	1.13	0.535	7.62	6.98
16	0.0469	1.095	0.91	0.185	2.64	4.34
50	0.0117	0.86	0.74	0.12	1.71	2.64
Pan	—	0.785	0.6	0.185	2.64	0.00

Table 29. AASHTO No. 57 Sieve analysis (DC tests).

Sieve No.	Sieve Size (inch)	Mass of Soil + Pan (g)	Mass of Pan (kg)	Mass of soil (kg)	Percent Retained	Percent Passing
1.5	1.5	1,476.1	1,476.1	0	0.00	100.00
1	1	1,127.1	1,127.1	0	0.00	100.00
0.75	0.75	2,311	1,393.4	917.6	12.09	87.91
0.50	0.5	5,052.1	1,087.8	3,964.3	52.22	35.69
0.375	0.375	2,739.5	1,102.7	1,636.8	21.56	14.13
4	0.187	2,308.8	1,514.8	794	10.46	3.67
8	0.0937	1,224.5	1,128.9	95.6	1.26	2.41
16	0.0469	981.1	909.8	71.3	0.94	1.47
200	0.0029	974.5	916.7	57.8	0.76	0.71
Pan	—	723.3	669.7	53.6	0.71	0.00

Table 30. AASHTO No. 9 Sieve analysis (DC tests).

Sieve No.	Sieve Size (inch)	Mass of Soil + Pan (g)	Mass of Pan (kg)	Mass of soil (kg)	Percent Retained	Percent Passing
0.75	0.75	0	1,393.21	0	0.00	100.00
0.50	0.5	0	1,087.95	0	0.00	100.00
0.375	0.375	0	1,102.79	0	0.00	100.00
4	0.187	1,785.33	1,514.98	270.35	5.78	94.22
8	0.0937	4,236.2	1,129.04	3,107.16	66.47	27.75
16	0.0469	1,791.1	909.95	881.15	18.85	8.90
50	0.0117	986.6	741.69	244.91	5.24	3.66
100	0.0059	830	809.4	20.6	0.44	3.22
200	0.0029	934.9	916.46	18.44	0.39	2.82
Pan	—	732.6	600.56	132.04	2.82	0.00

Table 31. AASHTO No. 8 Sieve analysis (TFHRC tests).

Sieve No.	Sieve Size (inch)	Mass of Soil + Pan (g)	Mass of Pan (kg)	Mass of soil (kg)	Percent Retained	Percent Passing
1	1	1,127.1	1,127.1	0	0.00	100.00
0.50	0.5	1,116.5	1,087.7	28.8	0.31	99.69
0.375	0.375	3,832	1,102.6	2,729.4	29.83	69.86
4	0.187	6,694.3	1,013.8	5,680.5	62.08	7.78
8	0.0937	1,688.5	1,128.7	559.8	6.12	1.66
10	0.079	1,398.7	1,374	24.7	0.27	1.39
16	0.0469	935	909.7	25.3	0.28	1.11
40	0.0165	810	793.1	16.9	0.18	0.93
50	0.0117	746.2	741.8	4.4	0.05	0.88
Pan	—	750.4	669.8	80.6	0.88	0.00

Table 32. AASHTO A-1-a (VDOT 21A) sieve analysis (TFHRC tests).

Sieve No.	Sieve Size (inch)	Mass of Soil + Pan (g)	Mass of Pan (kg)	Mass of soil (kg)	Percent Retained	Percent Passing
1	1	1,127.1	1,127.1	0	0.00	100.00
0.50	0.5	1,919.2	1,087.6	831.6	17.59	82.41
0.375	0.375	1,624.9	1,102.7	522.2	11.05	71.36
4	0.187	2,093.7	1,013.8	1,079.9	22.84	48.52
8	0.0937	1,757.5	1,129.6	627.9	13.28	35.24
10	0.079	1,489.5	1,374.7	114.8	2.43	32.81
16	0.0469	1,260.5	910.1	350.4	7.41	25.40
40	0.0117	1,206.5	793.1	413.4	8.74	16.66
200	0.0029	1,397.8	916.5	481.3	10.18	6.47
Pan	—	975.7	669.6	306.1	6.47	0.00

LSDS TESTING DATA

Table 33. Summary of AASHTO No. 8 LSDS results (DC tests).

Soil Type	Normal Stress (psi)	Max Shear (psi)	Peak Friction Angle (°)	Peak Dilation Angle (°)	Gap (inch)
8	5.051	9.5114	62.03	12.96	0.343
8	10.03	19.0619	62.25	11.65	0.343
8	20.03	30.533	56.73	6.35	0.343
8	30.02	45.6537	56.67	5.63	0.343

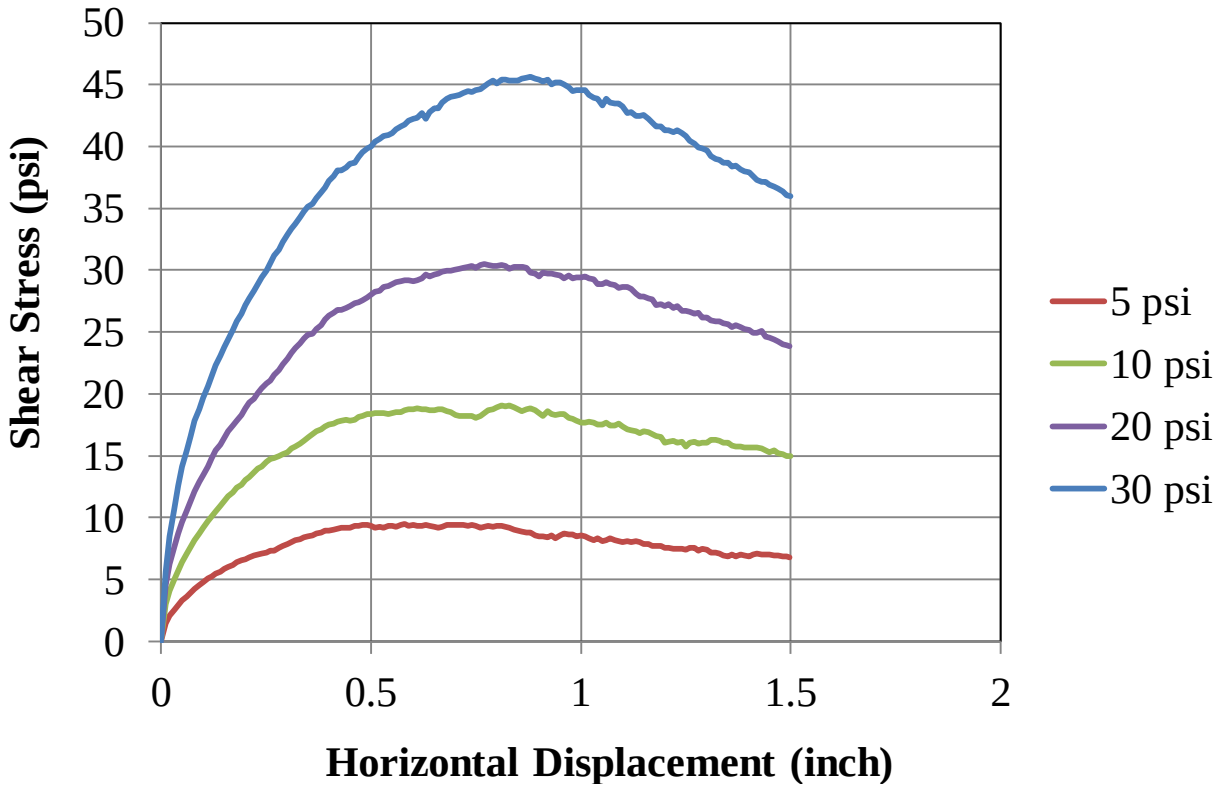

Figure 95. Graph. AASHTO No. 8 LSDS test results (DC tests).

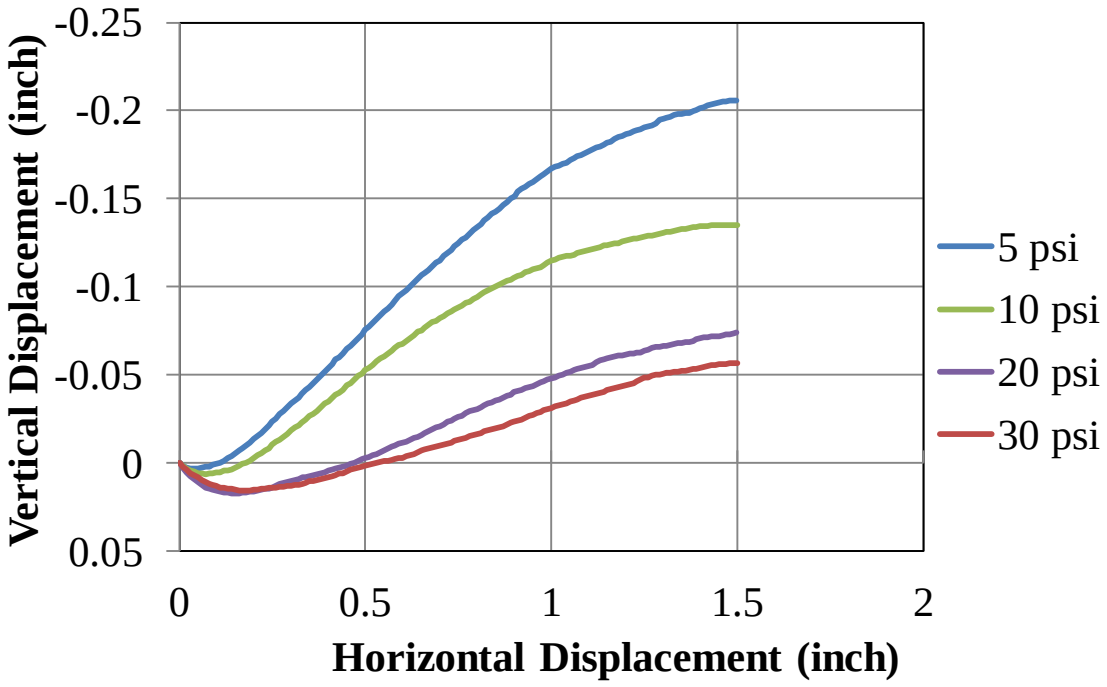

Figure 96. AASHTO No. 8 LSDS deformation test results (DC tests).

Table 34. Summary of AASHTO No. 8 pea gravel LSDS results (DC tests).

Soil Type	Normal Stress (psi)	Max Shear (psi)	Peak Friction Angle (°)	Peak Dilation Angle (°)	Gap (inch)
8P	5.022	7.5449	56.35	13.19	0.35
8P	10.05	15.00489	56.19	11.79	0.35
8P	20.01	21.238	46.71	5.96	0.35
8P	30.01	35.1467	49.51	6.04	0.35

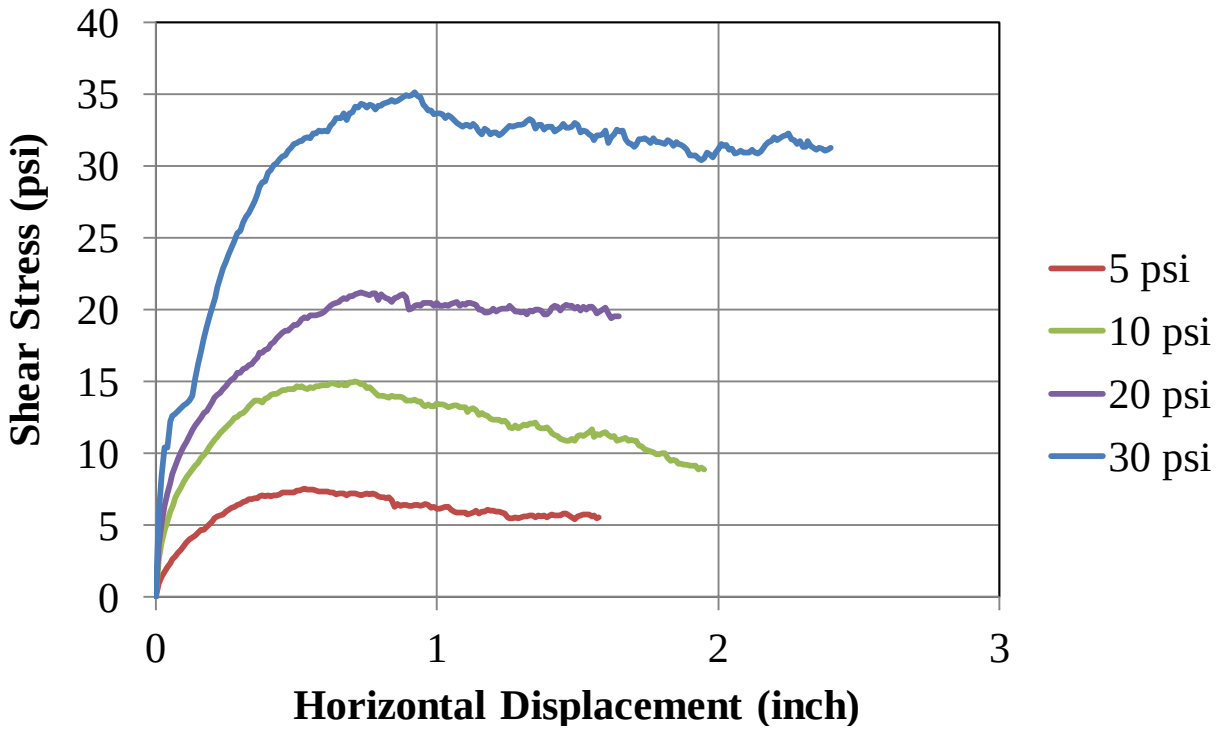

Figure 97. Graph. AASHTO No. 8 pea gravel LSDS test results (DC tests).

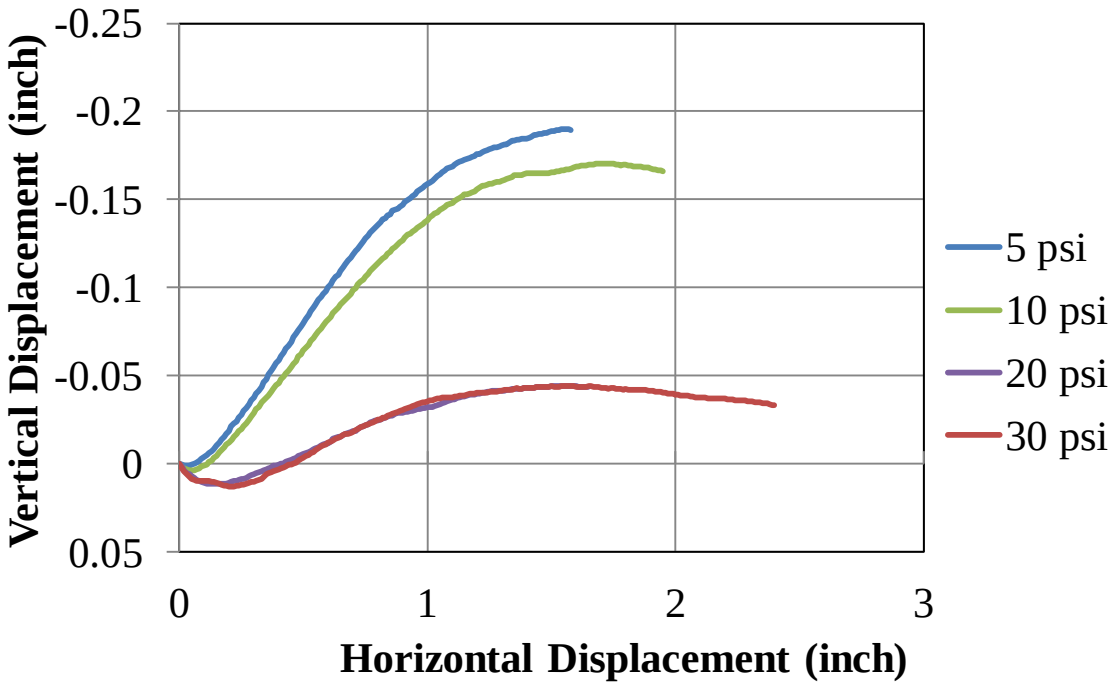

Figure 98. Graph. AASHTO No. 8 pea gravel LSDS deformation test results (DC tests).

Table 35. Summary of AASHTO No. 57 LSDS results (DC tests).

Soil Type	Normal Stress (psi)	Max Shear (psi)	Peak Friction Angle (°)	Peak Dilation Angle (°)	Gap (inch)
57	5.013	17.547	74.06	15.36	0.74
57	10.01	21.187	64.71	13.15	0.74
57	20.04	40.212	63.51	9.93	0.74
57	30.01	47.189	57.55	6.28	0.74

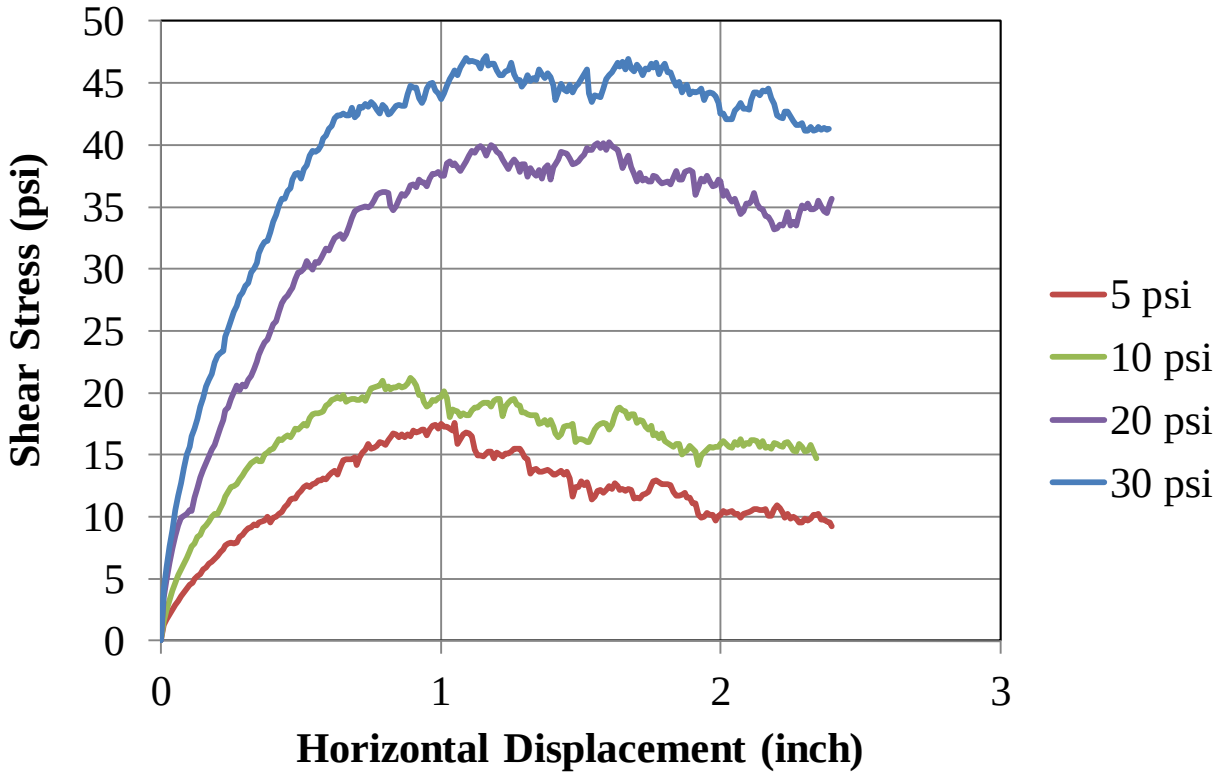

Figure 99. Graph. AASHTO No. 57 LSDS test results (DC tests).

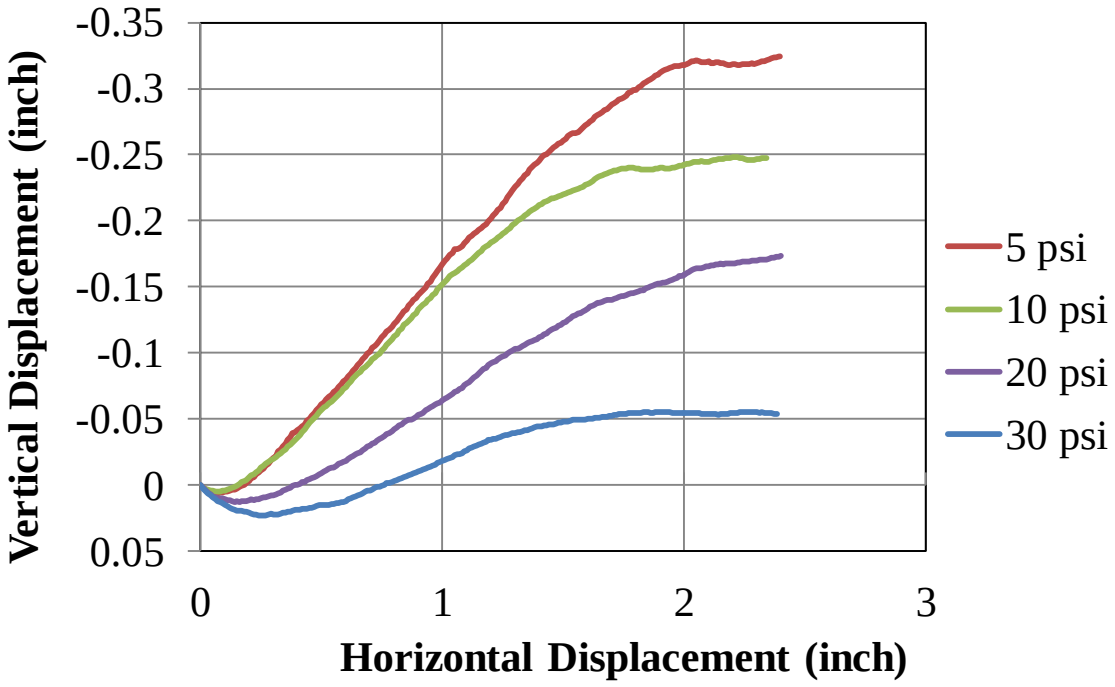

Figure 100. Graph. AASHTO No. 57 LSDS deformation test results (DC tests).

Table 36. Summary of AASHTO No. 9 LSDS results (DC tests).

Soil Type	Normal Stress (psi)	Max Shear (psi)	Peak Friction Angle (°)	Peak Dilation Angle (°)	Gap (inch)
9	5.053	9.7334	62.56	13.64	0.175
9	10.04	17.698	60.43	10.38	0.175
9	20.01	31.97	57.96	5.82	0.175
9	30.02	42.8381	54.98	4.73	0.175

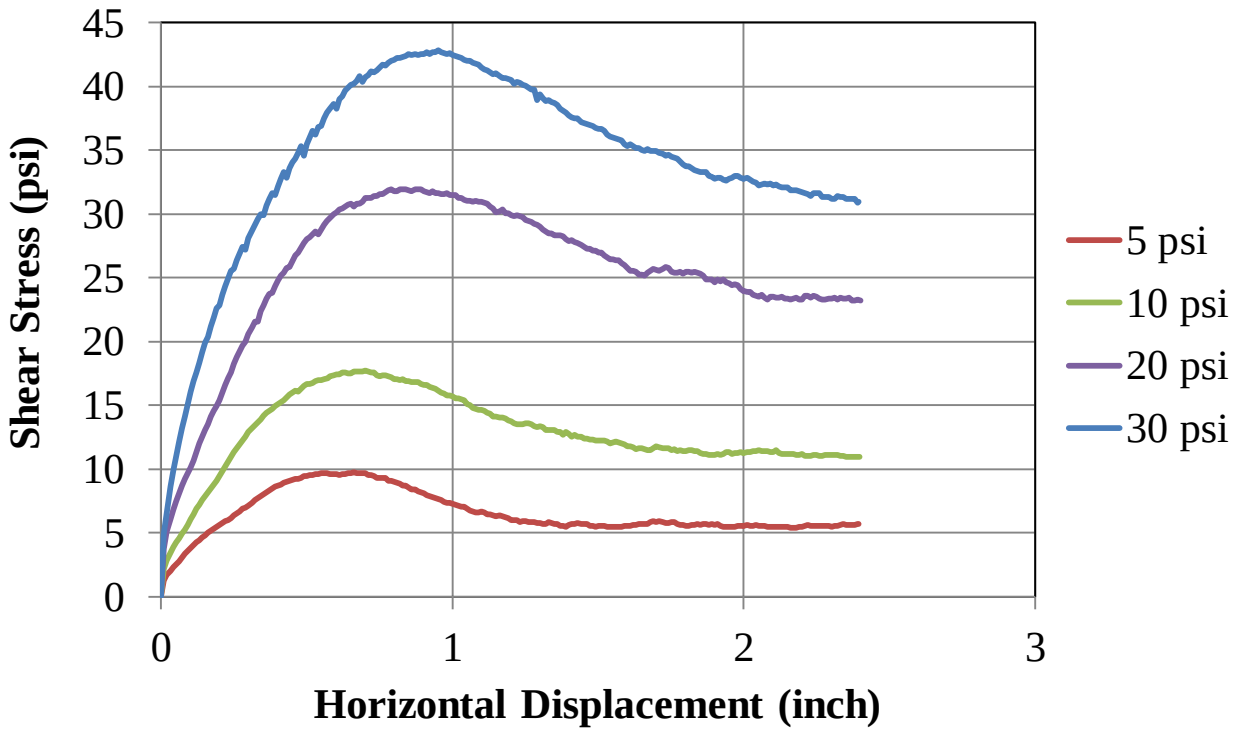

Figure 101. Graph. AASHTO No. 9 LSDS test results (DC tests).

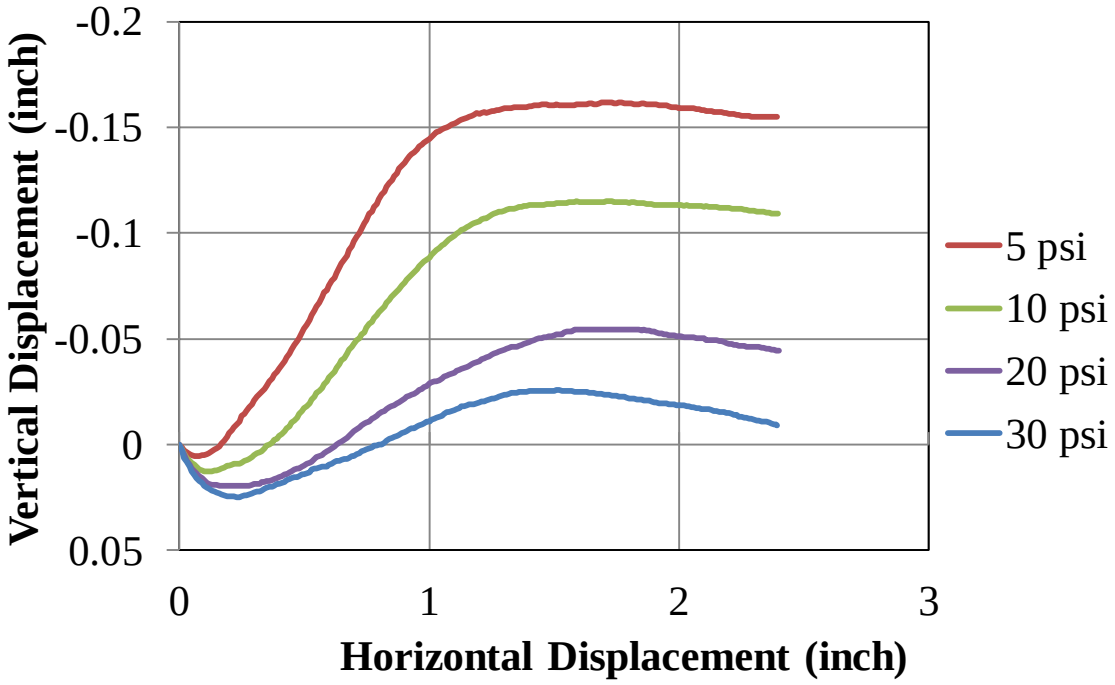

Figure 102. Graph. AASHTO No. 9 LSDS deformation test results (DC tests).

Table 37. Summary of AASHTO No. 8 LSDS results (TFHRC tests).

Soil Type	Normal Stress (psi)	Max Shear (psi)	Peak Friction Angle (°)	Peak Dilation Angle (°)	Gap (inch)
8	5.04	15.220948	71.68	15.66	0.443
8	10.06	26.73174	69.38	11.01	0.443
8	20.03	39.8865	63.34	8.07	0.443
8	30.02	52.54942	60.26	5.10	0.443

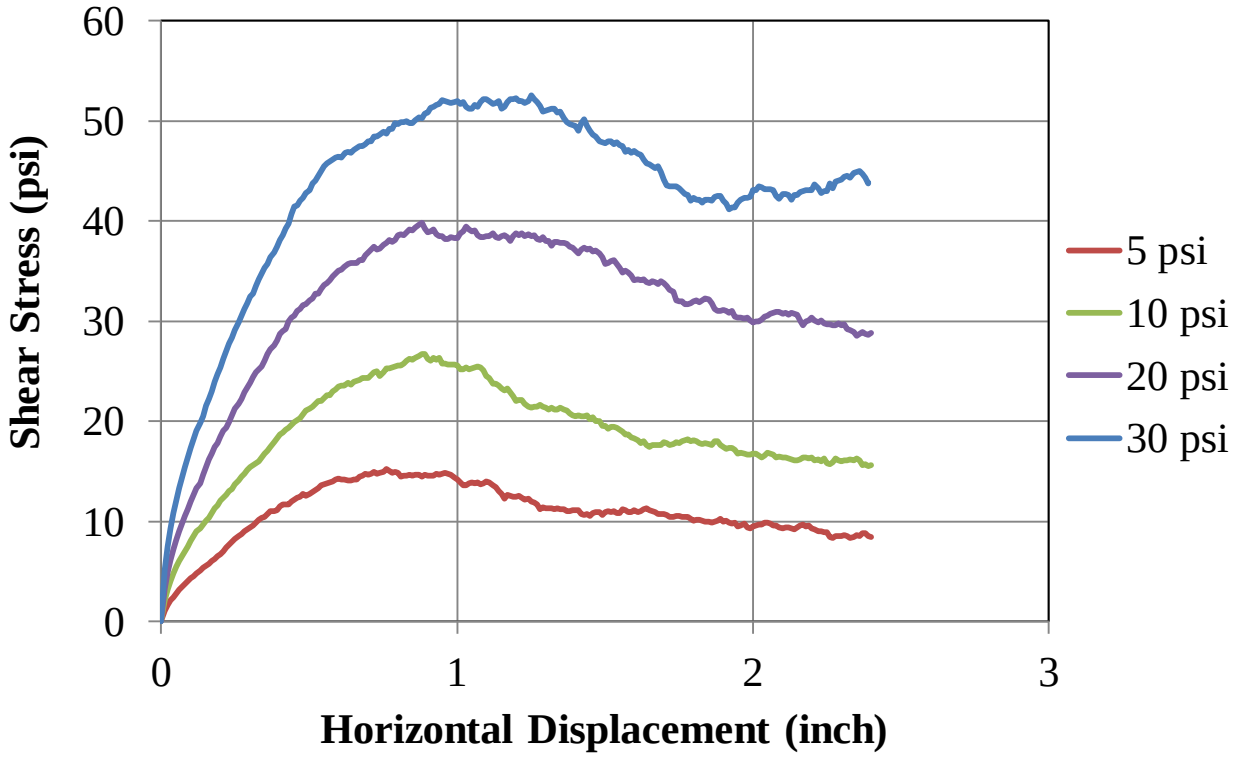

Figure 103. Graph. AASHTO No. 8 LSDS test results (TFHRC tests).

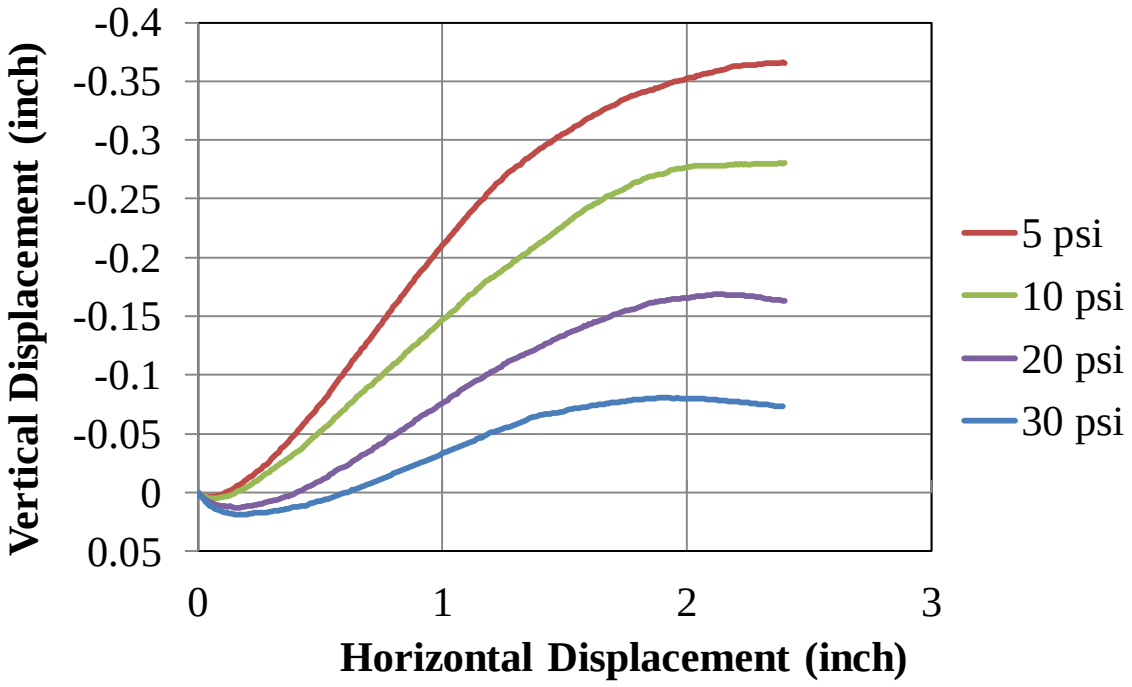

Figure 104. Graph. AASHTO No. 8 LSDS deformation test results (DC tests).

Table 38. Summary of AASHTO A-1-a (VDOT 21A) LSDS results (TFHRC tests).

Soil Type	Test Condition	Normal Stress (psi)	Max Shear (psi)	Peak Friction Angle (°)	Peak Dilation Angle (°)	Gap (inch)
21A	Dry	5.046	17.305	73.74	26.08	0.58
21A	Dry	10.05	23.6762	67.00	20.48	0.58
21A	Dry	20.02	40.35021	63.61	12.58	0.58
21A	Dry	30.03	50.135	59.08	11.05	0.58
21A	Saturated	4.99	5.46532	47.60	0.00	0.58
21A	Saturated	9.991	14.2569	54.98	0.05	0.58
21A	Saturated	19.98	25.034	51.41	0.00	0.58
21A	Saturated	29.99	36.2423	50.39	0.00	0.58

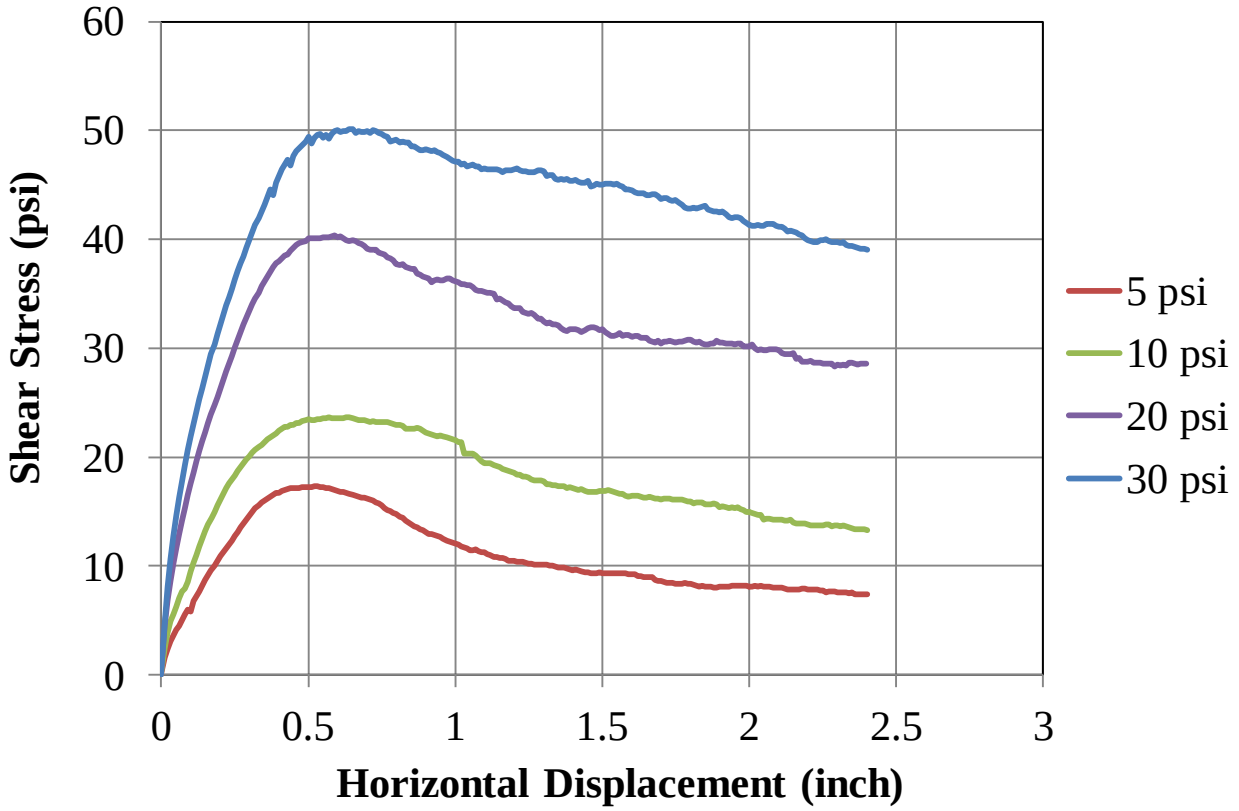

Figure 105. Graph. AASHTO A-1-a (VDOT 21A) LSDS test results (TFHRC tests).

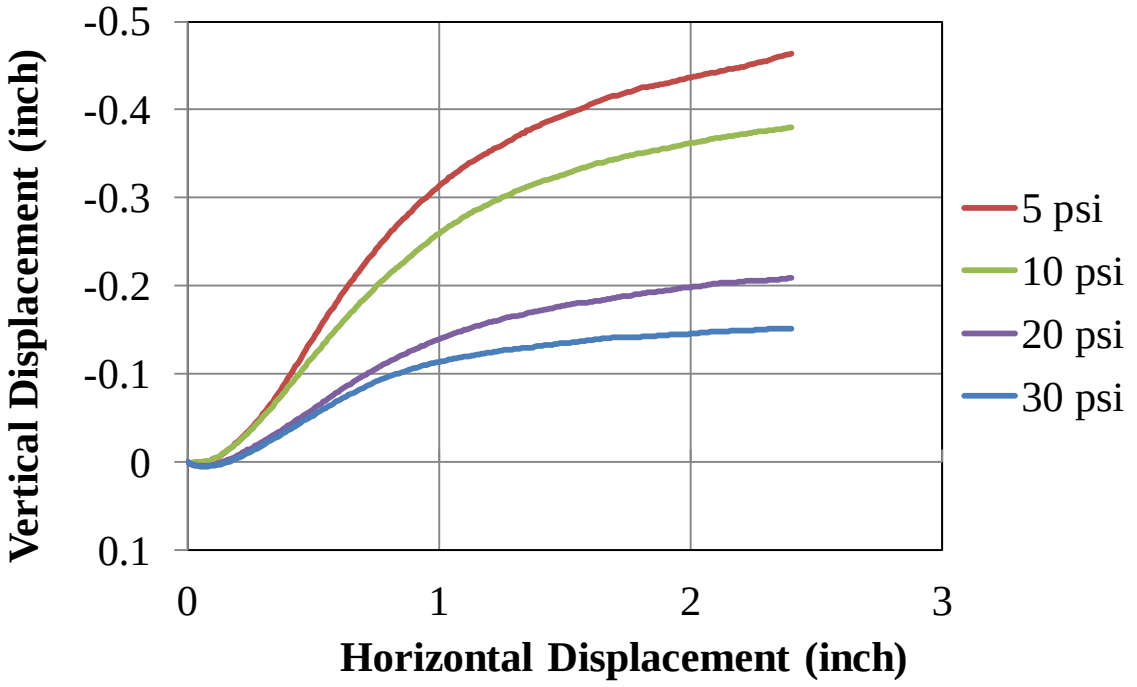

Figure 106. Graph. AASHTO A-1-a (VDOT 21A) LSDS deformation test results (DC tests).

APPENDIX B. NUCLEAR DENSITY TESTING FOR TFHRC PTS

Table 39. TF-2 Nuclear density test results.

Lift	Depth (inch)	γ_d (pcf)	Percent of Proctor	ω (percent)
1	backscatter	107.8	95.6	1.2
	backscatter	109.2	96.8	1.4
2	4	107	94.8	1.4
	6	112.8	100.0	1.2
3	4	101	89.5	1.1
	6	104.6	92.7	0.8
4	4	109.9	97.4	1
	6	110	97.5	1
5	4	111.6	98.9	0.7
	6	114.7	101.7	0.8
6	4	109.1	96.7	1.7
	6	111	98.4	1.3
7	4	110.9	98.3	1.9
	6	110.7	98.1	0.9
8	4	117.2	103.9	1.2
	6	113.4	100.5	1.4
9	4	111.4	98.7	1.1
	6	115	101.9	0.8
10	4	111.7	99.0	1.9
	6	110.3	97.8	0.9

Table 40. TF-2 Nuclear density test results.

Lift	Depth (inch)	γ_d (pcf)	Percent of Proctor	ω (percent)
1	4	148.5	99.7	5.5
	6	149.8	100.6	7.2
2	4	147	98.7	6.7
	6	145.5	97.7	6
3	4	145.6	97.8	6.9
	6	147.6	99.1	6.3
4	4	141.9	95.3	6.6
	6	141.5	95.0	6.3
5	4	147.2	98.9	5.9
	6	148.6	99.8	6.2
6	4	145.5	97.7	6.2
	6	146.2	98.2	6.8
7	4	146.4	98.3	6.4
	6	145.8	97.9	5.8
8	4	147.3	98.9	6
	6	146.2	98.2	6.1
9	4			
	6			
10	4			
	6			

Blank cell = no data available.

Table 41. TF-3 Nuclear density test results.

Lift	Depth (inch)	γ_d (pcf)	Percent of Proctor	ω (percent)
1	4	147.9	99.3	6.7
	6	148.1	99.5	7
2	4	146.1	98.1	6.7
	6	150.8	101.3	6.6
3	4	147.4	99.0	6.2
	6	149	100.1	5.9
4	4	146.2	98.2	6.8
	6	149.5	100.4	6.1
5	4	149.7	100.5	5.5
	6	149.1	100.1	6.5
6	6	147.3	98.9	7.8
7	6	147.2	98.9	7.9
8	6	149.3	100.3	6.4
9	6	151.3	101.6	6.1
10	6	151.1	101.5	6.6

Table 42. TF-4 Nuclear density test results.

Lift	Depth (inch)	γ_d (pcf)	Percent of Proctor	ω (percent)
1	4	149.2	100.2	6.3
2	6	147.6	99.1	6.3
3	6	147.7	99.2	6.2
4	6	147.9	99.3	7.3
5	6	149	100.1	7
6	6	149.7	100.5	7.1
7	6	149.4	100.3	6.8
8	6	151.1	101.5	6.2
9	6	152.6	102.5	5.6
10	6	151.1	101.5	6.8

Table 43. TF-5 Nuclear density test results.

Lift	Depth (inch)	γ_d (pcf)	Percent of Proctor	ω (percent)
1	6	148.1	99.5	4.9
2	6	148.1	99.5	6.1
3	6	150.2	100.9	6.5
4	6	151.7	101.9	6.3
5	6	152.7	102.6	5.7
6	6	148	99.4	6.5
7	6	151	101.4	5.7
8	6	151	101.4	5.7
9	6	148.7	99.9	6.1
10	6	154.5	103.8	5.4

Table 44. TF-6 Nuclear density test results.

Lift	Depth (inch)	γ_d (pcf)	Percent of Proctor	ω (percent)
1	6	148.9	100.0	6.4
2	6	147.9	99.3	6
3	6	150.1	100.8	6.5
4	6	151	101.4	6.5
5	6	149.9	100.7	6.7
6	6	149.6	100.5	6.5
7	6	150.3	100.9	6.9
8	6	151.9	102.0	5.8
9	6	150.7	101.2	5.5
10	6	148.9	100.0	6.2

Table 45. TF-7 Nuclear density test results.

Lift	Depth (inch)	γ_d (pcf)	Percent of Proctor	ω (percent)
1	6	150.1	100.8	6.3
2	6	151.2	101.5	5.9
3	6	150.1	100.8	6.2
4	6	149.1	100.1	6.1
5	6	152.3	102.3	6.1
6	6	150.2	100.9	5.8
7	6	151	101.4	5.9
8	6	148.9	100.0	6.3
9	6	149.5	100.4	5.9
10	6	152.5	102.4	5.9

Table 46. TF-8 Nuclear density test results.

Lift	Depth (inch)	γ_d (pcf)	Percent of Proctor	ω (percent)
1	6	149.1	100.1	7.1
2	6	148.7	99.9	6.9
3	6	151	101.4	6.4
4	6	150.6	101.1	6.3
5	6	151.5	101.7	6.5
6	6	150.5	101.1	6.5
7	6	151.2	101.5	6.3
8	6	151.1	101.5	6.4
9	2	147.6	99.1	6.2
10	2	146.9	98.7	6.5
10	2	150.8	101.3	5.9

Table 47. TF-9 Nuclear density test results.

Lift	Depth (inch)	γ_d (pcf)	Percent of Proctor	ω (percent)
1	6	150.9	101.3	5.9
2	8	150.2	100.9	5.9
3	6	148.9	100.0	5.4
4	8	147.4	99.0	5.5
5	6	151.1	101.5	6.1
6	8	147	98.7	6.5
7	6	151.3	101.6	6.3
8	8	150.1	100.8	6.3
9	6	150.1	100.8	6.3
10	8	150.6	101.1	6

Table 48. TF-10 Nuclear density test results.

Lift	Depth (inch)	γ_d (pcf)	Percent of Proctor	ω (percent)
1	6	148.5	99.7	5.1
2	8	146.5	98.4	5.4
3	6	150.5	101.1	5.6
4	8	148.5	99.7	6.5
5	6	148.4	99.7	7.4
6	8	148.7	99.9	6.6
7	6	149.1	100.1	6.3
8	8	149.2	100.2	6.5
9	6	149.3	100.3	6.7
10	8	151	101.4	6.6

Table 49. TF-11 Nuclear density test results.

Lift	Depth (inch)	γ_d (pcf)	Percent of Proctor	ω (percent)
1	2	148	99.4	6.8
	2	150.2	100.9	6.5
2	2	153.2	102.9	5.5
	2	149.8	100.6	6.2
3	2	149.8	100.6	6.1
	2	150.4	101.0	5.8
4	2	151.8	101.9	5.8
	2	151.8	101.9	5.7
5	2	150.6	101.1	6.2
	2	148.2	99.5	6.1
6	2	149.9	100.7	5.8
	2	149.3	100.3	5.5
7	2	147.4	99.0	5.6
	2	150.6	101.1	5.7
8	2	149.9	100.7	5.5
	2	150	100.7	5.8
9	2	150.2	100.9	5.4
	2	152.3	102.3	5.4
10	2	149.9	100.7	5.8
	2	149.8	100.6	5.9

Table 50. TF-12 Nuclear density test results.

Lift	Depth (inch)	γ_d (pcf)	Percent of Proctor	ω (percent)
1	2	149	100.1	6
	2	148.7	99.9	5.8
2	2	148.1	99.5	5.7
	2	149	100.1	6.3
3	2	150.3	100.9	6.5
	2	148.2	99.5	6.6
4	2	149.3	100.3	6.4
	2	148.5	99.7	6.0
5	2	147.6	99.1	5.8
	2	150.4	101.0	5.9
6	2	148	99.4	6
	2	148.8	99.9	5.5
7	2	148.5	99.7	6
	2	152.2	102.2	5.6
8	2	147.9	99.3	6.1
	2	148	99.4	6.4
9	2	151.1	101.5	6.2
	2	149	100.1	6.1
10	2	149.9	100.7	5.0
	2	151.1	101.5	5.0

Table 51. TF-13 Nuclear density test results

Lift	Depth (inch)	γ_d (pcf)	Percent of Proctor	ω (percent)
1	4	148	99.4	6.8
	4	146.6	98.5	6.3
	4	147.4	99.0	5.7
2	4	147.6	99.1	5.8
	4	147.8	99.3	5.7
	4	150.9	101.3	5.7
3	6	151.9	102.0	6.8
	4	150.5	101.1	6.6
4	6	149.9	100.7	6.3
	4	147	98.8	5.9
5	8	146.8	98.6	6
	4	150.6	101.1	6.4
6	6	152.4	102.4	6
	4	148.2	99.50	5.8
7	6	149.4	100.3	5.9
	4	153.2	102.9	5.7

Table 52. TF-14 Nuclear density test results.

Lift	Depth (inch)	γ_d (pcf)	Percent of Proctor	ω (percent)
1	6	147.8	99.3	4.4
	4	150.5	101.1	6.6
2	6	150.6	101.1	6.8
	4	148	99.4	5.6
3	6	148.3	99.6	5.8
	4	149.7	100.5	5.5
4	6	150.6	101.1	7
	4	147.9	99.3	7.4
5	6	147.4	99.0	7.4
	4	148.5	99.7	7
6	6	150	100.7	6.2
	4	148	99.4	7.1
7	6	150.2	100.9	6.7
	4	147.8	99.3	6.6

APPENDIX C. DEFORMATION INSTRUMENTATION LAYOUTS FOR PTS

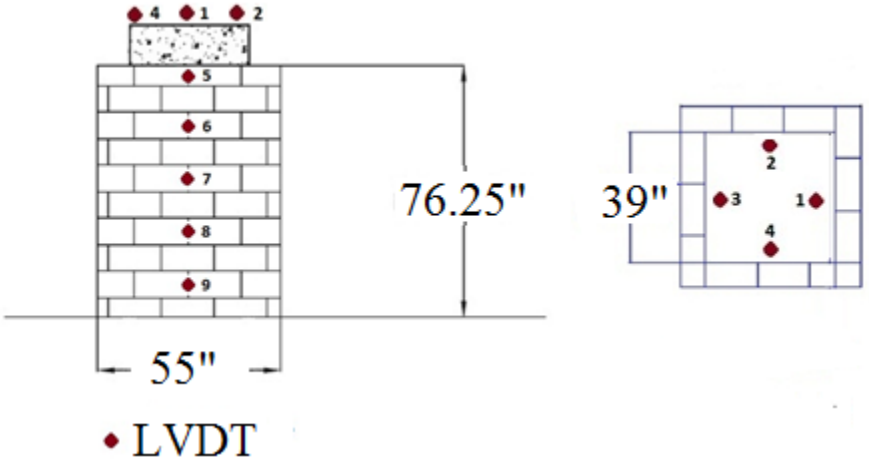

Figure 107. Illustration. Instrumentation layout for DC tests and TF-1.

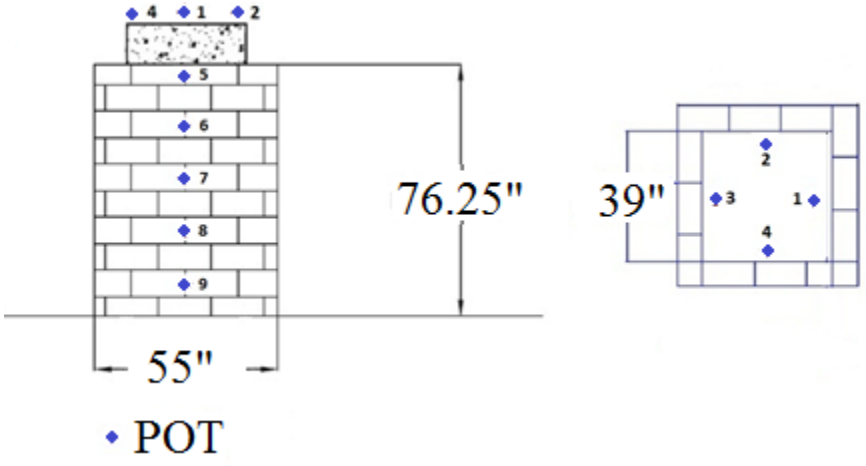

Figure 108. Illustration. Instrumentation layout for TF-2, TF-9.

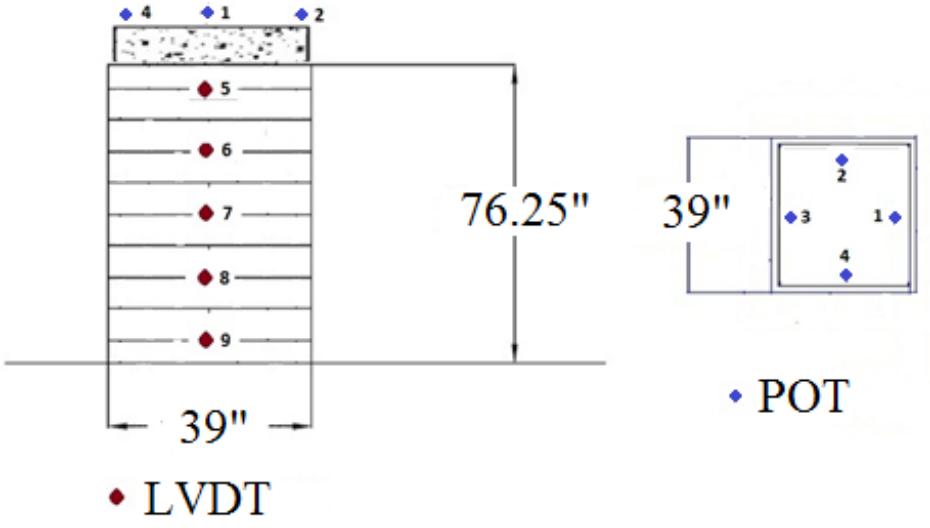

Figure 109. Illustration. Instrumentation layout for TF-3, TF-4.

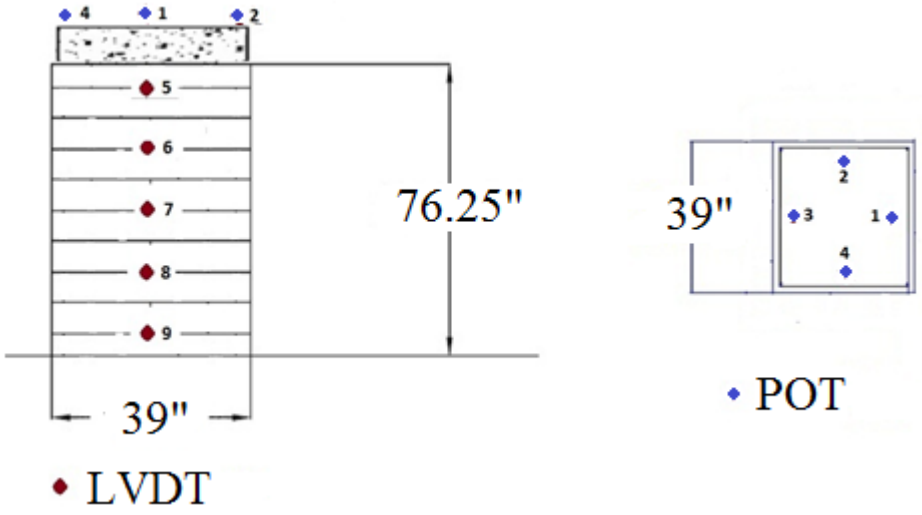

Figure 110. Illustration. Instrumentation layout for TF-5, TF-7.

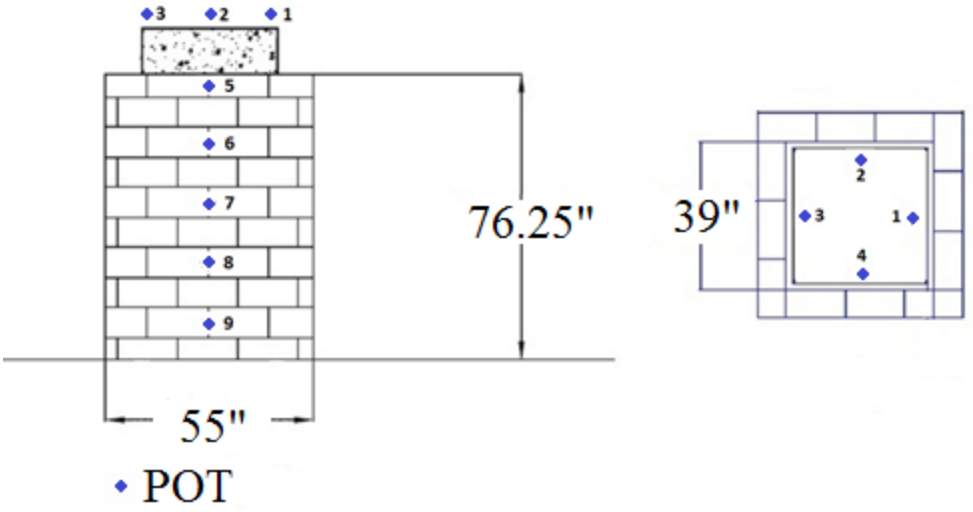

Figure 111. Instrumentation layout for TF-6, TF-12.

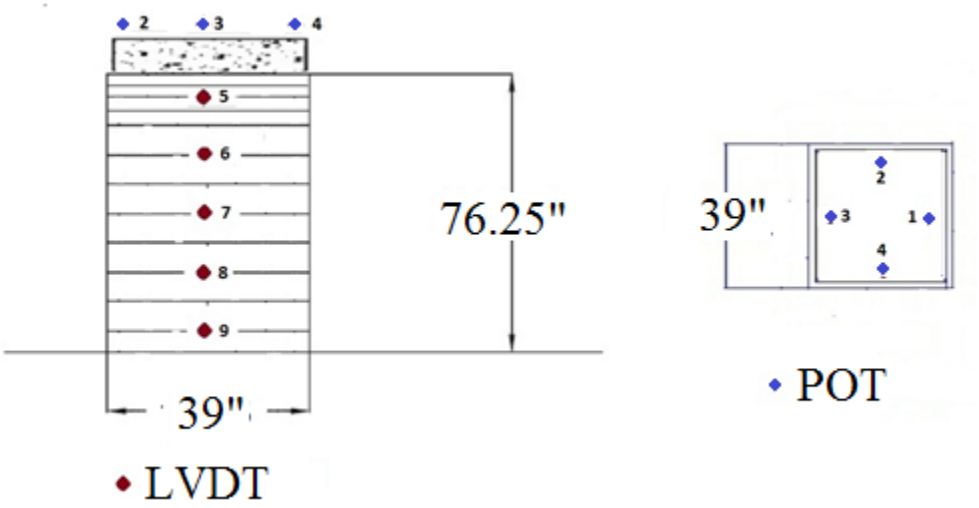

Figure 112. Illustration. Instrumentation layout for TF-8.

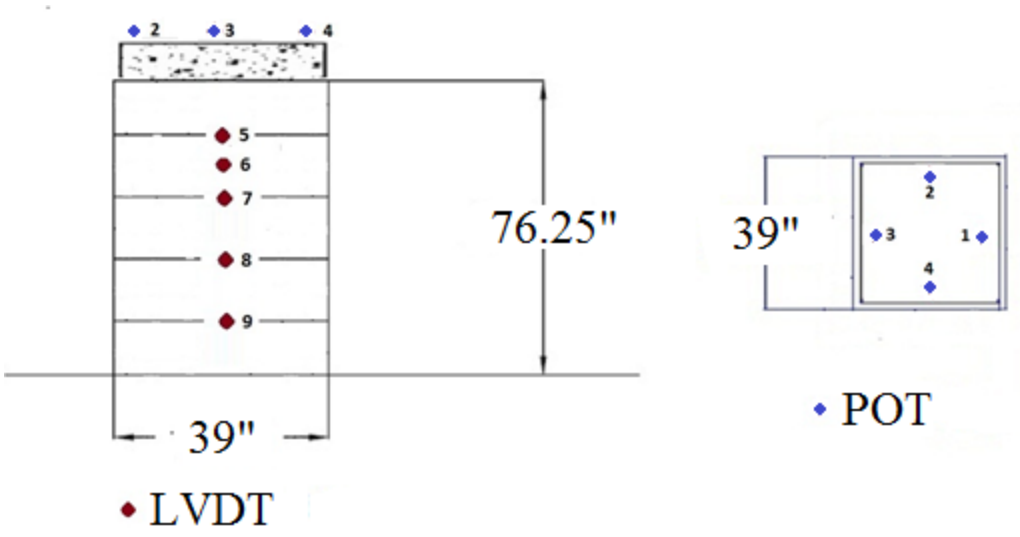

Figure 113. Illustration. Instrumentation layout for TF-10.

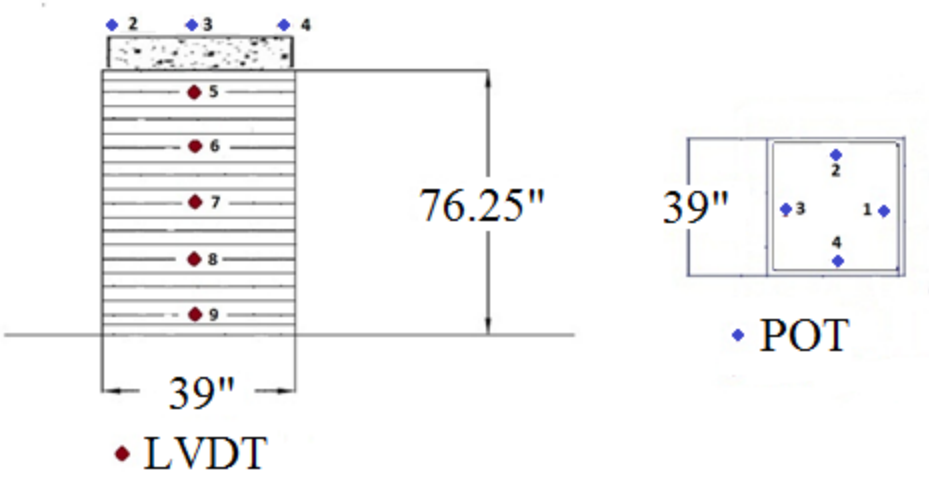

Figure 114. Illustration. Instrumentation layout for TF-13

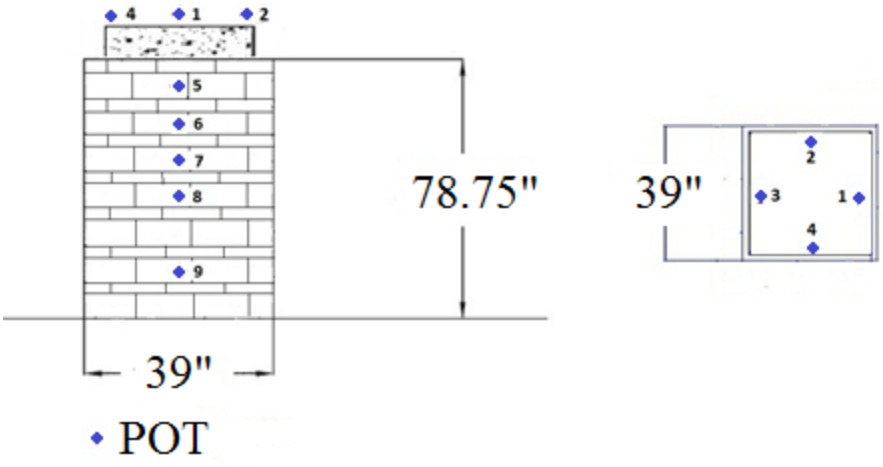

Figure 115. Illustration. Instrumentation layout for TF-14.

APPENDIX D. RAW DATA FOR PTS

Table 53. DC-1 PT Data.

Average Load (lb/jack)	Applied Pressure (psf)	Vertical Settlement (inch)	Vertical strain (percent)
0.00	0.00	0.00	0.00
6,000.29	2,666.80	0.33	0.43
7,691.24	3,418.33	0.43	0.56
10,891.56	4,840.69	0.58	0.76
13,882.17	6,169.85	0.82	1.08
16,743.42	7,441.52	1.02	1.34
18,617.17	8,274.30	1.19	1.56
20,737.31	9,216.58	1.35	1.78
23,679.35	10,524.15	1.56	2.05
26,749.52	11,888.68	1.85	2.43
29,760.19	13,226.75	2.12	2.79
32,796.45	14,576.20	2.60	3.43
36,725.03	16,322.23	2.99	3.93
38,843.79	17,263.90	3.24	4.26
41,800.05	18,577.80	3.57	4.70
45,218.53	20,097.12	3.82	5.02
49,169.75	21,853.22	4.20	5.52
52,488.78	23,328.34	6.04	7.95

Table 54. DC-2 PT Data.

Average Load (lb/jack)	Applied Pressure (psf)	Vertical Settlement (inch)	Vertical strain (percent)
0.00	0.00	0.00	0.00
5,787.51	2,572.23	0.59	0.78
7,200.47	3,200.21	0.75	0.99
8,940.54	3,973.57	0.92	1.21
10,952.92	4,867.97	1.17	1.53
12,974.76	5,766.56	1.40	1.83
15,051.84	6,689.71	1.64	2.15
17,077.36	7,589.94	1.88	2.46
19,204.93	8,535.52	2.17	2.84
21,211.57	9,427.36	2.50	3.28
25,264.01	11,228.45	3.19	4.18
27,203.24	12,090.33	3.50	4.59
29,368.95	13,052.87	3.73	4.89
31,354.88	13,935.50	4.01	5.26
34,309.37	15,248.61	4.47	5.86
37,455.51	16,646.89	4.76	6.24
40,418.89	17,963.95	4.83	6.34
43,298.49	19,243.77	4.90	6.43
51,134.47	22,726.43	5.37	7.04

Table 55. DC-3 PT Data.

Average Load (lb/jack)	Applied Pressure (psf)	Vertical Settlement (inch)	Vertical strain (percent)
0.00	0.00	0.00	0.00
1,649.95	733.31	0.24	0.31
4,305.23	1,913.44	0.52	0.68
6,976.55	3,100.69	0.78	1.03
9,692.94	4,307.98	1.03	1.35
12,450.76	5,533.67	1.29	1.70
14,973.40	6,654.85	1.54	2.02
17,582.22	7,814.32	1.83	2.41
20,165.77	8,962.56	2.12	2.78
23,249.20	10,332.98	2.42	3.19
26,217.45	11,652.20	2.77	3.64
29,407.36	13,069.94	3.08	4.05
32,442.93	14,419.08	3.37	4.43
35,518.85	15,786.16	3.70	4.87
38,565.19	17,140.08	4.04	5.32
41,538.90	18,461.73	4.42	5.82

Table 56. DC-4 PT Data.

Average Load (lb/jack)	Applied Pressure (psf)	Vertical Settlement (inch)	Vertical strain (percent)
0.00	0.00	0.00	0.00
2,724.22	1,210.76	0.16	0.22
5,017.17	2,229.85	0.38	0.51
7,568.27	3,363.68	0.59	0.77
9,949.51	4,422.01	0.82	1.08
12,971.35	5,765.05	1.11	1.46
15,926.47	7,078.43	1.40	1.84
19,025.69	8,455.86	1.70	2.24
21,821.66	9,698.52	1.98	2.61
24,883.53	11,059.35	2.26	2.97
27,993.61	12,441.61	2.58	3.40
30,894.62	13,730.94	2.94	3.87
34,053.34	15,134.82	3.30	4.34
36,906.96	16,403.09	3.54	4.66
39,975.59	17,766.93	3.91	5.15
42,919.44	19,075.31	4.25	5.60
45,841.51	20,374.00	4.52	5.95
47,205.64	20,980.28	4.70	6.18
50,450.81	22,422.58	4.95	6.52
55,229.31	24,546.36	5.36	7.06
60,188.19	26,750.31	5.81	7.64

Table 57. DC-5 PT Data.

Average Load (lb/jack)	Applied Pressure (psf)	Vertical Settlement (inch)	Vertical strain (percent)
0.00	0.00	0.00	0.00
622.79	276.79	0.37	0.48
2,739.19	1,217.42	0.68	0.89
4,857.51	2,158.89	0.96	1.26
7,021.37	3,120.61	1.20	1.57
9,060.95	4,027.09	1.43	1.88
11,088.41	4,928.18	1.68	2.21
14,307.26	6,358.78	2.02	2.66
17,440.25	7,751.22	2.41	3.17
20,525.62	9,122.50	2.83	3.73
23,676.51	10,522.90	3.26	4.29
26,657.83	11,847.92	3.84	5.05
29,865.77	13,273.68	4.24	5.58
32,794.82	14,575.47	4.64	6.10
35,897.19	15,954.31	5.05	6.64
43,500.00	19,333.33	5.92	7.79
48,500.00	21,555.56	7.92	10.42

Table 58. TF-1 PT Data.

Applied Pressure (psf)	Vertical Settlement (inch)	Vertical strain (percent)
0.00	0.00	0.00
369.70	0.08	0.10
556.35	0.08	0.11
978.69	0.16	0.21
1,842.65	0.33	0.43
2,804.93	0.55	0.72
3,696.98	0.75	0.99
4,646.86	0.99	1.30
5,578.45	1.22	1.59
6,465.19	1.45	1.90
7,448.68	1.70	2.22
8,340.86	1.96	2.57
9,232.90	2.24	2.94
10,164.52	2.51	3.29
11,057.92	2.80	3.67
11,952.08	3.08	4.04
12,761.14	3.28	4.31
13,472.62	3.86	5.07
14,465.32	4.76	6.24
15,231.20	4.99	6.54
16,000.57	5.31	6.96
16,994.27	5.55	7.27
17,862.85	6.13	8.04
18,781.38	7.36	9.66
20,486.98	8.31	10.90

Table 59. TF-2 PT Data.

Applied Pressure (psf)	Vertical Settlement (inch)	Vertical strain (percent)
0.00	0.00	0.00
829.67	0.03	0.03
1,760.89	0.09	0.12
2,604.89	0.17	0.22
3,559.11	0.25	0.33
4,509.78	0.35	0.46
5,438.67	0.46	0.60
6,372.00	0.57	0.75
8,220.00	0.83	1.09
10,084.00	1.13	1.48
11,006.67	1.29	1.70
13,812.44	1.92	2.53
16,591.11	2.64	3.48
19,472.89	4.22	5.55
22,352.00	6.47	8.51
25,278.67	8.71	11.46

Table 60. TF-3 PT Data.

Applied Pressure (psf)	Vertical Settlement (inch)	Vertical strain (percent)
0.00	0.00	0.00
883.61	0.03	0.04
2,692.89	0.25	0.33
3,590.22	0.41	0.54
5,333.33	1.01	1.33
6,311.11	1.22	1.60
8,088.89	1.98	2.60
9,866.67	2.67	3.50
10,755.56	3.13	4.10
13,333.33	4.42	5.80
14,666.67	5.41	7.10
16,156.89	7.52	9.87
17,503.56	10.52	13.80

Table 61. TF-4 PT Data.

Applied Pressure (psf)	Vertical Settlement (inch)	Vertical strain (percent)
0.00	0.00	0.00
1,496.46	0.04	0.06
2,157.57	0.08	0.10
3,211.69	0.27	0.36
4,128.22	0.47	0.62
5,072.21	0.70	0.92
6,015.01	0.94	1.23
6,930.25	1.16	1.53
8,837.16	1.71	2.25
10,703.07	2.34	3.08
14,250.89	3.34	4.40

Table 62. TF-5 PT Data.

Applied Pressure (psf)	Vertical Settlement (inch)	Vertical strain (percent)
0	0	0
1,152	0.046214	0.060808
2,736	0.09353	0.123066
4,176	0.126134	0.165966
4,608	0.1733	0.228046
5,472	0.289825	0.381349
6,480	0.455363	0.599162
8,352	0.892178	1.173918
10,080	1.466227	1.929246
11,088	1.761062	2.317187
13,968	2.954815	3.887914
16,704	4.390352	5.776779
19,584	5.947989	7.826301
22,464	8.176841	10.759
25,344	9.917697	13.0496
10,944	9.843107	12.95146
0	8.705762	11.45495
0	8.700209	11.44764
2,448	0.512515	12.12201
3,744	0.663577	12.32077
5,616	0.822237	12.52953
8,496	1.007906	12.77384
11,232	1.19151	13.01542
16,992	1.785724	13.79728
22,464	3.312276	15.8059
25,920	4.924452	17.92719

Table 63. TF-6 PT Data.

Applied Pressure (psf)	Vertical Settlement (inch)	Vertical strain (percent)
0.00	0.00	0.00
889.74	0.06	0.08
1,764.73	0.20	0.27
2,522.17	0.26	0.34
3,718.49	0.38	0.50
4,546.27	0.48	0.64
5,357.84	0.65	0.85
6,255.09	0.73	0.96
8,011.64	0.93	1.22
9,850.08	1.82	2.39
13,449.91	2.27	2.99
18,706.79	3.16	4.15
21,447.16	3.68	4.84
24,041.44	4.24	5.58
26,687.14	4.76	6.27
29,321.85	5.34	7.02
30,643.85	5.79	7.62
31,937.57	6.25	8.22
33,305.27	6.83	8.99
35,809.33	7.66	10.08
38,714.79	8.76	11.52
41,250.78	10.75	14.15
43,827.56	11.95	15.73

Table 64. TF-7 PT Data.

Applied Pressure (psf)	Vertical Settlement (inch)	Vertical strain (percent)
0	0	0
906.5827	0.14	0.19
1,843.848	0.31	0.40
2,727.728	0.48	0.63
3,579.004	0.65	0.86
4,443.513	0.90	1.19
5,359.769	1.08	1.42
6,237.56	1.29	1.70
7,992.877	1.75	2.30
9,808.05	2.29	3.01
10,739.62	2.59	3.41
13,366.63	3.65	4.80
15,953.95	4.89	6.44
18,656.81	6.54	8.61
21,257.23	7.80	10.27
24,085.41	9.54	12.55
26,573.67	12.46	16.39

Table 65. TF-8 PT Data.

Applied Pressure (psf)	Vertical Settlement (inch)	Vertical strain (percent)
0.00	0.00	0.00
901.25	0.19	0.24
1,784.19	0.39	0.51
2,673.33	0.60	0.78
3,610.08	0.81	1.07
4,460.27	1.00	1.32
5,317.64	1.20	1.58
6,194.72	1.42	1.87
7,942.55	1.87	2.46
9,762.13	2.38	3.13
10,636.89	2.66	3.50
13,345.60	3.62	4.76
16,003.43	4.70	6.18
18,547.61	5.90	7.76
21,274.89	7.35	9.67
23,999.31	8.62	11.34
26,608.37	10.10	13.29
29,178.74	13.51	17.77

Table 66. TF-9 PT Data.

Applied Pressure (psf)	Vertical Settlement (inch)	Vertical strain (percent)
0.00	0.00	0.00
434.85	0.06	0.08
573.32	0.07	0.09
746.42	0.09	0.12
1,225.31	0.14	0.19
1,898.80	0.24	0.31
2,541.19	0.32	0.42
3,146.98	0.41	0.54
3,725.78	0.50	0.65
4,334.89	0.63	0.84
5,585.85	0.85	1.12
6,790.22	1.08	1.43
7,433.04	1.24	1.63
9,292.90	1.74	2.29
11,195.61	2.46	3.24
13,072.80	3.36	4.43
14,953.66	5.17	6.80
16,806.30	6.49	8.53
18,680.80	8.05	10.59
20,537.79	9.95	13.09
22,360.24	11.83	15.56

Table 67. TF-10 PT Data.

Applied Pressure (psf)	Vertical Settlement (inch)	Vertical strain (percent)
0.00	0.00	0.00
375.25	0.09	0.12
1,115.40	0.28	0.37
1,443.58	0.35	0.46
1,641.11	0.39	0.51
2,060.36	0.50	0.66
2,478.58	0.64	0.84
2,915.38	0.77	1.02
3,691.10	1.07	1.40
4,536.46	1.46	1.92
4,958.59	1.68	2.22
6,186.24	2.53	3.33
7,432.09	3.86	5.08
8,625.99	6.32	8.32
8,838.17	9.05	11.91
10,339.14	10.85	14.28

Table 68. TF-11 PT Data.

Applied Pressure (psf)	Vertical Settlement (inch)	Vertical strain (percent)
0.00	0.00	0.00
1,321.94	0.08	0.10
1,712.69	0.21	0.27
2,676.26	0.35	0.46
3,506.48	0.50	0.66
4,368.60	0.67	0.89
5,242.11	0.87	1.15
6,148.03	1.08	1.43
7,785.80	1.56	2.05
9,525.78	2.15	2.83
10,468.16	2.54	3.34
13,028.22	3.65	4.81
15,745.28	5.04	6.63
18,444.67	7.03	9.25
21,111.16	8.68	11.43
23,276.92	9.72	12.79

Table 69. TF-12 PT Data.

Applied Pressure (psf)	Vertical Settlement (inch)	Vertical strain (percent)
0.00	0.00	0.00
995.38	0.11	0.14
2,018.60	0.20	0.26
3,079.10	0.29	0.39
4,185.50	0.39	0.52
5,360.08	0.51	0.67
6,463.52	0.63	0.82
7,552.20	0.75	0.98
9,702.94	1.02	1.34
11,883.24	1.32	1.74
12,969.50	1.54	2.03
16,219.10	2.27	2.99
19,473.98	4.39	5.77
22,908.22	7.05	9.28
26,174.57	9.09	11.96
29,062.81	10.16	13.37

Table 70. TF-13 PT Data.

Applied Pressure (psf)	Vertical Settlement (inch)	Vertical strain (percent)
0	0	0
762.3172	0.098888	0.125573
1,333.227	0.162839	0.20678
1,879.568	0.26315	0.334158
2,320.298	0.38099	0.483797
3,020.67	0.511435	0.649442
3,600.98	0.668502	0.848892
3,931.689	0.836782	1.06258
5,394.454	1.27596	1.620266
6,626.904	1.847268	2.345737
7,227.084	2.249614	2.856652
9,002.369	4.368862	5.547761
10,789.2	6.084915	7.726876
12,984.6	9.703566	12.32199

Table 71. TF-14 PT Data.

Applied Pressure (psf)	Vertical Settlement (inch)	Vertical strain (percent)
0.00	0.00	0.00
580.06	0.16	0.21
1,191.94	0.25	0.32
1,829.39	0.35	0.46
2,466.98	0.45	0.59
3,001.13	0.54	0.71
3,611.30	0.64	0.84
4,225.24	0.74	0.98
5,402.42	0.94	1.24
6,620.61	1.15	1.51
7,233.56	1.28	1.68
9,042.58	1.65	2.18
10,965.38	2.07	2.72
12,738.15	2.53	3.33
14,571.33	3.08	4.05
16,460.84	3.68	4.84
18,314.54	4.45	5.85
20,140.13	5.51	7.25
22,071.79	7.13	9.39
23,603.11	9.65	12.69

ACKNOWLEGEMENTS

The authors would like to acknowledge the hard work and effort of Ms. Jan Li, Mr. Moustafa Ibrahim-Awad, Mr. Tim Tuggle, Mr. Jeffrey Lin, and Mr. Daniel Powers in helping to construct and test the performance tests at Turner-Fairbank Highway Research Center. In addition, thanks to Dr. Fassil Beshah for coordinating use of the Structures Laboratory. For the tests conducted in Defiance County, OH, the authors wish to thank Mr. Warren Schlatter and Mr. Jeff Timbrook, along with the participants of each GRS EDC Validation Session. Finally, the authors would also like to extend their appreciation for the technical review comments prepared by (in alphabetical order) Mr. Daniel Alzamora of the Resource Center, Khalid Mohamed of the Office of Bridge Technology, and Dr. Justin Ocel of the Office of Infrastructure Research and Development.

REFERENCES

1. Adams, M., Nicks, J., Stabile, T., Wu, J., Schlatter, W., and Hartmann, J., "Geosynthetic Reinforced Soil Integrated Bridge System Interim Implementation Guide". *Report*, FHWA-HRT-11-026, Federal Highway Administration, McLean, VA, 2011a.
2. Adams, M.T., Lillis, C.P., Wu, J.T.H., and Ketchart, K., "Vegas Mini Pier Experiment and Postulate of Zero Volume Change," *Proceedings, Seventh International Conference on Geosynthetics*, Nice, France, 2002, pp. 389–394.
3. ASTM D7181, "Standard Test Method for Consolidated Drained Triaxial Compression Test for Soils," *Annual Book of ASTM Standards*, ASTM International, West Conshohocken, PA, 2011.
4. Adams, M.T., Ketchart, K., and Wu, J.T.H., "Mini Pier Experiments: Geosynthetic Reinforcement Spacing and Strength as Related to Performance," *Geotechnical Special Publication 165, Geosynthetics in Reinforcement and Hydraulic Applications*, Geo-Denver *2007*, ASCE, Denver, CO, 2007.
5. Adams, M., Nicks, J., Stabile, T., Wu, J., Schlatter, W., and Hartmann, J., "Geosynthetic Reinforced Soil Integrated Bridge System Synthesis Report," *Report*, FHWA-HRT-11-027, Federal Highway Administration, McLean, VA, 2011b.
6. Juran, I., Guermazi, A., Chen, C.L. and Ider, M.H., "Modeling and simulation of load transfer in reinforced soils: Part 1". *International Journal for Numerical and Analytical Methods in Geomechanics, 12*(2), John Wiley and Sons, 2005, pp. 141–155.
7. Ketchart, K. and Wu, J.T.H. "Performance Test for Geosynthetic-Reinforced Soil including Effects of Preloading," *Report*, FHWA-RD-01-018, Federal Highway Administration, McLean, VA, 2001. <http://www.tfhrc.gov/structur/gtr/01-018.pdf>, retrieved on December 6, 2012.
8. Elton, D.J. and Patawaran, M.A.B., "Mechanically Stabilized Earth (MSE) Reinforcement Tensile Strength from Tests of Geotextile Reinforced Soil," *Technical Report*, Alabama Highway Research Center, Auburn University, Auburn, AL, 2005.
9. Wu, J.T.H., Adams, M., Pham, T.Q., Lee, S.H., and Ma, C.Y., "A generic soil-geosynthetic composite test," *International Journal of Geotechnical Engineering*, *6*(1), 2012, pp. 103–116.
10. AASHTO, "LRFD Bridge Design Specifications, Edition 5," *Report*, American Association of State Highway and Transportation Officials, Washington, DC, 2012.
11. Wu, J.T.H., Pham, T.Q., and Adams, M.T., "Composite Behavior of Geosynthetic-Reinforced Soil (GRS) Mass," *Report*, FHWA-HRT-10-077, Federal Highway Administration, McLean, VA, 2010.
12. Wu, J.T.H. and Pham. T.Q., "Load-Carrying Capacity and Required Reinforcement Strength of Closely-Spaced Soil-Geosynthetic Composites," *ASCE Journal of Geotechnical and Geoenvironmental Engineering, 139*(1), Reston, VA, 2013.
13. ASTM D3080, "Standard Test Method for DIRECT Shear Test of Soils Under Consolidated Drained Conditions," *Annual Book of ASTM Standards*, ASTM International, West Conshohocken, PA, 2004.
14. ASTM D4595, "Standard Test Method for Tensile Properties of Geotextiles by the Wide-Width Strip Method," *Annual Book of ASTM Standards*, Vol. 4.13, ASTM International, West Conshohocken, PA, 2006, pp. 40–50.
15. AASHTO T-99, "Standard test methods for moisture density relations of soils and soil aggregate mixtures using 5.5 lb rammer and 12 in. drop. Standard specifications for highway

materials and methods of sampling and testing," American Association of State Highway Transportation Officials, Washington, DC, 2011.
16. ASTM D4253, "Standard Test Methods for Maximum Index Density and Unit Weight of Soils Using a Vibratory Table," *Annual Book of ASTM Standards*, ASTM International, West Conshohocken, PA, 2000.
17. Industrial Fabrics, "Geotext 200 ST Product Data Sheet," < http://www.ind-fab.com/downloads/200st.pdf>, retrieved on December 6, 2012.
18. Propex, "Geotex Woven Geotextiles Product Information," <http://geotextile.com/product/geotex.html>, retrieved on December 6, 2012.
19. US Fabrics, "US 3600/3600 Product Information," <http://www.usfabricsinc.com/products/us-3600-3600>, retrieved on December 6, 2012.
20. ASTM D4632, "Standard Test Method for Grab Breaking Load and Elongation of Geotextiles, Annual Book of ASTM Standards," ASTM International, West Conshohocken, PA, 2008.
21. Briaud J.-L., "Introduction to Soil Moduli," *Geotechnical News*, June 2001, BiTech Publishers Ltd, Richmond, BC, Canada, 2001. (geotechnicalnews@bitech.ca).
22. Adams, M.T., "Performance of a Prestrained Geosynthetic-Reinforced Soil Bridge Pier," *International Symposium on Mechanically Stabilized Backfill*, Wu, J.T.H. (ed), Denver, Balkema, 1997, pp. 35–53.
23. Wu, J.T.J., Ketchart, K., and Adams, M. "GRS Bridge Piers and Abutments," *FHWA Research Report*, FHWA-RD-00-038, FHWA, McLean, VA, 2000.
24. Meyerhof, G.G., "The ultimate capacity of foundations on slopes," *Procs., 4th Int. Conf. on Soil Mechanics and Found. Engrg., London, August*, London, England, 1957, pp. 384–386.
25. Pham, T.Q., "Investigating Composite Behavior of Geosynthetic Reinforced Soil (GRS) Mass," *Ph.D. Thesis*, University of Colorado, Denver CO, 2009.
26. NAVFAC, "Soil Mechanics Design Manual 7.01," Naval Facilities Engineering Command, Alexandria, VA, 1986.
27. Gibson, R.E., "Some results concerning displacements and stresses in a non-homogeneous elastic half space," *Geotechnique*, Vol. 17, 1967, pp. 58–67.
28. Poulos, H.G. and Davis, E.H., "Elastic Solutions for Soil and Rock Mechanics," John Wiley and Sons, New York, 1974.
29. Samtani, N.C., Nowatzki, E.A., and Mertz, D.R., "Selection of Spread Footings on Soils to Support Highway Bridge Structures," *Report*, FHWA-RC/TD-10-001, FHWA Resource Center, Matteson, IL, 2010.
30. Nicks, J.E., Adams, M., Wu, J., "A new approach to the design of closely spaced geosynthetic reinforced soil for load bearing applications," *TRB Annual Compendium of Papers*, Transportation Research Board, Washington DC., 2013a.
31. VanBuskirk, C.D., "Adoption and Implementation of GRS design concepts," *19th Vancouver Geotechnical Society Symposium*, Vancouver Geotechnical Society, Vancouver, Canada, 2010.
32. Nicks, J.E., Adams, M.T., and Alzamora, D.A., "Implications of MSE Connection Criteria for Frictionally Connected GRS Structures," *Proceedings of Geosynthetics 2013*, Long Beach, CA, 2013b.
33. Wu, J.T.H., Lee, K.Z.Z., Helwany, S.B., and Ketchart, K., "Design and Construction Guidelines for GRS Bridge Abutment with a Flexible Facing," *Report*, No. 556, National Cooperative Highway Research Program, Washington, DC, 2006.

34. Bathurst, R.J. and Benjamin, D.J., "Failure of a Geogrid-Reinforced Soil Wall," *Report*, Transportation Research Board, Washington, DC, 1990, pp. 109–116.
35. Barker, R.M., Duncan, J.M., Rojiani, K.B., Ooi, P.S.K., Tan, C.K., and Kim, S.G., "Manuals for the Design of Bridge Foundations," *NCHRP Report 343*, Transportation Research Board, Washington, DC, 1991.
36. Paikowsky, S.G., Canniff, M.C., Lesny, K., Kisse, A., Amatya, S., and Muganga, R., "LRFD design and construction of shallow foundations for highway bridges," *NCHRP Report 651*, Transportation Research Board, Washington DC, 2010.
37. Kulicki, J.M., Prucz, Z., Clancy, C.M., Mertz, D.R., and Nowak, A.S., "Final Report for NCHRP Project 20-7/186: Updating the Calibration Report for AASHTO LRFD Code," *Report*, Transportation Research Board, Washington, DC., 2007
38. Benjamin, C.V.S., Bueno, B.S., Lodi, P.C. and Zornberg, J.G., "Installation and ultraviolet exposure of geotextiles," *Fourth European Geosynthetics Conference, EuroGeo4*, Edinburgh, United Kingdom, 8–10 September, 2008, pp. 18.
39. Grouni, H.N. and Nowak, A.S., "Calibration of the Ontario Bridge Design Code 1983 Edition," *Canadian Journal of Civil Engrg. 11*(4), 1984: pp. 760–770
40. Paikowsky, S. G., with contributions from Birgisson, B., McVay, M., Nguyen, T., Kuo, C., Baecher, G., Ayyab, B., Stenersen, K., O'Malley, K., Chernauskas, L., and O'Neill, M., "Load and Resistance Factor Design (LRFD) for Deep Foundations, NCHRP (Final) Report 507," *Report*, Transportation Research Board, Washington, DC, 2004.
41. Bathurst, R.J., Allen, T.M., and Nowak, A.S., "Calibration concepts for load and resistance factor design (LRFD) of reinforced soil walls," *Canadian Geotechnical Journal*, NRC Canada, Volume 45, 2008, pp. 1,377–1,392.

HRDI-40/08-13(WEB)E